High precision penetration depth measurements: Probing the superfluid density and the order parameter of high-T_c superconductors

Christos Panagopoulos
Trinity College
Cambridge

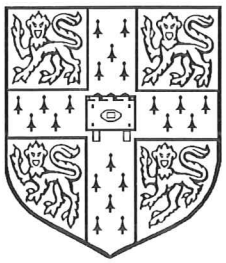

A dissertation submitted for the degree of Doctor of Philosophy at the University of Cambridge

June 1997

Αφιερωνω αυτη την εργασια στο Χαρουμακι μου και τον αγαπημενο μας υιο Οδυσσεα – Νοζομι για την συμπαρασταση και ατελειωτη αγαπη τους

Ευχαριστω

Summary

The symmetry of the order parameter of high- T_c superconductors (HTSC) has been extensively discussed in the past few years. A sensitive probe of the energy gap is the temperature (T) dependence of the superfluid density as obtained from the measurement of the penetration depth, λ.

We present some new results on the T dependence and the absolute values of the in-plane, λ_{ab}, and out-of-plane, λ_c, penetration depths obtained for several HTSC using the low field ac-susceptibility technique.

We have found that the presence of the linear term in $\lambda_{ab}(T)$, characteristic of d-wave superconductivity, is independent of the number of CuO_2 planes per unit cell, carrier concentration, crystal structure, presence of chains and the anisotropy. The superconducting energy gap of BCS d- wave cuprate superconductors was found to scale linearly with T_c. It was shown experimentally that for HTSC with tetragonal symmetry and moderate anisotropy the Cu 4s orbital is important for the c-axis hopping of holes. Namely a T^5 dependence of $\lambda_c(T)$ was observed for $HgBa_2CuO_{4+\delta}$ and a T^2 law for more anisotropic materials (e.g. $HgBa_2Ca_2Cu_3O_{8+\delta}$). $\lambda_c(T)$ for $YBa_2Cu_3O_{6.7}$ and $YBa_2Cu_3O_{6.57}$, which have similar anisotropy to Hg-1223, also varied as T^2. $YBa_2Cu_3O_7$ shows a flatter but linear T dependence in $\lambda_c(T)$ at low T. Zinc substitution in $YBa_2Cu_3O_7$ affects the anisotropy and the residual density of states. Finally, results for $Ba_{0.6}K_{0.4}BiO_3$ emphasise the importance of the CuO_2 planes for d- wave pairing symmetry.

Statement of Originality

I declare that the work presented herein is my own original work and contains nothing that is the result of collaboration, except where specifically stated in the text. In addition it has not been submitted previously at Cambridge or any other university for a degree or diploma. In accordance with the regulations this thesis does not exceed 60,000 words in length.

Christos Panagopoulos

Trinity College

Cambridge

June 1997

Acknowledgements

I would like to acknowledge the constant interest and encouragement of my supervisor, Dr. J.R. Cooper. Without his experience and enthusiasm this project would never have been fruitful.

Technical support from the staff of the IRC in Superconductivity workshop is deeply acknowledged. The experience and skills of S. Smith and S. Brown, have been of great help.

I would also like to acknowledge the generous provision of samples of high quality $HgBa_2Ca_2Cu_3O_{8+\delta}$, $HgBa_2CuO_{4+\delta}$ and $Ba_{0.6}K_{0.4}BiO_3$, by Professor P.P. Edwards and G. Peacock of the School of Chemistry, University of Birmingham and Drs. W. Schmidbauer and J.W. Hodby of Clarendon Laboratory, University of Oxford, respectively.

The enlightening discussions and advice of Drs. T. Xiang, W. Zhou and J. Chrosch of the IRC in Superconductivity proved invaluable.

The interest of Dr. S.R. Julian in my work is very much appreciated, as his permission to perform susceptibility experiments (in progress) using the dilution refrigerator in the Cavendish laboratory.

I am also grateful to all the students and research staff at the IRC for numerous scientific discussions and for providing a very pleasant working and social environment.

Special thanks must also go to Professor W.Y. Liang for believing in the success of the project from the beginning, and his encouragement and help in various aspects of the project.

Financial support from the Cambridge Commonwealth Trust, Overseas Research Students awards and Trinity College Cambridge is also deeply acknowledged.

An overall view of the thesis

Detailed knowledge of the behaviour of the density of the superfluid and the identification of the symmetry of the energy gap are crucial to the understanding of the physical properties of high- T_c superconductors (HTSC). One of the best probes of the superfluid density and the symmetry of the energy gap is the penetration depth, λ. The way λ varies with temperature, T, provides important information about the behaviour of the superfluid, in particular, whether the energy gap is conventional or unconventional. Moreover the values at $T = 0$ (i.e., $\lambda(0)$) can be used to relate the superfluid density to the critical temperature T_c.

In this work considerable attention has been given to sample preparation. The growth of single crystals is hampered by their chemical complexity and obtaining homogeneously doped crystals is very difficult. As an alternative approach we have prepared magnetically aligned powders dispersed in epoxy. In contrast to single crystals, one can easily prepare high purity powders. High degree of alignment, crucial for accurately determining the anisotropic properties, is consistently achieved and a new characterisation method using high-resolution X-ray diffractometers, constructed by Professor E. Salje and his colleagues, in combination with integration techniques has been developed.

Sample surface deterioration was found to cause problems in measurements of the low temperature magnetisation of HTSC and consequently λ. The necessary preparation and heat treatment conditions to obtain clean surfaces have been found and it is shown that these have significant effects on our data.

We present some new results for the T dependence and the absolute values of the in-plane, λ_{ab}, and out-of-plane, λ_c, penetration depths obtained for several HTSC using the low field ac-susceptibility technique. We have further verified the validity of our $\lambda_{ab}(0)$ values by muon spin relaxation measurements performed at the Paul-Scherrer Institute in Switzerland on some of our samples.

$HgBa_2Ca_2Cu_3O_{8+\delta}$ was first prepared in 1993 and presently has the highest known critical temperature. Thus, it is very important to obtain information regarding its physical properties. To this aim we measured the temperature dependences of λ_{ab} and λ_c down to 4.2 K and found them to be markedly different. This is believed to arise from the large anisotropy ratio $\gamma \cong 30$. The behaviour of $\lambda_{ab}(T)$ is indicative of *d*-wave superconductivity while $\lambda_c(T)$ is similar to the behaviour expected for a superconductor with intrinsic Josephson coupling between the CuO_2 planes. Similar measurements on the isotropic perovskite $Ba_{0.6}K_{0.4}BiO_3$ superconductor showed that $Ba_{0.6}K_{0.4}BiO_3$ is an *s*-wave superconductor. The latter result is a strong indication of the importance of the CuO_2 planes for *d*-wave symmetry.

We have extended our study on Hg-cuprates by measuring the low T dependence of λ of magnetically aligned powders of $HgBa_2Ca_{n-1}Cu_nO_{2n+2+\delta}$ (n=1 and 3) down to 1.2 K. For both members $\lambda_{ab}(T)$ is strongly linear whereas $\lambda_c(T)$ for n=1 and 3 varies as T^5 and T^2, respectively. The results are discussed in terms of $d_{x^2-y^2}$- wave symmetry of the order parameter.

Also we report the T and oxygen concentration dependences of λ_{ab} and λ_c of grain aligned $YBa_2Cu_3O_{7-\delta}$ with $\delta = 0.0$, 0.3 and 0.43. The values of $\lambda_{ab}(0)$ and $\lambda_c(0)$ and the ratio $[\lambda_c(0) / \lambda_{ab}(T)]$ were found to increase with increasing δ. The linear term in $\lambda_{ab}(T)$ also increases with δ, which in conjunction with our results for $HgBa_2Ca_{n-1}Cu_nO_{2n+2+\delta}$ (n = 1 and 3) suggests that in *d*- wave cuprates T_c may scale with the superconducting energy gap. The low T dependence of λ_c changed from linear for $\delta = 0.0$ to T^2 for both $\delta = 0.3$ and 0.43.

Finally, we show recent $\lambda_{ab}(T)$ and $\lambda_c(T)$ results of $YBa_2(Cu_{1-x}Zn_x)_3O_7$ with x = 0.00, 0.02, 0.03 and 0.05. The information obtained allowed us to determine the fundamental effects of Zn doping on $\lambda(T)$ and the anisotropy of the system. $\lambda_{ab}(T)$ and $\lambda_c(T)$ for x =0.00 showed excellent agreement with the behaviour predicted for a *d*-wave superconductor. The $\lambda_{ab}(0)$ and $\lambda_c(0)$ values were found to increase strongly with increased Zn concentration whereas the anisotropy ratio $\gamma = [\lambda_c(0) / \lambda_{ab}(0)]$ decreased. With increased Zn doping the $[\lambda_{ab}(0) / \lambda_{ab}(T)]^2$ and $[\lambda_c(0) / \lambda_c(T)]^2$ curves systematically approach each other.

It is widely accepted that the understanding of the physical properties of HTSC is one of the major challenges in modern physics. The present work provides a systematic study of the behaviour of the superfluid and the unconventional energy gap of high T_c cuprates. It may prove that a detailed understanding of the superfluid and the energy gap symmetry is a crucial clue towards developing a successful theory of superconductivity in the cuprates.

Contents

Chapter 1

In this chapter, we introduce the fundamental theoretical ideas of superconductivity that are relevant to the main subject of this thesis, an introduction to high-T_c superconductors, and a brief account on the status of the subject under investigation.

Introduction

At a critical temperature (T_c) the electrical resistance of certain substances becomes zero. This phenomenon was discovered in 1911 by H.K. Onnes [1] when measuring the resistance of Hg and was given the name "superconductivity".

Investigations have shown that superconductivity can be destroyed not only by increasing the temperature, T, but also by applying a sufficiently strong magnetic field. If a metal is placed in a magnetic field smaller than a critical field H_c, then upon transition to the superconducting state the field is expelled from its interior (Meissner effect).

1.1 Cooper pairs

The theory of superconductivity was formulated by Bardeen, Cooper, and Schrieffer (BCS) in their paper in 1957 [2]. The basic concept of the BCS theory is that superconductivity results from a dynamic *pairing* of the conduction electrons of the material to form the so-called superfluid. These pairs are superimposed in quantum mechanical phase and the pairing creates an energy gap (or order parameter) in the electron energy spectrum. The long range phase coherence means that superconductivity is one of the most striking macroscopic examples of quantum mechanics in action.

In simple terms, let us suppose that two electrons which lie in the neighbourhood of the Fermi surface attract each other. Cooper [3] showed that the two electrons would then

form a bound state, provided that they were very close to the Fermi surface. Note that in a bound state, electrons are paired to form a single system, and their motions are correlated. These two electrons are called a "Cooper pair". The binding energy is strongest when the electrons forming the pair have opposite moments and opposite spins. It follows, therefore, that if there is any attraction between them, then all the electrons in the neighbourhood of the Fermi surface condense into a system of Cooper pairs. These pairs sometimes called superelectrons, have a binding energy corresponding to an "energy gap" Δ.

The question that arises is how does this attraction came about in the first place. In superconductive materials, it results from the electron-lattice interaction. Such a possibility was primarily indicated by the discovery of the isotope effect [4] where the T_c of a superconductor was found to be related to its isotope mass M, as $T_c \sim M^{-1/2}$. Suppose that the two electrons, 1 and 2, pass each other. Because electron 1 is negatively charged, it attracts positive ions toward itself (electron-lattice interaction). Thus electron 2 does not "see" the bare electron 1. Electron 1 is screened by ions. The screening may greatly reduce the effective charge of this electron; in fact, the ions may overrespond and produce a net positive charge. If this happens, then electron 2 will be attracted toward 1. This leads to a net attractive interaction, as required for the formation of the Cooper pair.

As a result of this binding between electron 1 and electron 2, an energy gap appears in the excitation spectrum of the system. This gap straddles the Fermi energy.

1.2 The upper and lower critical fields

The Meissner effect implies a critical field, H_c, above which superconductivity will be destroyed. Since $H^2/8\pi$ is the magnetic energy density, the difference between the Helmholtz free energy in the normal and superconducting states per unit volume is

$$F_n(T) - F_s(T) = \frac{H_c(T)^2}{8\pi} . \qquad (1.1)$$

Within the BCS theory the experimental results can be approximately described by a quadratic temperature dependence,

$$H_c(T) = H_c(0)\,[1-(T/T_c)^2], \tag{1.2}$$

with $H_c(0)$ values less than 10^3 G for the elements of the periodic table that superconduct. Geometrical (sample shape dependent) effects may cause the magnetic field to exceed H_c in some parts of the sample, while $H < H_c$ in other parts of the sample. This is the intermediate state. Superconducting materials which go through the intermediate state are called type I.

Not all superconductors pass directly from the Meissner state to the normal state. In the presence of a magnetic field a second type of superconductors (type II) go through the "mixed state" which adjoins the superconducting phase at H_{c1} (the lower critical field) and the normal phase at another field H_{c2} (the upper critical field). At H_{c2} superconductivity disappears and the break-up of Cooper pairs occurs as a result of the curving of their trajectory in the magnetic field. H_{c1} and H_{c2} can be related to the thermodynamic H_c as

$$H_{c2} \sim \sqrt{2}\kappa H_c\,,\; H_{c1} \sim \frac{H_c}{\sqrt{2}\kappa}\ln\kappa\,,\; H_{c1}H_{c2} \sim H_c^2\ln\kappa \tag{1.3}$$

κ is called the Ginzburg-Landau parameter and is equal to λ_{eff}/ξ. Here λ_{eff} and ξ are the effective penetration depth and the coherence length, respectively [5]. An analytical discussion leading to the above relation can be found in most solid state books. The penetration depth is the region where the screening currents, which circulate to cancel the flux inside the sample, flow. The coherence length characterises the distance over which the superconducting order parameter can vary without substantial energy increase. Borrowing an idea from the mean free path in a normal metal alloy in the presence of

Within the BCS theory the experimental results can be approximately described by a quadratic temperature dependence,

$$H_c(T) = H_c(0)\,[1-(T/T_c)^2], \tag{1.2}$$

with $H_c(0)$ values less than 10^3 G for the elements of the periodic table that superconduct. Geometrical (sample shape dependent) effects may cause the magnetic field to exceed H_c in some parts of the sample, while $H < H_c$ in other parts of the sample. This is the intermediate state. Superconducting materials which go through the intermediate state are called type I.

Not all superconductors pass directly from the Meissner state to the normal state. In the presence of a magnetic field a second type of superconductors (type II) go through the "mixed state" which adjoins the superconducting phase at H_{c1} (the lower critical field) and the normal phase at another field H_{c2} (the upper critical field). At H_{c2} superconductivity disappears and the break-up of Cooper pairs occurs as a result of the curving of their trajectory in the magnetic field. H_{c1} and H_{c2} can be related to the thermodynamic H_c as

$$H_{c2} \sim \sqrt{2}\kappa H_c\,,\; H_{c1} \sim \frac{H_c}{\sqrt{2}\kappa}\ln\kappa\,,\; H_{c1}H_{c2} \sim H_c^2\ln\kappa \tag{1.3}$$

κ is called the Ginzburg-Landau parameter and is equal to λ_{eff}/ξ. Here λ_{eff} and ξ are the effective penetration depth and the coherence length, respectively [5]. An analytical discussion leading to the above relation can be found in most solid state books. The penetration depth is the region where the screening currents, which circulate to cancel the flux inside the sample, flow. The coherence length characterises the distance over which the superconducting order parameter can vary without substantial energy increase. Borrowing an idea from the mean free path in a normal metal alloy in the presence of

impurity scattering, ξ might be expected to be related to the mean free path (l) by an equation of the type $(1/\xi) = (1/\xi_0) + (1/l)$ where ξ_0 is the coherence length of the pure material. Normally, $\xi_0 << l$, the so-called clean limit. Increased electron-impurity scattering, leads to $l << \xi_0$, and then $\xi \sim l$, the dirty limit.

In the mixed state, vortices which act as tiny bar magnets and repel each other penetrate into the sample. The net repulsion energy is minimized when the vortices form close-packed, hexagonal array, called a vortex lattice.

1.3 The penetration depth

The perfect diamagnetism of a superconductor in the Meissner state prevents electric currents from flowing through the body of the material. On the other hand, current cannot be confined entirely to the surface because, if this were so, there would be an infinite current density there. In fact the currents flow within a surface layer called the penetration depth which is of the order of μm or less. To examine this quantitatively we assume that at $T < T_c$, only a fraction $n_s(T)/n$ of the total number of conduction electrons n, participate in a supercurrent. $n_s(T)$ is the density of superconducting electrons. Note: $n_s \rightarrow n$ for $T \rightarrow 0$ and $n_s \rightarrow 0$ for $T \rightarrow T_c$ (from below).

Suppose that an electric field, $\boldsymbol{E}$, momentarily arises within a superconductor. The superconducting electrons will be freely accelerated without dissipation so that their mean velocity $\boldsymbol{v}_s$ will satisfy

$$m \frac{d\boldsymbol{v}_s}{dt} = -e\boldsymbol{E} , \tag{1.4}$$

where e ($e > 0$) is the electronic charge. But since the current due to the superconducting electrons is given by $\boldsymbol{J} = -e\boldsymbol{v}_s n_s$, eq. (1.4) can be written as

$$\frac{d\boldsymbol{J}}{dt} = \frac{n_s e^2}{m} \boldsymbol{E} . \tag{1.5}$$

We identify the effective number density of superelectrons n_s as the total number density of electrons n.

Substituting eq. (1.5) into Faraday's law of induction, $[(1/c)d\boldsymbol{B}/dt] = -\nabla \times E$, gives the following relation between current density and magnetic field:

$$\frac{\partial}{\partial t}[\nabla \times \boldsymbol{J} + \frac{n_s e^2}{mc}\boldsymbol{B}] = 0. \tag{1.6}$$

This relation, together with the Maxwell equation

$$\nabla \times \boldsymbol{B} = \frac{4\pi}{c}\boldsymbol{J} \tag{1.7}$$

determines the magnetic fields and current densities that can exist within a perfect conductor. Note in particular that any static field $\boldsymbol{B}$ determines a static current density $\boldsymbol{J}$ through eq. (1.7). Since any time independent $\boldsymbol{B}$ and $\boldsymbol{J}$ are trivial solutions to eq. (1.6), the two equations are consistent with an arbitrary static magnetic field. This is incompatible with the observed behaviour of superconductors in small magnetic fields $H < H_{c1}$, the lower critical field, where no fields are permitted in their interior in the Meissner state. The London brothers [6] pointed out that this characteristic behaviour could be obtained by restricting the full set of solutions of eq. (1.6) to those that obey

$$\nabla \times \boldsymbol{J} + \frac{n_s e^2}{mc}\boldsymbol{B} = 0 \tag{1.8}$$

which is known as the London equation. Equation (1.6), which characterises any medium that conducts electricity without dissipation, requires that the left hand side of eq. (1.8) is independent of time; the more restrictive London equation, which specifically characterises superconductors and distinguishes them from mere "perfect conductors",

requires in addition that the time-independent value be zero. Equations (1.7) and (1.8) imply that

$$\nabla \times \nabla \times \boldsymbol{B} + \frac{4\pi n_s e^2}{mc^2}\boldsymbol{B} = 0 \qquad (1.9)$$

and

$$\nabla \times \nabla \times \boldsymbol{J} + \frac{4\pi n_s e^2}{mc^2}\boldsymbol{J} = 0. \qquad (1.10)$$

Now $\nabla \times \nabla \times \boldsymbol{B} = \nabla(\nabla \bullet \boldsymbol{B}) - \nabla^2 \boldsymbol{B}$, but from Maxwell's equations $\nabla \bullet \boldsymbol{B} = 0$, so equations (1.9) and (1.10) become

$$\nabla^2 \boldsymbol{B} = \beta^2 \boldsymbol{B} \quad \text{and} \quad \nabla^2 \boldsymbol{J} = \Lambda^2 \boldsymbol{J},$$

respectively, where $\Lambda^2 = (4\pi n_s e^2 / mc^2)$. These equations, in turn, predict that currents and magnetic fields die away exponentially inside a superconductor, falling to e^{-1} of their values at a layer of thickness λ of the surface, where λ, known as the London penetration depth, is given by

$$\lambda = \frac{1}{\Lambda} = \sqrt{\frac{mc^2}{4\pi n_s e^2}} \qquad (1.11)$$

The penetration depth does not have a fixed value but varies with temperature due to the temperature dependence of n_s; the penetration depth λ becomes infinite when T approaches the transition temperature since the density of superconducting electrons n_s goes to zero at T_c. In BCS theory the detailed temperature dependence of $[\lambda(T)/\lambda(0)]$ depends on the ratio $\xi_0/\lambda(0)$. Here $\lambda(0)$ is the value of λ at 0 K and ξ_0 is the coherence length of the pure material.

In the limit where $\lambda << \xi_0$ but still negligible scattering with the mean free path $l >> \xi_0$ we get [5]

$$\lambda_\infty \cong [(\sqrt{3}/2\pi)\ \lambda^2\ \xi_0]^{1/3} \qquad (1.12)$$

Clean aluminium with $\lambda = 50$ nm and $\xi_0 = 160$ nm is close to this limit.

In the local limit we have $l << \lambda$ and

$$\lambda_{dirty} \cong \lambda\ [1 + \xi_0/\lambda]^{1/2} \qquad (1.13)$$

This expresses the fact that shortening the mean free path, for example by alloying the superconductor, increases the penetration depth.

1.4 High-T_c superconductors

1.4.1 Introductory remarks

In 1986, J. G. Bednorz and K. A. Müller [7], discovered a material with a T_c greater than 30 K. This T_c had never been thought possible, according to the Bardeen-Cooper-Schrieffer (BCS) theory [2], which was developed for conventional superconductors (superconductors that do not contain Cu-O planes). The material was La_2CuO_4 in which ions of Ba^{2+} and later Sr^{2+}, or Ca^{2+} replaced some of the La^{3+} ions. These new materials were given the name high-T_c superconductors and their discovery introduced doubts on the validity of the BCS theory to high-T_c superconductors.

Shortly afterwards, $YBa_2Cu_3O_{7-\delta}$ was discovered [8,9], with T_c of ~ 92 K, above the boiling point of liquid nitrogen (77.3 K). A year later, the Bi-Sr-Ca-Cu-O [10-12] and Tl-Sr-Ca-Cu-O [13-16] systems were prepared with T_c's in the range 110 - 120 K. In all these oxides superconductivity is obtained by introducing holes through doping at atmospheric pressure. Later on electron doped copper oxide superconductors, the $Ln_{2-x}Ce_xCuO_{4-y}$ system (Ln=Nd, Sm, Pr) with T_c up to 24 K for $x = 0.15$, were discovered [17,18]. In 1993 a new system, Hg-Ba-Ca-Cu-O was found with a T_c ~ 135 K [19-20], the highest reported to date.

Another type of oxide superconductors is the $BaBiO_3$ family. In 1975, it was discovered that $Ba(Bi_{1-x}Pb_x)O_3$ was superconducting over a large range of x with a maximum $T_c = 13$ K [21]. More recently, $Bi_{0.6}K_{0.4}BiO_3$ was found to have T_c ~ 30 K [22]. Although T_c is small compared with that of some high-T_c superconductors, it is certainly high in comparison with conventional superconductors.

1.4.2 Crystal structures

In addition to their high T_c values, the large spatial anisotropy of the high-T_c superconductors, except $(Bi_{0.6}K_{0.4})BiO_3$ which is isotropic, is striking. The anisotropy is due to the layered crystal structure, which is currently believed to be essential for the existence of high-T_c superconductivity. The layers are composed of CuO_2 planes, separated from each other by planes of various other oxides, which form inert charge reservoir layers.

A detailed account on the structures of all high -T_c superconductors can be found in a number of books dedicated to high temperature superconductivity [23]. Here we focus on the structure of the materials investigated in this thesis.

$YBa_2Cu_3O_{7-\delta}$ (YBCO): The crystal structure of YBCO is shown in fig.1.1. For δ = 0, YBCO has an orthorhombic structure, all the oxygen sites along the *b* direction of the basal plane are empty, and all of those along the *a* direction occupied. Thus CuO chains appear along the *a* direction. The absence of oxygen atoms allows the Cu atoms to move slightly closer together along the *b* direction, by inducing an orthorhombic distortion with $a > b$.

Hg-Ba-Ca-Cu-O compounds: The superconducting compounds in the Hg-Ba-Ca-Cu-O system form a hierarchy of tetragonal structures which differ in the number of CuO_2 planes and they follow the general chemical formula of $HgBa_2Ca_{n-1}Cu_nO_{2n+2+\delta}$. The structures consist of n = 1, 2, 3 CuO_2 planes. The individual CuO_2 layers are separated by Ca layers which contain no oxygen and the CuO_2 layer groups are intercalated by two Ba-O layers. The compound with a CuO_2 trilayer in one unit cell exhibits the highest T_c of about 135 K. The structure can be viewed as a series of active CuO_2 planes with the Hg-O layers acting as a charge reservoir. Figure 1.2 shows the structures for the series $HgBa_2Ca_{n-1}Cu_nO_{2n+2+\delta}$ (n = 1, 2 and 3; δ=0).

$BaBiO_3$-type superconductors: $BaBiO_3$ has an almost undistorted ABO_3, cubic perovskite structure. Each Bi atom is octahedrally coordinated to six O atoms. When

undoped, it is not a metal. However, when doped on the A site with potassium, it becomes metallic and superconducting. The superconducting phase, is cubic, thus making $Ba_{1-x}K_xBiO_3$ similar to the isotropic lower T_c superconductors such as the Nb compounds. Its parent structure is $BaBiO_3$, and the superconductor contains potassium which occupies the barium sites in the structure shown in fig. 1.3. Superconductivity occurs only in the cubic perovskite phase which exists for $0.37 < x < 0.5$ in $Ba_{1-x}K_xBiO_3$. This compound has not been widely studied and there is little information available on its basic properties.

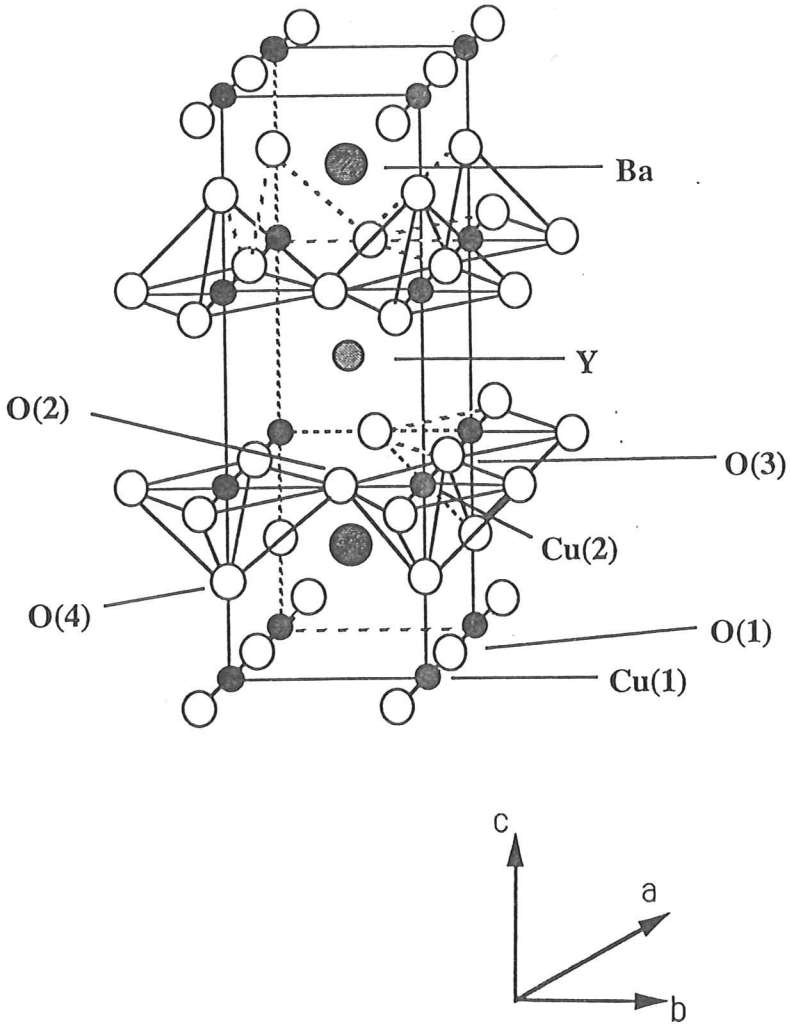

Fig. 1.1. The orthorhombic $YBa_2Cu_3O_7$ structure.

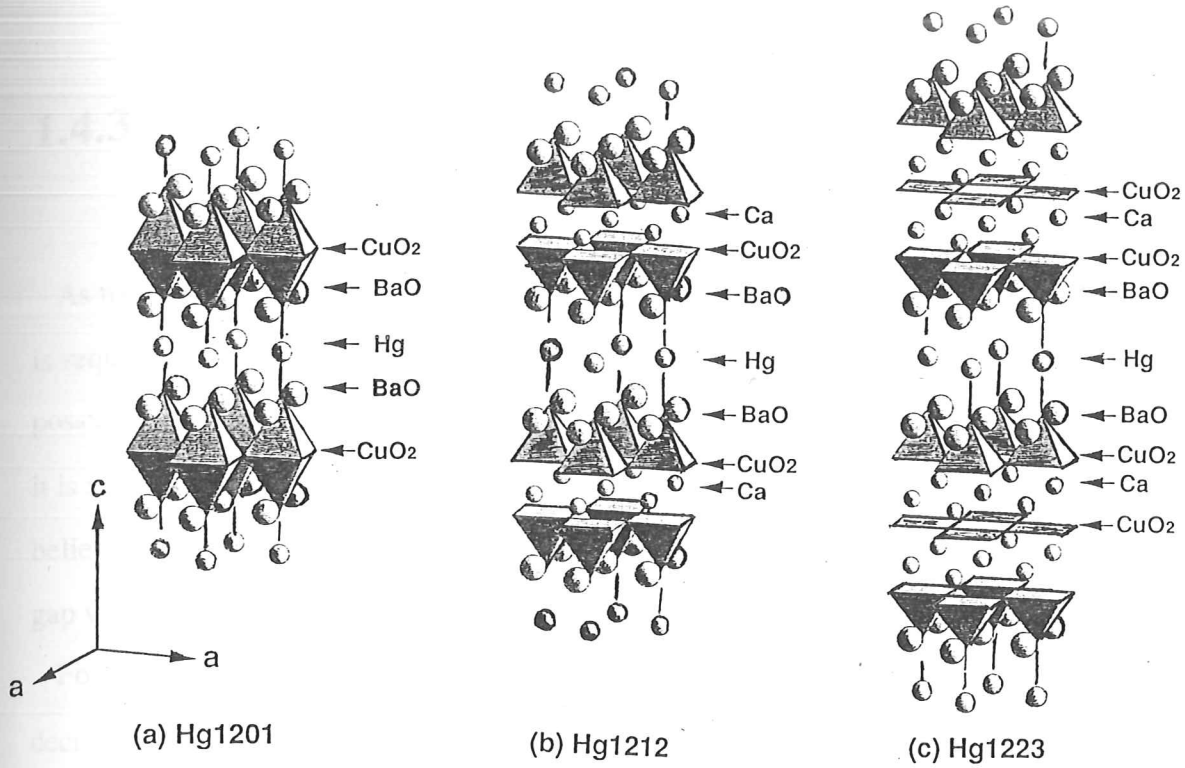

Fig. 1.2. The structures for the series $HgBa_2Ca_{n-1}Cu_nO_{2n+2+\delta}$ (n = 1, 2 and 3; δ =0). (a) $HgBa_2CuO_4$ (Hg-1201) (b) $HgBa_2CaCu_2O_6$ (Hg-1212) and (c) $HgBa_2Ca_2Cu_3O_8$ (Hg-1223).

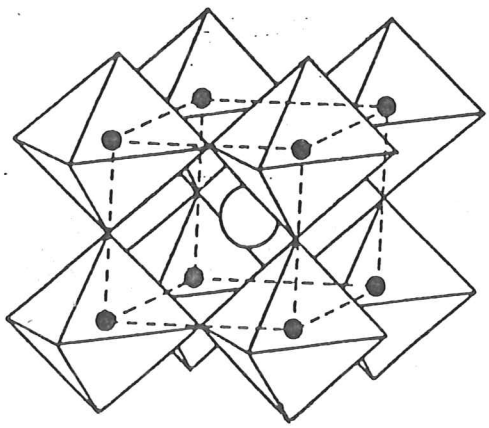

Fig. 1.3. The structure of $BaBiO_3$, the parent structure of $Ba_{1-x}K_xBiO_3$. Potassium occupies the barium sites.

1.4.3 Superconducting gap and penetration depth measurements in high-T_c superconductors

As mentioned earlier, in the superconducting state a minimum energy, the gap energy, is required to break up a superconducting (Cooper) pair. No electronic excitations are possible below the gap. In conventional *s*-wave superconductors the gap (Δ) is isotropic; it is roughly the same everywhere on the Fermi surface. In superfluid ^{3}He and also, it is believed, in the novel class of metals known as the heavy fermion superconductors the gap vanishes along lines or at points on the Fermi surface.

For conventional, BCS like, superconductors, at low temperatures ($T/T_c < 0.3$), $\Delta(T)$ decreases exponentially with temperature, as

$$\Delta(T) = \Delta_0 - [2\pi T\Delta_0 (1-T/8\Delta_0)\exp -(\Delta_0/k_BT)], \qquad (1.14)$$

changing only slightly in a broad range of temperature. Δ_0 is the gap at $T = 0$. As the temperature increases, more quasiparticles become thermally excited and near T_c the energy gap varies as [5]:

$$\Delta(T) / \Delta_0 \sim 1.74 (1 - T/T_c)^{1/2}. \qquad (1.15)$$

The physical properties that are associated with the energy gap are also expected to vary exponentially at very low temperatures.

The principle behind using $\lambda(T)$ as a probe of the pairing state is relatively straightforward. If there is a gap whose minimum value over the Fermi surface at $T = 0$ is Δ_0, then at low temperatures the variation of $\lambda(T)$ with temperature is given by

$$[\frac{\lambda(T)}{\lambda(0)} - 1] \sim \sqrt{\frac{2\pi\Delta_0}{k_BT}} \exp(\frac{-\Delta_0}{k_BT}) \qquad (1.16)$$

where k_B is the Boltzmann constant. Thus, in principle, observation of an exponential temperature dependence at low temperatures would enable the gap, Δ_0, to be inferred. Hence, if it were to be shown that, at the lowest temperatures, the exponential form was absent, then it could be concluded that there are nodes of some topology in the gap. Conversely, observation of an exponential temperature dependence at low temperatures would not imply that the superconductor is conventional but rather, would only indicate that there is no nodal structure.

In high-T_c superconductors superconductivity is believed to occur in the two-dimensional CuO_2 planes. The high T_c values and experimental evidence for a mechanism other than the standard BCS electron pairing have motivated the investigation of many different pairing mechanisms. Evidence is now growing that one of the most fundamental properties of the superfluid, the energy gap, is very different to that assumed by the *s*-wave BCS model. We consider the paired electrons and hence the energy gap to be confined to the CuO_2 planes. In conventional superconductors the energy gap has "*s*-wave" symmetry, i.e. in the case of high-T_c superconductors the gap has the same magnitude and phase for all directions in a CuO_2 plane. In high-T_c superconductors, some have argued that the energy gap has "*d*-wave" symmetry, leading to a directional dependence in a CuO_2 plane resembling a four-leaf clover described by x^2-y^2 for points (x,y) on a circle. Detailed knowledge of the behaviour of the density of the superfluid and the identification of the symmetry of the energy gap are crucial to the understanding of the physical mechanism of high -T_c superconductors.

Theoretical models have been developed to explain the unconventional behaviour of the copper oxide superconductors. It is beyond the scope of this thesis to give a review of these theories, but we will consider one model (*d*-wave model) that we found to describe closer our results. Excellent accounts on the theory can be found in the review articles written by J.F. Annett et al. [24,25].

This model suggested that the presence of strong antiferromagnetic spin fluctuations in the normal state might favour a BCS like singlet but with nodes in the gap function, so

called *d*-wave superconductivity [26-29]. In the case where we have unconventional states with gap nodes the superfluid density has a stronger temperature dependence and it should follow the general behaviour [24]

$$[\frac{\lambda(T)}{\lambda(0)} - 1] \sim A_n (\frac{k_B T}{\Delta_{max}})^n \qquad (1.17)$$

where A_n is a constant, the exponent n depends on the type of nodes and their relative orientation to the applied magnetic field, and Δ_{max} is the maximum value of the gap function over the Fermi surface. For line nodes this formula leads to an exponent $n = 1$ and to a linear temperature dependence of the penetration depth, $\lambda \sim T$, for very low temperatures [30,31].

In a *d*-wave model, disorder gives rise to a finite density of states at zero energy [32]. Impurities can cause strong localisation of the low energy excitations and affect the linear temperature dependence of λ. The induced scattering is found to alter the linear T dependence of λ to T^2 at low temperatures [33,34].

There has been a great number of measurements of both the magnitude and T dependence of λ for the high-T_c superconductors, but the results are often conflicting. Several experimental techniques have been applied in order to determine λ. Below we present a brief account on the status of the subject discussed in this thesis.

Detailed λ studies on $Ba_{1-x}K_xBiO_3$ are not available and here we provide direct evidence for it being a conventional superconductor. $La_{2-x}Sr_xCuO_4$ on the other hand, was given a little more attention. The existing results for $La_{1.85}Sr_{0.15}CuO_4$ single crystals [35], the only composition of the series studied to date, suggest that it follows a BCS like behaviour, although no "clean" low temperature, $T / T_c < 0.25$, data is available.

The most "popular" superconductor seems to be $YBa_2Cu_3O_{7-\delta}$ for well known reasons (e.g. relatively easy to prepare, stable with promising technological applications). Data for this material was far from conclusive until Hardy et al., [36] measured the in-plane penetration depth of $YBa_2Cu_3O_{7-\delta}$ single crystals using the microwave technique.

Unfortunately, however, with the microwave technique it is not easy to determine the $\lambda(0)$ values directly.

$Bi_2Sr_2Ca_2CuO_{8-\delta}$ has also been studied to a certain extent but deserves more attention. Recent microwave measurements show a linear temperature dependence of the in-plane penetration depth down to 5 K [37,38].

A report on $Tl_2CaBa_2Cu_2O_{8-\delta}$ single crystal showed that both in-plane and out-of plane components of the penetration depth varied linearly with temperature [39]. However, there has been no confirmation of the result and no studies on the single and triple layered members of the Tl family.

$HgBa_2Ca_{n-1}Cu_nO_{2n+2+\delta}$ had not been studied prior to our investigation and we are able to provide the first penetration depth measurements and the accompanying physical conclusions in this cuprate family.

Studies on the electron doped cuprate superconductor $Nd_{1.85}Ce_{0.15}CuO_4$ (NCCO) point towards a single conclusion: an *s*-wave order parameter [40]. However, we would like to note that the literature on this material is not extensive and any conclusion should await wider confirmation. Furthermore, a recent comment by J.R. Cooper [41] shows that the low temperature measurements on this material are very sensitive to the strong paramagnetism arising from the Nd^{3+} ions and that NCCO is probably also *d*-wave.

Finally, a systematic study of impurity effects in cuprates was not available prior to the present work. Here we provide the first systematic evidence for the effects of non magnetic impurities to the anisotropic penetration depth of $YBa_2Cu_3O_{7-\delta}$.

In brief, the data published on the T dependence of λ is partly controversial and no significant improvements can be made unless the samples under investigation are well characterised before any attempt of data interpretation. Furthermore, no definite comparison can be made between different experimental groups unless both $\lambda(T)$ and $\lambda(0)$ are determined from the same samples and if possible using the same technique.

It is thus necessary to have a technique which allows us to simultaneously determine both $\lambda(0)$ and $\lambda(T)$ and can study accurately a wide range of high-T_c superconductors.

The technique presented in this thesis is based on the idea first suggested and employed for the study of conventional superconductors by D. Shoenberg at the Cavendish laboratory in the middle of this century [42]. The method has since been employed by several groups [43] for the investigation of high-T_c superconductors.

As we discuss in Chapter 2 with this technique one measures the susceptibility of powder samples at low fields and frequencies. Although one would always tend to prefer results obtained from a single crystal in practice there are only few high-T_c superconductors for which good single crystals with a volume greater than 10^{-7} cm^3 can be grown. Furthermore, it is often very difficult to obtain good quality doped crystals and doping studies have proved to be very important for high temperature superconductivity. Also microwave studies of single crystals are often unable to determine the magnitude of λ, and measure only relative changes $\delta\lambda = \lambda(T) - \lambda(T_0)$, where T_0 is typically 1.2 K.

Employing low fields and frequencies and well characterised clean materials we are able to perform an extensive and systematic study of both $\lambda(0)$ and $\lambda(T)$ on several high-T_c superconductors. In this thesis we report the details of the technique and new results on some high-T_c superconductors which we have been able to investigate to date.

References

[1] H. K. Onnes, Commun. Phys. lab. Univ. Leiden, Nos. 119b, 120b, 122b, 124c (1911).

[2] J. Bardeen, L. N. Cooper and J. R. Schrieffer, Phys. Rev. **106**, 162(1957) ; **108** 1175 (1957).

[3] L. N. Cooper, Phys. Rev. **104**, 1189 (1956).

[4] C.A. Reynolds *et al*, Phys. Rev. **78**, 487 (1950); E. Maxwell, Phys. Rev. **78**, 477 (1950).

[5] M. Tinkham: Introduction to Superconductivity, eds. B. Bayne and M. Gardner (McGraw-Hill, New York, 1975).

[6] F. London and H. London, Proc. R. Soc. London Ser. A. **149**, 71 (1935) ; Physica **2**, 341 (1935).

[7] J. G. Bednorz and K. A. Müller, Z. Phys. B **64**, 189 (1986) .

[8] C.N. Chu *et al.*, Phys. Rev Lett. **58**, 405 (1987).

[9] M.K Wu *et al.*, Phys. Rev Lett. **58**, 908 (1987).

[10] H. Maeda *et al*, Jpn. J. Appl. Phys. **27**, L209 (1988).

[11] C. Michel *et al*, Z. Phys. B **68**, 421 (1987).

[12] J. Akimitsu *et al*, Jpn. J. Appl. Phys. **26**, L2080 (1987).

[13] Z.Z. Sheng and A.M. Hermann, Nature **332**, 55 (1988).

[14] Z.Z. Sheng *et al*, Phys. Rev. Lett. **60**, 937 (1988).

[15] R.M. Hazen *et al*, Phys. Rev. Lett. **60**, 1657 (1988).

[16] S.S.P. Parkin *et al*, Phys. Rev. Lett. **61**, 750 (1988).

[17] Y. Tokura, H. Takagi and S. Uchida Nature **337**, 345 (1988).

[18] H. Takagi, S. Uchida and Y. Tokura, Phys. Rev. Lett. **62**, 1197 (1989).

[19] A. Schilling, M. Cantoni, J.D. Guo and H.R. Ott, Nature **363**, 56 (1993).

[20] S.N. Putlin, E.V. Antipov, O. Chmaissem and M. Marezio, Nature **362**, 226 (1993).

[21] A.W. Sleight, J.C. Gillson and P.E. Bierstedt, Solid State Commun., **17**, 27 (1975).

[22] R.J. Cava *et al.*, Nature **332**, 814 (1988).

[23] For example, G. Burns: High Temperature Superconductivity (An Introduction), (Academic Press, Inc, San Diego, 1992).

[24] J.F. Annett, N. Goldenfeld and S.R. Renn in "Physical Properties of High Temperature Superconductors II" ed. D.M. Ginsberg, Singapore 1990.

[25] J.F. Annett, N. Goldenfeld and A. J. Leggett in "Physical Properties of High Temperature Superconductors" ed. D.M. Ginsberg, (in press).

[26] D.J. Scalapino, E. Loh Jr and J.E. Hirch, Phys. Rev. B **34**, 8190 (1986).

[27] P. Monthoux, A.V Balatsky and D. Pines, Phys. Rev. Lett. **67**, 3448 (1991).

[28] P.A. Lee and N. Read, Phys. Rev. Lett. **58**, 2691 (1987).

[29] C. Gross, R. Joynt and T.M. Rice, Z. Phys. B 68, 425 (1987).

[30] P. Arberg, M. Mansor and J.P Carbotte, Sol. State Commun. **86**, 671 (1993).

[31] M. Prohammer and J.P Carbotte, Phys. Rev. B **43**, 5370 (1991).

[32] P.A. Lee, Phys. Rev. Lett. **71**, 1887 (1993).

[33] J.F. Annett, N. Goldenfeld and S.R. Renn, Phys. Rev. B **43**, 2778 (1991).

[34] P.J. Hirschfeld and N. Goldenfeld, Phys. Rev. B **48**, 4219 (1993).

[35] T. Shibauchi *et al.,* Phys. Rev. Lett. **72**, 2263 (1994).

[36] W.N. Hardy *et al.,* Phys. Rev. Lett. **70**, 3999 (1993).

[37] T. Jacobs *et al.,* Phys. Rev. Lett. **75**, 4516 (1996).

[38] S.F. Lee *et al.,* Phys. Rev. Lett. **77**, 735 (1996).

[39] H. Ning et al., J. Superconductivity **5**, 503 (1992).

[40] S.M. Anlage et al., Phys. Rev. B **50**, 523 (1994).

[42] D. Shoenberg, Nature **143**, 434 (1939).

[43] D.K. Finnemore *et al.*, Phys. Rev. B **35**, 5319 (1987), D.E. Farrell *et al.*, Phys. Rev. B **35**, 8797 (1987), J.R. Cooper *et al.,* Phys. Rev. B **37**, 638 (1988).

Chapter 2

Experimental

2.1 Preface

There are four main techniques for measuring λ, namely optical conductivity, microwave surface impedance, muon spin relaxation, and low field alternating current (ac) magnetic susceptibility. The optical conductivity technique has been used to determine the absolute value $\lambda(0)$. Measurements as a function of temperature are in principle possible but very time consuming since one needs to accurately obtain the oscillator strength sum rule for the conductivity for several temperatures. The microwave method can only accurately determine relative changes of the temperature dependence of λ, $\delta\lambda(T)$, and not $\lambda(0)$. The muon spin relaxation method on the other hand, can measure accurately only $\lambda(0)$ in the CuO_2 planes. The ac susceptibility technique is the only reliable method which can simultaneously determine directly $\lambda(0)$ as well as $\lambda(T)$ both in or perpendicular to the planes. It is based on the fact that when a small magnetic field is applied to a superconductor, the latter expels the field from its interior and the field can only penetrate a short distance. This distance, the penetration depth, increases as we raise the temperature of the superconductor and becomes infinite at T_c. Consequently, the magnetic field in the sample increases with temperature and the sample's disturbance of the magnetic field distribution in its vicinity is reduced. However, for maximum sensitivity the sample should have a dimension that is comparable to the penetration depth and a powder sample (grains of average diameter size of the order of 10^{-4} cm), is the best choice for the investigation of the penetration depth with the low field ac susceptibility technique (see section 2.2).

However, two major complications, which do not apply in the type of materials studied by Shoenberg, hamper the application of the ac susceptibility technique to the study of high-T_c superconductors. Firstly, λ in high-T_c superconductors is anisotropic. This means that the random alignment of powder grains that Shoenberg was able to use will *not* give useful information for these layered oxides. Secondly, the surfaces of the high-T_c superconductors, particularly in the powder form, are environmentally sensitive and can thus be easily contaminated.

In order to explore the possibility of successfully employing the ac susceptibility technique to study high-T_c superconductors the first task is to align the CuO_2 planes of all grains in parallel. If all planes are parallel then one can study λ in the two orientations relative to the planes. Each grain of the powder contains a number of CuO_2 planes all parallel within the grain. The major task is to have all the grains of the powder oriented so that all CuO_2 planes of the powder are parallel. The latter was achieved by dispersing the powder in epoxy (section 2.4). The mixture is placed in a high magnetic field, using a special probe, while the epoxy is in the liquid state, and is held in the field until the epoxy cures. The product is a solid composite containing ~0.1 grams of superconductor i.e., approximately 10^8 grains fixed in place with their CuO_2 planes parallel to within ~ 1° (section 2.5, chapter 3). This degree of alignment was achieved using the procedure described in section 2.5. The schematic diagram, D.1., below shows the sample before and after alignment. The magnetic properties of these samples can be viewed as the sum of the properties of the thousands of little grains "enclosed" in the composite. The degree of alignment of the planes is the highest reported to date and a new method was developed (chapter 3) for assessing the alignment using high-resolution x-ray diffractometers.

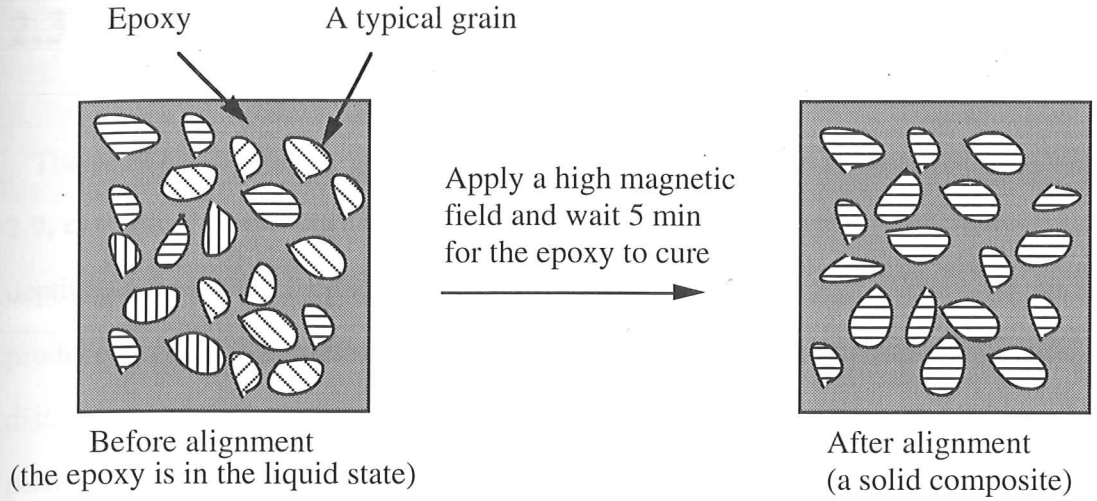

D.1. Schematic representation of the alignment of the grains. The lines in the grains represent the CuO_2 planes. The grains rotate with the application of magnetic field so that all CuO_2 planes align perpendicular to the field.

Penetration depth results obtained from high-T_c superconducting powders can sometimes be misleading due to grains with damaged surfaces produced after grinding a bulk polycrystalline piece into fine powder. We have found for the first time the preparation and heat treatment conditions necessary for obtaining clean surfaces and in a careful study, we show that these lead to a large increase in the quality of the measurements (chapter 4).

In what follows we describe the experimental techniques and procedures used to prepare, characterise, and measure the high -T_c superconductors presented in this thesis.

2.2 Sample preparation

The high -T_c superconductors studied here were prepared using appropriate methods for each material. Brief information on the preparation procedures is given in the respective chapters of this thesis.

2.3 Sieving and sedimentation

The presence of very large grains in a sample, as we explain in more detail in section 2.9, can cause severe uncertainties in the calculated absolute values of the penetration depth (details on the calculation procedure are given in section 2.9). We should therefore produce small size particles that have the required mean value and the generation of a distribution with a sharp cut off. The two procedures followed to produce small size particles with a distribution which has a sharp cut off were:

Sieving: For this method a 20μm aperture sieve was used, fabricated from a perforated stainless steel sheet (Endecotts Co. Ltd). The high-T_c superconductor was ground by hand (in an argon glove box to avoid surface degradation during grinding; details are given in chapter 4) in an agate mortar and repeatedly spread across the sieve using a plastic brush. The powder was sieved (in an argon atmosphere) through the 20μm sieve.

Sedimentation: For this method a special glass tube was designed (based on the design of H. M. Cheah [1]) as illustrated in fig. 2.1. The glass tube was then built at the glassware workshop of the Cavendish laboratory by R. Smith. In a typical sedimentation procedure $YBa_2Cu_3O_{7-\delta}$ powder was initially ground in an agate mortar in air. The powder was put into the glass tube that was filled up to the top with acetone. The glass tube was then reversed and shaken vigorously several times to obtain a homogeneous mixture. The drag force for a spherical body that falls through a homogeneous fluid of infinite extent is given by $F_d = 6\pi\,\eta\,v_t\,r$. Here η is the viscosity of the fluid, v_t is the terminal velocity of the body and r is its radius. Combining this equation with Newton's law of motion one gets $(6\pi\,r\,\eta v_t) = [(m-m_f)g\,]$ where m is the mass of the body and m_f is the mass of the fluid displaced.

Since m = dV, where d is the density and V the volume of the spherical body, we have $v_t=[2\,r^2\,(d-d_f)\,g\,/\,9\eta]$, where d_f is the density of the fluid. Allowing particles to fall a pre-

specified distance for a certain period of time would allow the separation of particles of a particular radius. For example, on the basis of the last formula the glass tube was then left in a vertical position for approximately 1.1 min to allow complete sedimentation of the $YBa_2Cu_3O_{7-\delta}$ heavy particles in the bottom part C (fig. 2.1).The mixture of the non sedimented powder and acetone was then separated from the rest of the material through plug B. The remains of the procedure were collected from part C and sedimented again. This procedure was repeated several times with intermediate grindings until most of the grains with radius < 10 μm were collected. The powder : acetone mixture was then left to dry in an externally vented fume cupboard for several hours until the acetone had evaporated and eventually the sedimented powder was collected. The collected powder was then heat treated to cure the surface of the grains (details on the heat treatment are discussed in chapters 3 and 4).

Typical scanning electron microscopy photographs of powders collected by either sieving ($HgBa_2Ca_2Cu_3O_{8+\delta}$, $Ba_{0.6}K_{0.4}BiO_3$) or sedimentation ($YBa_2Cu_3O_{7-\delta}$) are shown in fig. 2.2.

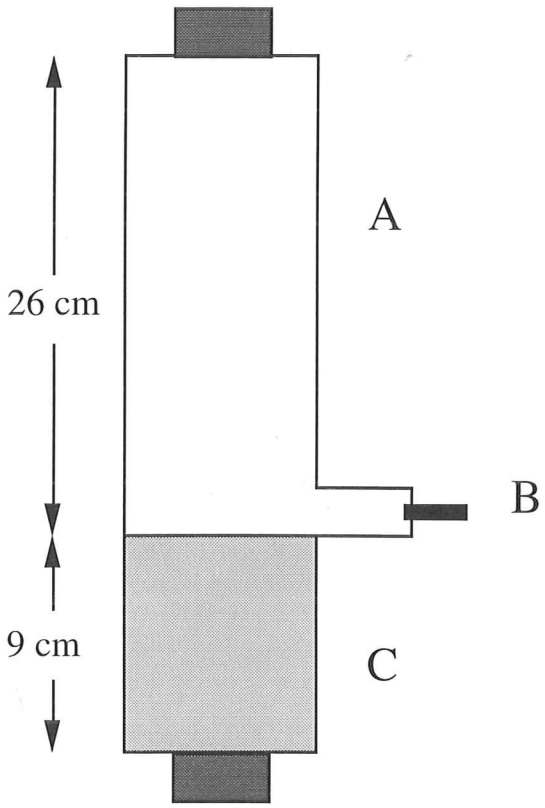

Fig. 2.1. Glass tube used for sedimentation.

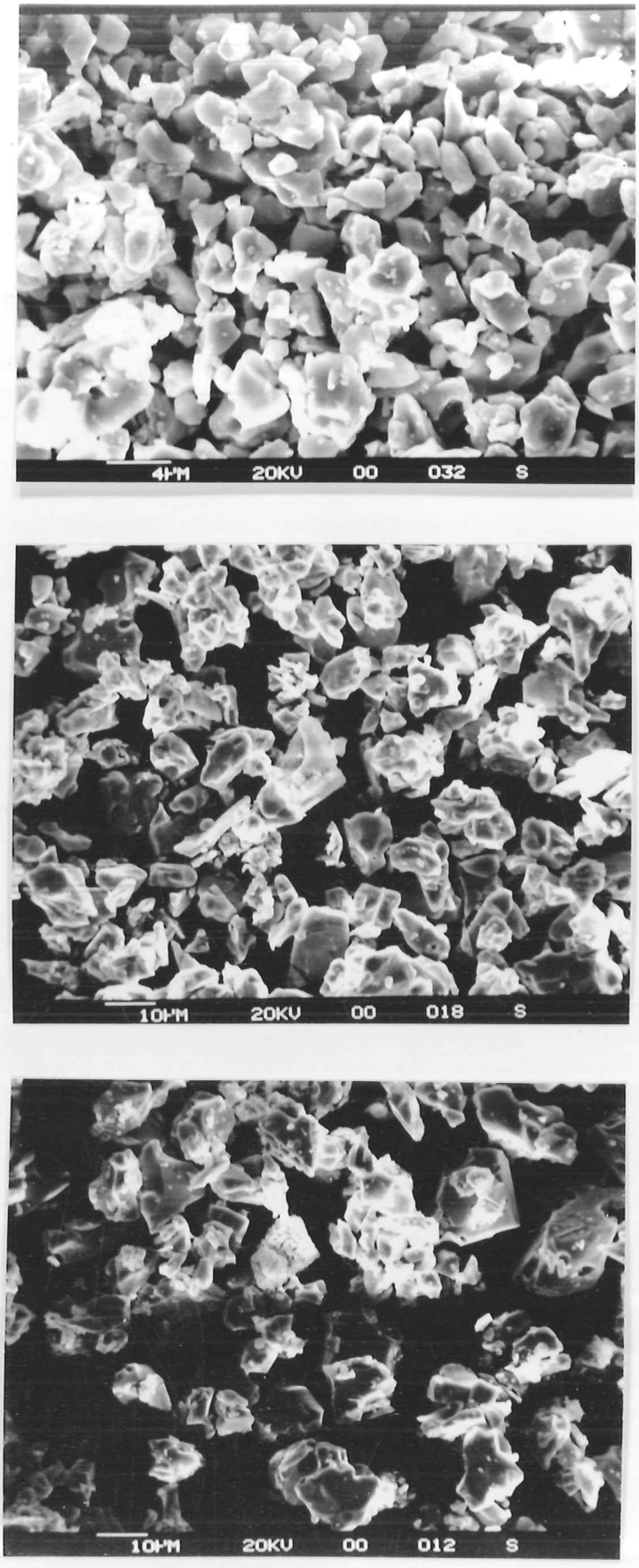

Fig. 2.2. Typical scanning electron microscopy photographs of $YBa_2Cu_3O_{7-\delta}$ (top), $HgBa_2Ca_2Cu_3O_{8+\delta}$ (middle) and $Ba_{0.6}K_{0.4}BiO_3$ (bottom).

2.4 Annealing

The necessary annealing procedures to obtain the desired T_c's are specified in the respective chapters when applicable.

2.5 Alignment procedure

The sieved and sedimented powders were magnetically aligned after being heat treated (when necessary). We have been able to significantly improve the technique of magnetically aligning ceramic copper oxide superconductors, first introduced by Farrell et al. [2]. Having improved the technique we systematically achieved high degree of alignment for several copper oxide superconductors.

To magnetically align the samples, the powder was mixed with a 5 min fast curing epoxy (Double Bubble; Perma Bond Europe) with a typical weight ratio superconductor : epoxy = 1 : 5. The mixture was used to fill gelatine capsules which were positioned vertically in a copper block of a special probe designed for this purpose (fig. 2.3). The probe was built at the IRC in Superconductivity by S. Smith.

The Cu block was fixed with a screw on a copper-nickel (Cu-Ni) thin tube. A vacuum sealed 10 pin PYE connector was soldered to the top end of the Cu-Ni tube to allow the required electrical connections to be made. The probe details are shown in fig. 2.3.

The probe was inserted in a static field of either 7 or 12 T (the magnitude of field used for each material is specified in the respective chapters) at room temperature for 5 min. Since the sample space of the magnet is always much lower than room temperature a heater made of Mn wire bifilarly wound around the copper block was used to heat the latter. The temperature was monitored by a platinum temperature sensor, calibrated at room temperature against a standard thermometer, which was inserted in the Cu block and was in good thermal contact with the samples.

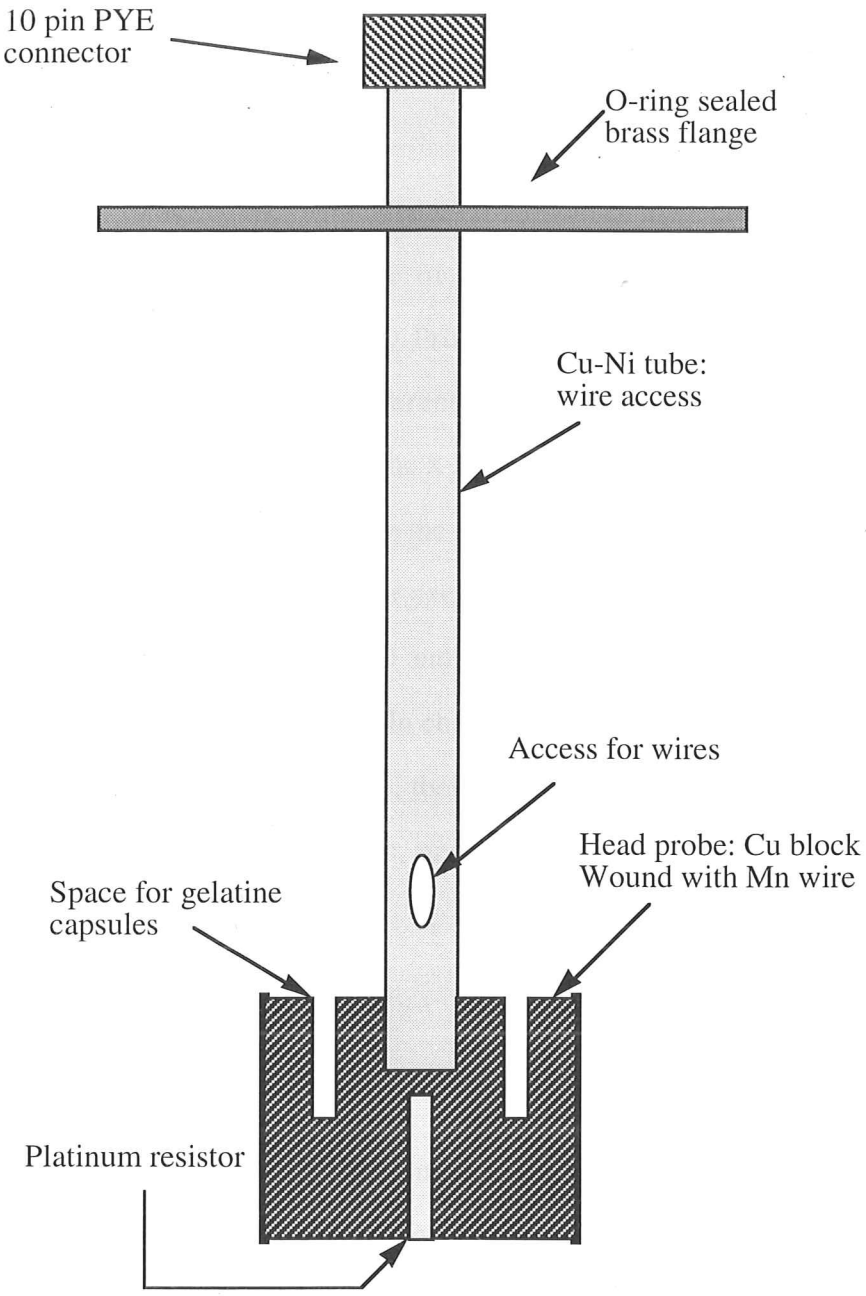

Fig. 2.3 Probe used to magnetically align the powders.

2.6 Characterisation of the degree of alignment

A unique way to determine the degree of alignment of magnetically oriented powders was developed. In brief, the degree of alignment was determined by using high-resolution x-ray machines (set up by Professor E. Saljie at the Department of Earth Sciences) in combination with different integration techniques in order to obtain quantitative and qualitative results. The x-ray beam is strictly monochromatic ($CuK\alpha_1$) and focused with a long focal length on the sample. The sample goniometer can be rotated and shifted around three perpendicular axes and two translation directions, respectively. The instruments are equipped with 1D and 2D detectors and their distance to the sample can be varied between 10 and 30 cm. In chapter 3 we describe the experimental methods connected with this special technique, their application to the analysis of the degree of alignment in several of our samples, and compare the results to those obtained by standard diffraction methods.

2.7 QD Squid

A model 1822 Quantum Design Superconducting Quantum Interference Device (SQUID) was used for the normal state magnetic susceptibility experiments employed to characterise the quality of some of our samples.

A superconducting magnet provides static magnetic fields up to ± 5.5 T. A National Bureau of Standards (NBS) platinum standard was used to calibrate the magnetometer in these fields and the calibration factors were adjusted in order to obtain the correct moment for the standard with an accuracy 0.1%. The principal of operation is to measure the magnetic flux by moving the sample near the pickup coil in the presence of a magnetic field. The detection coil consists of three coils (centre, upper and lower), wound in a second derivative configuration in which the upper and lower coils each contain half the

number of turns of the counterwound centre coil. The SQUID detectors can measure signals with a sensitivity of 10^{-8} emu. The magnetic moment is computed by summing the squares of the individual readings, taking the square root of the result and multiplying by the system's calibration factors. The temperature control module provides precision regulation of the thermal environment at a temperature range from 2 to 400 K.

The sample was placed in a plastic holder. The background from the holder was measured separately and was always subtracted from the data. All the measurements were performed at 5T for the temperature range 5 - 300 K. Intermediate measurements in different fields from 0 to 5T were taken to verify the field dependence at 100 K and at 300 K. The magnetic susceptibility was calculated from the net magnetic moment.

2.8 Ac-susceptometry

Ac susceptometers have been used quite extensively in the study of the magnetic properties of materials. The principle of operation involves subjecting the sample material to a small alternating magnetic field. The flux variation due to the sample is picked up by a sensing coil surrounding the sample and the resulting voltage induced in the coil is detected. This voltage is directly proportional to the magnetic susceptibility, χ, of the sample. In the case of granular superconductors, when the grains are fully coupled, the entire volume of a granular sample including voids and non-superconducting phases is shielded and $\chi = -1$. When the grains are uncoupled, which is the case in our samples as we discuss in later chapters, the inductive susceptibility signal represents a summation of shielding signals from many grains; voids and non superconducting phases do not contribute.

Two susceptometers were used for the susceptibility measurements performed in order to determine the low field susceptibility and consequently the magnetic penetration depth. One susceptometer was home-made and was used to measure the susceptibility of some of the samples at temperatures in the range 1.2 - 40 K. The second susceptometer was a

commercially available one which was used to obtain data in the temperature range 4.2 - 150 K.

2.8.1 Home - made ac susceptometer

For the purpose of some of the work presented in this thesis a new ac susceptometer probe was designed. The probe was then built by S. Smith and S. Brown at the workshop of the IRC in Superconductivity. The aim was to obtain high resolution and low temperatures, down to 1.2 K, when desired. In this section we outline the important elements of the design and construction.

The probe head was made of a new material developed for the purpose of the experiment. This material is made of Stycast 1266 epoxy being mixed with 20 μm insulated copper wires in a mass ratio 7:1. The mixture was pumped in a desiccator to minimise the presence of air bubbles, and then allowed to cure at room temperature. The purpose of this composite was to improve the thermal conductivity of the epoxy by the presence of the copper wires and eliminate the possibility of eddy currents being set up during the measurements. The solid product was machined at the IRC in Superconductivity workshop by S. Brown.

Two different designs of probe heads were constructed. The main component of the probe heads including the coils and temperature sensor is shown in fig. 2.4. The low temperature work presented in this thesis was carried out using probe head (b).

The machined block was fixed with GE varnish to a thin walled non-magnetic copper-nickel (Cu-Ni) tube. Three 3mm holes at 180° to each other were drilled at the lower end of the tube to allow access to the miniature coaxial cables, used for the coil connections as we describe below, and the Cu wires used for the Allen Bradley resistor (the temperature sensor). Three oxygen free copper discs were soldered (equally spaced) on the Cu-Ni tube to act as radiation shields. A vacuum sealed brass cylindrical box was soldered to the top end (room temperature part) of the tube to facilitate the electrical feed throughs. The

probe details are shown in fig. 2.5. The entire probe is suspended into a glass dewar (inner dewar) which is filled with liquid helium. The glass dewar is sealed on the top by means of a brass cylinder and an O-ring in a manner which allows liquid helium transfer and gas input and output by using the appropriate valves. The inner dewar is in turn suspended into a second glass dewar (outer dewar) filled with liquid nitrogen.

Below we describe the essential features of the ac susceptometer in more detail.

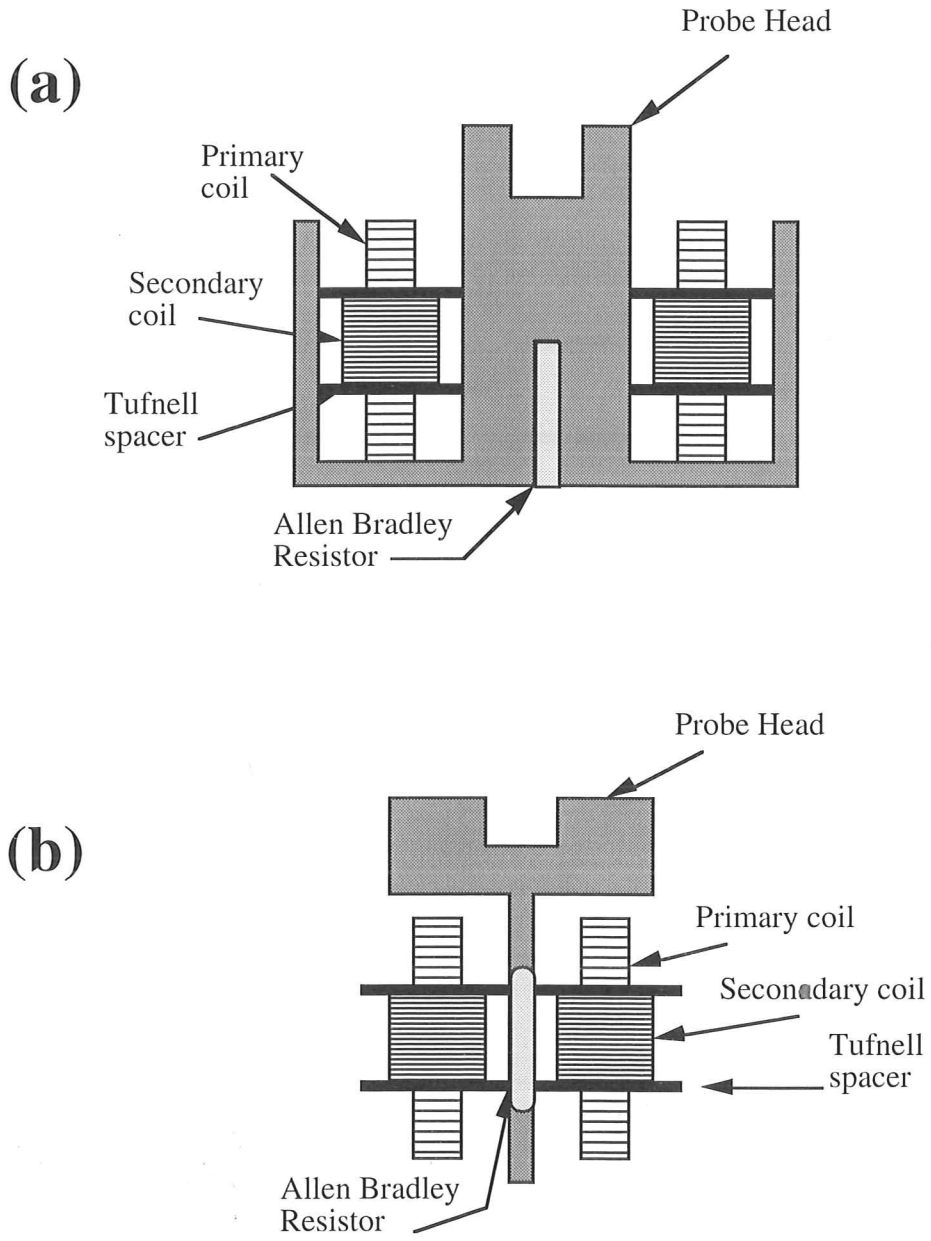

Fig. 2.4 Section view of the probe heads loaded with the coils and temperature sensor.

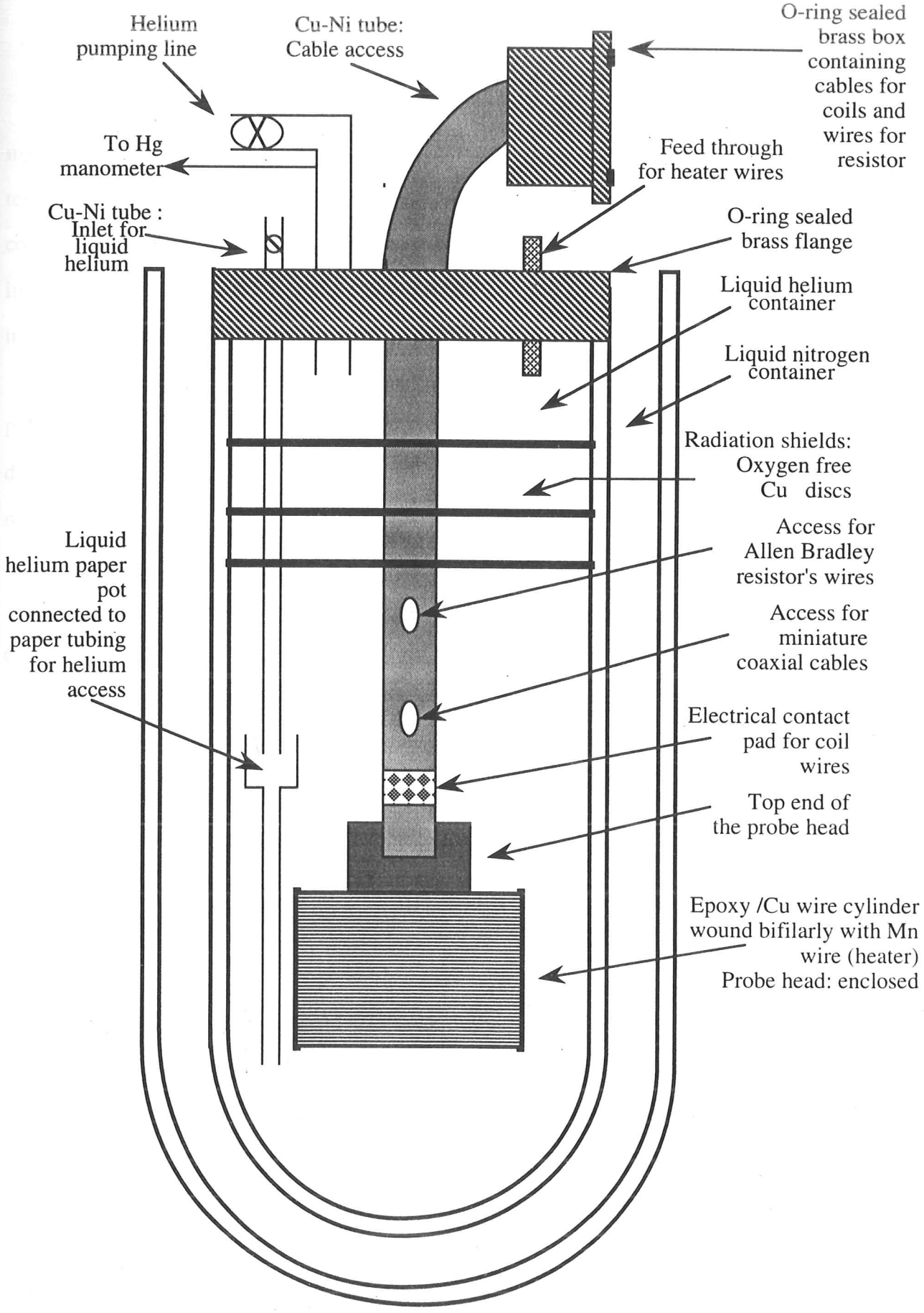

Fig. 2.5. Home-made ac susceptibility apparatus.

The coils had to be relatively rigid and so were to be wound on very thin (<100 μm) mylar tubing and set in GE varnish. Mylar has a negligible magnetic susceptibility at low temperatures and with both secondary coils wound on identical tubes, there is no contribution from the mylar once the two signals had been subtracted from each other. To improve rigidity with only a small loss of sensitivity, the primary coils were wound inside the secondary coils.

Each coil was wound on mylar tubing of 4.4 mm diameter. A single layer of a typical primary coil wire was wound with a total of 88 turns. The wire used was 100μm diameter insulated copper wire. Careful monitoring of the winding, through the microscope, ensured that the coil was wound as tightly as possible without allowing the wire to overlap the previous run. The coil was fixed in place with GE varnish.

Two tufnell spacer rings were placed over the primary coil and were fixed in place with GE varnish at a separation of 4 - 5mm (depending on the sample size). This formed a space for the secondary coil to be wound. The secondary coils, typically 1000 turns, were wound with 40μm diameter insulated copper wires and were fixed in place with GE varnish. A few centimetres of wire were left at each end to allow extra turns to be put on by hand at a later stage to balance the two secondary coils exactly.

The method used to balance the secondary coils is as follows. With the coils in the correct position but not firmly fixed in place, the magnitude and phase of the signal from just one of the secondary coils was measured at a chosen frequency and amplitude of drive signal. A similar measurement was made for both secondary coils, with the wires connected to their coils in opposing senses, to obtain the out-of-balance signal. The out-of-balance fraction, i.e., the ratio of the single to both secondary coils signal, could thus be calculated. This fraction when multiplied by the number of turns on a secondary coil gave an estimate of the number of turns which should be added to one of the coils to improve the balance. Once the required number of turns were added the wires to both primary and secondary coils were then secured to the head-probe with GE varnish. The sample was then placed and held by vacuum grease in one of the coil sets. A piece of

epoxy with no superconductor in it (same type, dimensions and weight of epoxy with the one the sample is made from) was placed in the other coil.

Miniature contact pads placed on the head probe allowed the very fine coil wires to be more easily connected to the main contact pad which was placed at the lower end of the Cu-Ni tube, and so to the connections at the top of the probe.

Thus, connections were then made from the contact pads to the individual components. The secondary coil wires were connected to their coils in opposing senses so that in effect one coil was nominally wound in a clockwise direction and the other anti-clockwise. On the other hand the pair of wires for the primary coils were connected in series so that both primary coils were wound in the same sense and produced alternating magnetic fields in the same direction when an alternating current was passed down the primary coil wires.

Temperature measurement below 60 K was achieved using a calibrated Allen Bradley resistor for measurements down to 4.2 K and the vapour pressure of liquid helium for temperatures between 4.2 and 1.2 K. The Allen Bradley resistor was calibrated using a calibration rhodium-iron resistor whose resistance was measured by a four contact method. The Allen Bradley and the standard Rh-Fe resistors were mounted on a probe purpose-built (this probe was supplied by Dr. J.R. Cooper at the IRC in Superconductivity) from copper to give excellent thermal contact. The Allen Bradley voltage and the Rh-Fe temperature were continuously recorded every 1 K during cooling and heating cycles at the same speed and the resulting data averaged to remove any possible thermal hysteresis effects.

To allow a varied temperature range to be obtained an independent heater was required. The heater coil, 100μm insulated Mn wire, was wound bifilarly on a cylinder, made of the same material as the head probe. The heater-cylinder was placed, by push fit and vacuum grease, over the head probe with two slits at the top and was closed at the bottom end but with four 3mm holes, to allow the flow of liquid helium in the sample area.

All necessary sets of cables were passed down the length of the Cu-Ni tube through two 3mm diameter holes which were drilled in the tube. Three lengths of Lake Shore

miniature, low temperature, low-noise coaxial cables were used: one for the primary coil and two for the secondary coils. One set of four and a set of two 100μm copper wire twisted pairs in PTFE sleeving were used to connect the Allen Bradley temperature sensor and the heater, respectively. Note that the heater wires were fed through the brass flange used to vacuum seal the glass dewar and not through the brass cylindrical box and Cu-Ni tube (fig. 2.5).

At the top of the Cu-Ni tube all cables and wires passed through a small hole in the vacuum sealed cylindrical brass box which was soldered to the tube. The box was machined to take three sealed BNC sockets, and one glass-to-metal seal 10 pin PYE connector. The BNCs were screwed and epoxied in place and electrically isolated from the chassis of the box, and the 10 pin plug was soft-soldered to it. One BNC socket was used for both secondary coils and one for a single secondary. The 10 pin plug was used to connect the wires for the temperature sensor. The lid of the box was then fixed firmly in place by six screws and an O-ring to ensure a good vacuum seal. The probe was placed in the "inner" dewar and was leak-tested successfully.

The signal used for determining the magnetic susceptibility was that of both secondary coils. The signal was generated by feeding the primary coils with an ac current generated by an ac current source that could produce currents in the range 10μA - 30 mA rms. The response from the secondary coils passed through a 1:100 transformer and the output signal fed to a lock-in amplifier. The Allen Bradley resistor was operated using a dc current supply and a digital multimeter for detecting the voltage. An independent current source was used to operate the heater surrounding the probe head. Temperatures below 4.2 K were achieved by pumping directly on liquid helium. The temperature was then determined from the vapour pressure. Note that for pumped He^4 above the lambda point there is only good correspondence between pressure and temperature when the pressure is being reduced. When the pressure is being increased there can be large temperature gradients in liquid He^4 above the lambda point.

2.8.2 Commercial ac susceptometer

Details on the cryostat and sample probe assembly can be found in the Lake Shore Cryotronics manual for Model 7000 ac susceptometer. In brief the susceptometer consists of one primary and two identical secondary coils. The primary coil is normally connected to a dc, ac current source that is able to create a static and alternating magnetic field. The secondary coils, are symmetrically positioned and wound oppositely in order to cancel any internal or external background. The sample is surrounded by a high thermal conductivity sapphire tube and its temperature is measured by a silicon diode resistor. Helium gas in the sample space provided good thermal contact to the thermometer and a vacuum isolation space supplied uniform temperature in the sample region, minimising evaporation of liquid helium during the measurement. The sample probe was made with a stainless steel tube that ended in a nylon holder where the sample was held. It had an adjustable seal to allow the positioning of the specimen in the middle of one of the sensing coils where the signal would be maximum. The ac susceptometer is illustrated in fig. 2.6.

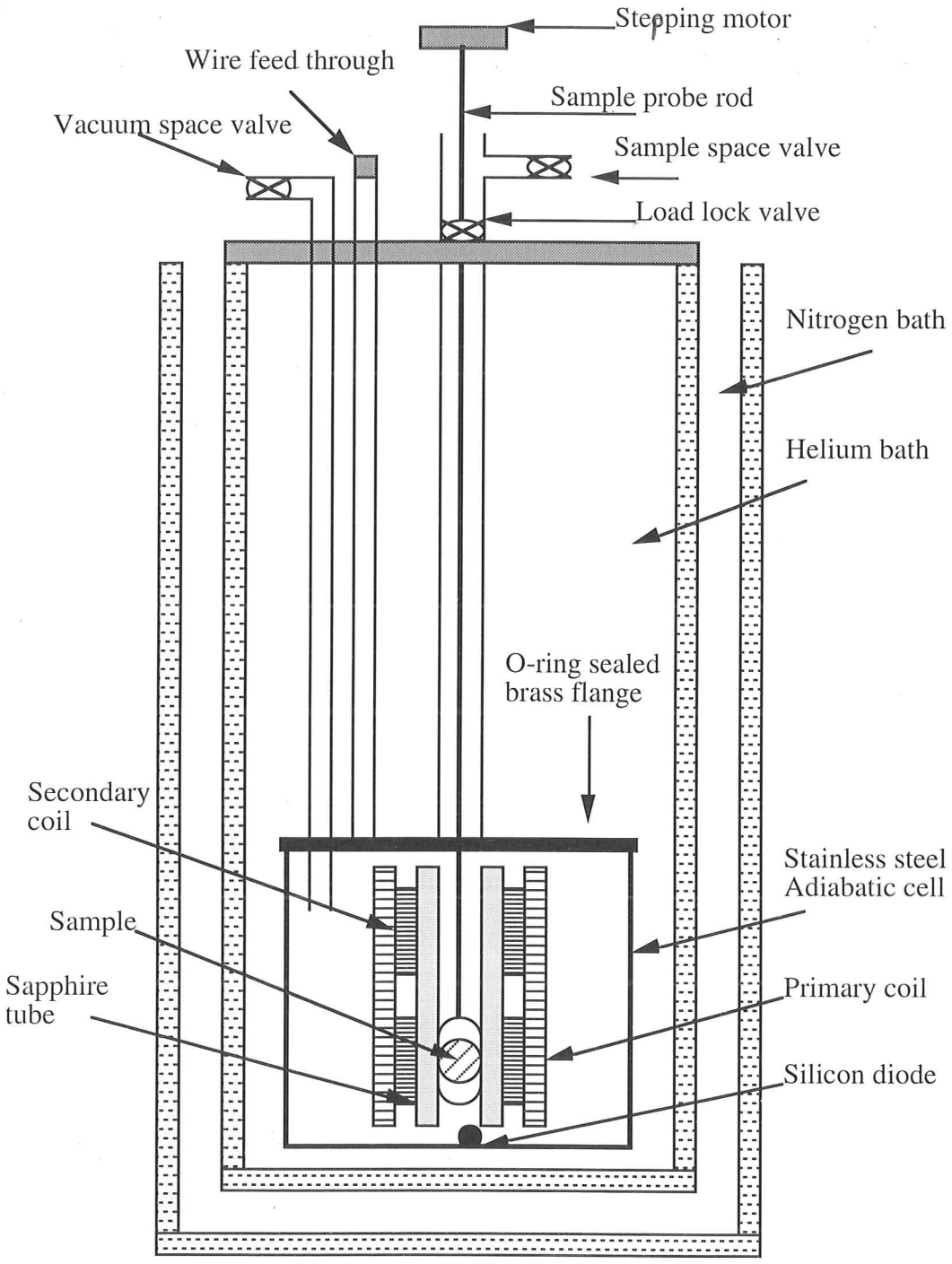

Fig. 2.6. Commercial ac susceptibility apparatus (Cryogenics, Model 7000).

2.8.3 Calibration

When the sample is placed in one of the secondary coils, the voltage balance is destroyed and the flux variation due to the sample is picked up by these coils. The voltage detected is directly proportional to the magnetic susceptibility of the sample:

$$\chi_m = a \frac{u_{RMS}}{fH_{RMS}V} \tag{2.1}$$

where a is the geometrical factor of the coil, u_{RMS} the measured voltage, f the frequency of the ac field, H_{RMS} the applied field and V is the volume of the sample. The measured susceptibility χ_m is complex, $\chi_m = \chi_m' + i\chi_m''$, with the real part χ_m' related to the occurrence of the Meissner effect and the imaginary part χ_m'' corresponding to the energy dissipation in the material.

The measured susceptibility should be corrected for demagnetisation effects, that depend on the geometry of the sample, in order to obtain the real susceptibility of the specimen χ_r. In general, both susceptibilities are related through the expression:

$$\chi_r = \frac{\chi_m}{1 - N\chi_m} \tag{2.2}$$

where N is the demagnetisation factor.

A common method for determining the calibration constant is through the use of known standards. By measuring the signal from a sample with known volume and susceptibility, eq. (2.1) can be used to determine the geometrical factor a. The calibration is strictly valid only for samples of the same size and shape as the standard.

In using calibration standards, particularly in the case of superconducting materials, corrections for the demagnetisation factor are taken into account. For example, for a superconducting sphere like lead (Pb) which has a demagnetisation factor of 1/3 and a

real susceptibility, χ_r, of -1 for perfect diamagnetism, from eq. (2.2) we find that the measured susceptibility will be -3/2 and this should be the value for χ_m used in eq. (2.1) in solving the calibration constant. More details on calibration of similar susceptometers can be found in refs. [3,4].

2.9 The relation between diamagnetic susceptibility and penetration depth

Because the penetration depth is small, ordinary sized specimens in a magnetic field appear to be perfectly diamagnetic. The penetration of the magnetic flux becomes noticeable, however, if we make measurements on small samples, such as powders, whose dimensions are not much greater than the penetration depth. In this case there is an appreciable magnetic flux density through the specimen; there is no longer perfect diamagnetism, and consequently the properties are rather different from those of a bulk superconductor. Measurement of the reduction in diamagnetic signal with respect to the full shielding signal, provides a measure of the magnetic penetration depth and since high-T_c superconductors are highly anisotropic, a grain aligned sample is the best choice for the investigation of the anisotropic penetration depth.

On the basis of scanning electron microscopy photographs most of the high-T_c superconductors, and all the ones discussed in this thesis (see e.g. fig. 2.2), consist of approximately spherical grains. According to London [5], the field and currents of a superconducting sphere of radius R can be determined in an applied magnetic field H_a. The field equations from magnetostatics for the region outside the sphere ($r \geq R$) in spherical polar coordinates r, θ, ϕ are as follows:

$$h_r = (H_a + \frac{2m}{r^3}) \cos\theta$$

$$h_\theta = (-H_a + \frac{m}{r^3}) \sin\theta \quad \text{for } r \geq R \tag{2.3}$$

$h_\phi = 0$

Here m is the induced magnetic moment of the sphere. For the interior $r \leq R$, one first takes the equation for the current:

$$\nabla \times \nabla \times \boldsymbol{J} + \beta^2 \boldsymbol{J} = 0. \tag{2.4}$$

Considering the assumed symmetry of the system and of the external field, one anticipates that there can only be a current parallel to the equator, $J_\theta = 0$, $J_r = 0$ and J_ϕ of the form

$$J_\phi = f(r) \sin \theta \ . \tag{2.5}$$

Substituting eq. (2.5) into (2.4) for $\boldsymbol{J}$ leads to an ordinary differential equation for $f(r)$:

$$f'' + \frac{2}{r} f' - [\frac{2}{r^2} + \beta^2] f = 0 \tag{2.6}$$

which has the general solution

$$f = \frac{A}{r^2} (\sinh \beta r - \beta r \cosh \beta r) + \frac{B}{r^2} (\cosh \beta r - \beta r \sinh \beta r) \tag{2.7}$$

where A and B are the integration constants. The part of the function whose coefficient is B becomes infinite for $r \rightarrow 0$. Hence it is necessary to set $B = 0$ in order to obtain a solution which is regular at the centre of the sphere. Thus one obtains

$$J_\phi = \frac{A}{r^2} (\sinh \beta r - \beta r \cosh \beta r) \sin \theta \ . \tag{2.8}$$

Using $\nabla \times \boldsymbol{J} = -\frac{n_s e^2 h}{mc}$, for $r \leq R$, we obtain

$$h_r = \frac{4\pi}{\beta^2 c}\left(\frac{1}{r\sin\theta}\right)\frac{\partial}{\partial\theta}(\sin\theta\ J_\phi)$$
$$= \frac{8\pi A}{\beta^2 c r^3}(\sinh\beta r - \beta r\ \cosh\beta r)\cos\theta$$

$$h_\theta = -\frac{4\pi}{\beta^2 c}\frac{1}{r}\frac{\partial}{\partial r}(r\ J_\phi) \qquad (2.9)$$
$$= \frac{4\pi A}{\beta^2 c r^3}\{(1+\beta^2 r^2)\sinh\beta r - \beta r\ \cosh\beta r\}\sin\theta$$

$$h_\phi = 0$$

By the two boundary conditions requiring h_r and h_θ to be continuous at $r = R$,

$$m = -\frac{H_a R^3}{2}\left(1 - \frac{3}{\beta R}\coth\beta R + \frac{3}{\beta^2 R^2}\right)$$

or (2.10)

$$m = -\frac{H_a R^3}{2}\left(1 - \frac{3\lambda}{R}\coth\frac{R}{\lambda} + \frac{3\lambda^2}{R^2}\right)$$

where $\beta = 1/\lambda$, and m is the magnetic moment. (When $\lambda << R$, $m = m_0 = -\frac{H_a R^3}{2}$, where m_0 is the diamagnetic moment of an unpenetrated sample.) The normalised susceptibility of a sphere is:

$$\frac{m}{m_0} = \frac{\chi}{\chi_0} = 1 - \frac{3\lambda}{R}\coth\frac{R}{\lambda} + \frac{3\lambda^2}{R^2} \qquad (2.11)$$

and when the susceptibility is measured for a large number of well separated grains (i.e., the field from one grain does not affect other grains) and the particle size distribution is taken into account the measured effective susceptibility becomes

$$(\frac{\chi}{\chi_0})_{eff} = \frac{\int [1 - \frac{3\lambda}{R} coth \frac{R}{\lambda} + \frac{3\lambda^2}{R^2}] R^3 g(R) dR}{\int R^3 g(R) dR} \qquad (2.12)$$

where χ_0 is the susceptibility in the absence of any flux penetration and g(R) is the measured grain size distribution. The term effective means the susceptibility measured for a certain field orientation with respect to the CuO_2 planes.

The magnetic penetration depth λ is calculated using the relative reduction of the diamagnetic moment with respect to m_0. Therefore, it is necessary to know m_0 before the calculation takes place. The maximum possible diamagnetism m_0 is calculated from the mass of the superconductor in the composite sample (superconductor : epoxy), its x-ray density and assuming the individual particles are spherical.

The normalised susceptibility has to be integrated over the measured distribution of particle size and the demagnetisation factor has to be considered. Taking them into account the measured effective susceptibility is given by

$$(\frac{\chi}{\chi_0})_{eff} = \frac{2}{3} \{ \frac{v_{ac}}{VD - Fv_{ac}(\frac{1}{3} - N)} \} \qquad (2.13)$$

where v_{ac} is the measured ac magnetisation signal (in μV), V is the volume of the superconductor (in mm^3), D is the calibration factor of the apparatus (in $\mu V / cm^3$) and F is the fraction of the superconducting volume to the total volume of the sample. N is the demagnetising factor of the composite epoxy and powder sample which for a spherical approximation is ~ 1/3. The factor 2/3 on the right hand side of the equation comes from the assumption that the particles are spherical. Details on the derivation of eq. 2.13 can be

found in Ref. 4. Combining eqs (2.12) and (2.13) one can derive the magnitude and temperature dependence of the magnetic penetration depth.

The errors associated with the penetration depth calculation arise mainly from the departure of the grains from spherical geometry and the uncertainty in the grain size distribution. To determine the grain size distribution several scanning electron microscopy photographs were taken for the powder used to align a sample and the analysis was done by measuring all grains appearing on each photograph along two perpendicular axes. The mean value of the two readings of each grain was taken as the length of the diameter and the cumulative volume was estimated. Deviation from the spherical geometry tends to increase the actual surface-area to volume ratio leading to an increased field penetration. The effect of this is less important when $\lambda \sim R$ in which case the ratio of penetrated to unpenetrated sample volume is similar for both spherical and non-spherical specimens. This creates the necessity of having a narrow and well defined grain size distribution with its mean being of the order of the measured penetration depth. Also, a large particle contributes a much larger diamagnetic signal than a small particle ($\lambda \sim R$) and hence the measured susceptibility is particularly sensitive to the number of large particles when the majority of particles have a size which is comparable to the penetration depth. The problem of uncertainty of the particle size was solved by sieving or sedimenting the powder before alignment as discussed in section 2.2.

When calculating values of λ from our experimental susceptibility data we often checked that the results were not too sensitive to the grain size distribution used. As a matter of fact, it was found that decreasing the number of measured grains by half led only to a 3% change in the calculated penetration depth, and left the temperature dependences unaltered, whereas shifts of the distribution by $\pm$ 1 μm did not affect the final values more than 2%.

Another possible source of error is the estimation of m_0 which directly depends on the mass of the superconductor under investigation. We find that 10% error in the estimation of the mass of the superconductor leads to ~ 10% error in the estimated fractional

diamagnetism, ~ 7% in $\lambda(0)$ but leaves the temperature dependence of λ almost unchanged. It is thus important to estimate the mass of the superconductor in the superconductor: epoxy composite very accurately. The sedimentation of the heavier grains during the alignment procedure, while the epoxy is in the liquid state, is the main contribution to this error. To overcome this complication we used the fast curing epoxy mentioned earlier in section 2.5 and made sure that our results were reproducible between different samples cut from the same capsule (which contained the composite superconductor : epoxy; see section 2.5) but from different parts (top to bottom).

Following the aforementioned arguments for the extraction of the penetration depth from the measured susceptibility it is rather straightforward to calculate $\lambda(T)$ from χ(T) for an isotropic material. However, all the high T_c copper oxide superconductors are highly anisotropic. It turns out that when the external field is parallel to the *c*-axis of the grains then the diamagnetic screening current flows entirely within the *ab*-planes of the sample so that the value of λ extracted is simply the in-plane penetration depth, λ_{ab}. In the case where the external field is parallel to the *ab*-plane, the screening currents flow in both the *ab* plane and *c* axis. In this case, only an effective penetration depth, λ_{eff}, that has contributions from both orientations can be deduced using the analysis described earlier. An approximate solution, $\lambda_{eff} \sim 0.7\lambda_c$ [6,7] in the limit of $\lambda_c >> \lambda_{ab}$, (which as we shall see is the case for all the anisotropic copper oxide superconductors studied here), can be used to estimate λ_c. Here λ_c is the out-of-plane penetration depth. Even for $[\lambda_c(0) / \lambda_{ab}(0)] \sim 4$, we have checked the original formulae relating χ (H_{ac} // *ab*) and λ_c in both the large [6,7] and small [8] grain limits to make sure that the relation $\lambda_c = 1.4\lambda_{eff}$ [6] remains valid. It turns out that any error from this source is negligible (< 2.5 %).

2.10 Muon-spin-relaxation experiments

Transverse-field muon-spin-relaxation (TF-μSR) experiments have revealed a remarkable correlation between T_c and the value of λ_{ab} at $T = 0$ ($\lambda_{ab}(0)$) [9]. The distribution of the precession frequencies and the resulting depolarisation rate (σ) of the initially polarised muon spins are a very sensitive, local probe for the field profile in the flux-line lattice (FLL) state of type II superconductors which is determined by the magnetic penetration depth. The copper oxide superconductors are highly anisotropic with $\lambda_c >> \lambda_{ab}$ and of extreme type II nature with $\lambda_{a,b,c} >> \xi_{a,b,c}$. λ_{ab} is generally assumed to be determined by the density of the superconducting condensate n_s and the effective mass m^*_{ab} of the carriers ($\lambda_{ab}^{-2} \sim n_s / m^*_{ab}$) [9].

Having obtained $\lambda_{ab}(0)$ of our samples using the susceptibility technique we decided to confirm our findings on some of our samples with TF-μSR measurements. The samples that were studied by μSR were polycrystalline pellets, with randomly oriented grains. This experiment serves two purposes. It gives the first direct evidence of the belief that μSR measurements on randomly oriented powders give accurate $\lambda_{ab}(0)$ values, in the case where the sample under investigation is anisotropic, and confirms our findings from the susceptibility technique.

The μSR experiments were performed at the "surface muon" beam lines at the Paul-Scherrer Institute (PSI) in Villigen, Switzerland. Here we only give a brief description of the technique and the data analysis.

The samples are field cooled below T_c in an external field of 3 kG to induce a homogeneous FLL. Positive muons from 100% "spin polarised" muon beam, with P_μ = 29 MeV/c, are implanted with their initial spin polarisation $P_\mu(0)$ transverse to B_{ext}. Without losing their initial spin polarisation the muons are rapidly thermalised (10^{-12} s) and are randomly distributed throughout the field profile of the FLL whose characteristic length scale λ is far larger than any lattice constant. Each muon spin starts to precess

around the local magnetic field B_{loc} with a characteristic frequency $\omega_\mu = \gamma_\mu B_{loc}$, where $\gamma_\mu = 2\pi$ 135.5 MHz / T is the gyromagnetic ratio of the muon.

The time resolved spin polarisation $P_\mu(t)$ is detected using parity violation that occurs in muon decay. Each positive muon decays (via the weak interaction) into two neutrinos and a positron, the latter being preferentially emitted in the direction of the muon spin at the instant of decay. The asymmetric positron emission rate $N_e^+(t)$ thus contains all the information on the precession and depolarisation of $P_\mu(t)$.

From a Fourier transform of $P_\mu(t)$ one obtains the distribution in the precession frequencies of the muon spins $F(\omega_\mu)$ and, in the case for which the flux lines run parallel to the external field, the field profile of the FLL $\eta(B_{\mathrm{loc}})$ [10]. For an ideal FLL of an isotropic superconductor the second moments $<\Delta\omega_\mu^2>$ and $<\Delta B^2>$ are directly related to the magnetic penetration depth ($<\Delta\omega_\mu^2> \propto <\Delta B^2> \propto \lambda^{-2}$). The so called line shape then is highly asymmetric and exhibits characteristic features such as a tail on the high-field side, steps at the maximum and minimum field values, and a pole at the saddle-point value [11].

For polycrystalline samples of the copper oxide high T_c superconductors one only observes a nearly symmetrical and Gaussian shaped distribution $F(\omega_\mu)$, the sharp features are smeared out [12]. For a Gaussian line-shape the second moment of $F(\omega_\mu)$ may be extracted by fitting the μSR-time spectrum by $P_\mu(t) \propto exp\ (-\sigma^2 t^2 / 2)$, where the depolarisation rate σ is proportional to the second moment of the distribution of the frequencies; that is $\sigma \propto <\Delta\omega_\mu^2>$. The more complicated analysis via the Fourier transformation of $P_\mu(t)$ may thus be avoided. Even though the flux lines for these highly anisotropic randomly oriented polycrystalline high T_c superconductors are no longer parallel to B_{ext}, the relation $\sigma \propto <\Delta\omega_\mu^2> \propto \lambda_{eff}^{-2}$ was shown to hold with $\lambda_{eff} = 1.23\ \lambda_{ab}$ for $\gamma = [\lambda_c\ (0)\ /\lambda_{ab}\ (0)] > 5$ [12]. Therefore, the experimentally determined depolarisation rate sigma of the muon spin polarisation provides a direct measure of the in-plane penetration depth λ_{ab} and hence the ratio of the superconducting condensate

density n_s to the effective mass m_{ab}^* for in-plane motion. All the data analysis was performed using the computer facilities of PSI.

References

[1] H.M Cheah, Ph.D thesis (Cambridge, 1991).

[2] D.E. Farrell *et al.*, Phys. Rev. B **36**, 4025 (1987).

[3] F.J. Blunt, Ph.D. thesis (Cambridge, 1990).

[4] D-N. Zheng, Ph.D. thesis (Cambridge, 1994).

[5] F. London, *Superfluids*, Vol. I, Wiley, 1950, p.34.

[6] J.R. Waldram and A.M. Campbell, private communication; H.M. Cheah, Ph.D. thesis, University of Cambridge (1991); approximate solution for anisotropic sphere.

[7] V.G. Kogan and J.R. Clem, Jpn. J. App. Phys. **26**, S1159 (1987).

[8] C. Baraduc and A. Buzdin, Physics Letters A **171**, 408 (1992).

[9] Y.J. Uemura *et al.*, Phys. Rev. Lett. **62**, 2317 (1989) and Phys. Rev. Lett. **66**, 2665 (1991).

[10] B. Pumpin *et al.*, Phys. Rev. B **42**, 8019 (1990).

[11] E.H. Brandt, Phys. Rev. B **37** 2349 (1988).

[12] W. Barford and J.M.F. Gunn, Physica C **156**, 515 (1988).

Chapter 3

High-resolution X-ray diffraction analysis of grain aligned high- T_c superconductors

3.1 Introduction

The growth of suitably large and good quality high-T_c superconducting crystals is quite often very difficult. Furthermore, it is very hard to obtain homogeneously doped crystals. On the other hand, high purity pollycrystalline samples are easier to prepare and it is also easier to vary their carrier concentration and impurity content. For this reason special methods have been used in recent years to orient the small crystallites of a superconducting powder sample magnetically by utilising the anisotropic paramagnetic susceptibility of these substances at room temperature [1].

The results of this procedure are grain-aligned ceramics with a preferred orientation, usually along the crystallographic *c*-axis. As a first check of the degree of alignment we often compare the powder diffraction pattern of the aligned material with that of a similar unaligned sample. The intensity ratios of "forbidden" lines still present in the aligned material to those in the unaligned one give a rapid guide to the unaligned fraction.

In this chapter we assess the degree of alignment using a new technique where we utilised recently developed high-resolution X-ray diffraction facilities [2] which combine a large number of rotational and translational degrees of freedom with 2D detectors and measured high-resolution rocking curves on the area detector on unaligned and magnetically aligned high-T_c superconducting ceramics. We then compare these results with data obtained using a 1D detector.

3.2 Experimental details

3.2.1 Diffraction geometry

The X-ray beam is strictly monochromatic (CuKα1) and its diameter adjustable between 0.05 mm and 5 mm. The possible movements of the sample with respect to the incoming beam include rotations around three perpendicular axes in 0.001° resolution (ω, χ and φ) and two perpendicular translations (x, y) by ±50 mm in steps of 0.01 mm (fig. 3.1).

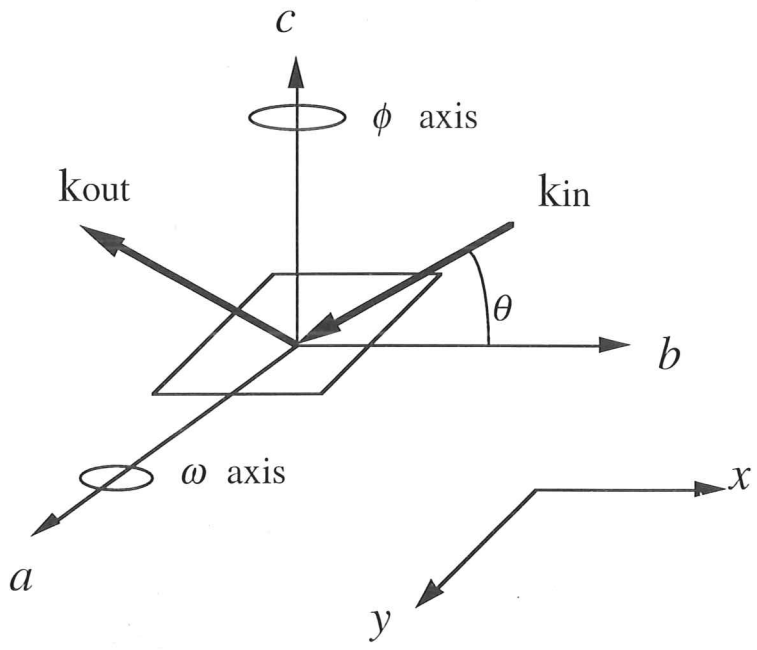

Fig. 3.1. Schematic representation of the possible rotation (ω, ϕ) and translation (x, y) axes of the X-ray diffractometers. The rotation axis χ (not shown) is the b axis and χ is the angle between the plane of k_{in}, k_{out} and axis a.

The diffracted beam is detected by either 1D or 2D detectors. Details on the two detectors are given in Ref. [3]. In brief, the 1D detector consists of a blade that forms the anode and a delay line constituting the cathode, contained within a gas mixture of argon-ethane held at constant pressure within the detector. High voltage is maintained between the two poles to accelerate charges that are freed by interactions of the gas with incoming X-rays. A cascade ensues, and the charges are collected by the cathode. All 4096 sections of the cathode are connected by a delay line that enables the discriminator electronics to determine the exact location of the incident phonon by measuring the difference in arrival time between the two ends of the line. The advantages of such a device are obvious, in that the measurements can be performed in real time as opposed to photographic methods, and the whole range of 120°, 2θ is covered simultaneously. The 2D detector, instead of a blade consists of a multiwire grid enclosed by pressurised xenon gas at approximately 4 bar. The X-rays enter through a concave beryllium window, causing ionisation of the gas. The multiwire grid feeds position sensitive decoding circuitry that generates the *x*-*y* coordinates of incident phonons. The resolution of the 512 × 512 pixel array can be varied by moving the detector away or towards the sample, with a maximum distance of 30 cm giving an average resolution of 0.028°.

In the actual experiment setting parameters such as tilt angle and counting time are strongly dependent on the information required from the data. In the case of diffuse scattering from microstructures in single crystals suitable Bragg reflections are chosen and the angle of incidence ω or rotation φ is varied over a comparatively small range (e.g. ±3° in 0.1° steps) with a counting time of 5 minutes or more per step. (Note that in the case of (00l) reflections $\omega = 2\theta/2$.) For the characterisation of thin films, on the other hand, where thickness, epitaxial alignment and grain (or domain) size of impurity phases can be determined by intensity comparison and rocking curve widths of substrate and film, respectively, tilt angle ranges are usually larger and counting times shorter [3].

In the case of ceramics where the grains can be distributed over a wide range in ω, χ and φ we varied the angle of incidence (ω) from 5° to 40° with a step size of 1° and a

counting time of 200 s. The rocking curve itself is then constructed by integrating a certain 'region of interest' of each spectrum (or 'frame' on area detector) with respect to the tilt angle yielding integrated intensities versus ω, $\chi(\varphi)$ or 2θ. By region of interest we mean a region of ~ $\pm 1°$ in 2θ or χ on the area detector (frame) of the intensity maximum.

As we show in detail in the following sections rocking curves of reflections (005), (006), and (007) were recorded, the intensities integrated (using a Lorentzian fitting procedure) and the data analysed with respect to variations in widths (in ω and along a χ cone of constant 2θ, 'powder line') and peak shapes, as well as intensity ratios (background-to-peak) to yield information on the quality and quantity of alignment, respectively.

3.2.2 Samples

For the study on degrees of grain alignment in superconducting ceramics, firstly a series of Zn-doped fully oxidised and oxygen deficient $YBa_2Cu_3O_{7-\delta}$ (YBCO) samples was used and secondly, we investigated the effect of different preparation techniques on the alignment of pure, fully oxidised and oxygen deficient YBCO, and $HgBa_2Ca_2Cu_3O_{8+\delta}$ (Hg-1223) for comparison. All other samples presented in this thesis, but not in this chapter, were also investigated by the method described here and the results are given in the respective chapters.

The preparation of $YBa_2(Cu_{1-x}Zn_x)_3O_{7-\delta}$ (Zn-doped YBCO) with x= 0.0, 0.02, 0.03, 0.05, 0.07, and 0.10 was carried out by the standard solid state reaction process. (The solid state reaction procedure was carried out by Dr. J.R. Cooper at the IRC in Superconductivity.) Then, a bulk piece from each different Zn composition was lightly ground and the powder sedimented in acetone to obtain well-defined grain size distributions as described in chapter 2. The sedimented powders were heat treated at 850°C and 380°C for 12 hrs and 24 hrs, respectively, in an oxygen atmosphere to cure any structural damages on the surface of the grains, which could have been caused by the

grinding and sedimentation process, and fully oxidise the samples (more details on the surface treatment are given in chapter 4). Part of the x = 0.03 powder was further annealed in pure oxygen atmosphere at 650° for 12 h and then quenched in liquid nitrogen to obtain δ = 0.3. The final oxygen contents of δ = 0.0 and δ = 0.3 were verified from the weight change of a fully oxygenated sintered sample used as a reference which was heat treated together with the powders. The average grain diameter was determined as described in the previous chapter (section 2.9) and the 50% cumulative volume point was 5μm for all values of x as well as for the oxygen deficient (δ = 0.3) samples with x = 0.03. The T_c's for the different Zn compositions were 92.5 K, 68.2 K, 55 K, 46.4 K, and 17 K for x = 0.0, 0.02, 0.03, 0.05, and 0.07, respectively. The x = 0.03, δ = 0.3 samples' T_c is 9 K. The samples with x = 0.10 are non-superconducting. Our T_c values are in reasonable agreement with values reported previously in the literature for fully oxygenated samples of similar Zn contents [4]. However, on the basis of Ref. [4] and our unpublished data for several sets of Zn : YBCO samples the T_c value of the 0.05 Zn samples corresponds to 0.045 Zn.

Hereafter T_c represents the temperature where the onset of superconductivity occurs in ac susceptibility measurements for a measuring field H_{ac}=3 G rms and frequency f=333 Hz. (Typical ac susceptibility data can be found in the following chapters.)

The Hg-1223 bulk pieces with T_c = 134.5 K were supplied by Prof. P.P. Edwards' group from the University of Birmingham. The bulk pieces were ground in argon atmosphere to minimise possible surface degradation as described in chapter 4. The average grain diameter was 10μm. More details on the sample preparation and grain size distribution of the Hg-cuprate samples used in this work are given in chapter 5.

In addition we compared the effect of different alignment methods on the degree of oriented grains in pure, fully oxidised and oxygen deficient, YBCO samples. The average grain diameters of the fully oxygenated and oxygen deficient samples were 5 and 10μm, respectively. All powders, except one set of samples which we describe below, were individually mixed with a 5 min fast curing epoxy (Double Bubble; Perma Bond Europe)

with a weight ratio powder : epoxy = 1:5, and placed in a static field of 12 T at room temperature for 5 min (method I). For one set of the oxygen deficient samples ($YBa_2Cu_3O_{6.7}$, T_c = 66 K), the powders were mixed with Stycast 1266 in the same ratio as above and placed in a static field of 12 T for 20 min at room temperature before being heated to 90°C in the field. The samples were kept at 12 T and 90°C for ~20 min to ensure that the Stycast was fully cured (method II). We note here that different magnitudes, between 7-12 T, of static field did not alter the degree of alignment. The separation of the grains in the superconductor : epoxy composites was confirmed by ac susceptibility measurements by checking the linearity of the pick-up voltage at 4.2 K for H_{ac} from 1 to 10 G rms and f from 16 to 667 Hz.

Reference samples were set in epoxy under the same conditions but in zero magnetic field. A rocking curve measurement was performed on the reference samples to be able to compare the data obtained from the aligned specimens to those of a randomly oriented powder sample.

3.3 Results and discussion

3.3.1 Assessment of the degree of alignment

The procedure of characterising the degree of alignment of a magnetically aligned powder involves two factors which are, firstly, the number of grains which are successfully oriented, their relative volume, i.e. *the quantity of aligned grains*, and secondly, the degree of their preferred orientation, i.e. *the quality of the alignment*. It is necessary to provide a method which yields accurate results for both quantities. An X-ray diffractometer equipped with an area detector is ideal for this purpose because it enables us to record rocking curves and polar plots simultaneously.

Figure 3.2 shows the ideal cases of diffraction patterns from either a single crystal (fig. 3.2(a)), an unaligned powder sample (fig 3.2(b)), and an aligned ceramic (fig. 3.2(c)) as

they would be displayed on our area detector. A picture on the area detector display at constant ω and integration in 2θ or χ gives a plot of intensity versus χ or 2θ, respectively. If we integrate either in 2θ or in χ for the whole ω range we obtain a plot of intensity versus ω.

We define a single crystal in terms of alignment in the way that 100% of its 'grains' are oriented perfectly, i.e. within ~0.01°. That means that all full width at half maxima (FWHM) of a single crystal's rocking curves and pole figures with respect to any of the relevant angles (ω, χ, φ, and 2θ) are of the order of 0.01°, and in particular, that their respective ratios are equal to 1. In addition, the background-to-peak intensity ratios in every direction are the same and of the order of ~0.01, that is the peak is 100 times stronger compared to the background. We note that in our calculations on assessing the degree of alignment we take the ratio of peak to background intensities, so any effects of counting time, crystal size and mosaic spread on the peak intensity will have similar effects to the background intensity and thus their ratio will not be affected.

In an unaligned powder sample, on the other hand, we find the following characteristics. The width in 2θ varies according to the grain size and is typically of the order of 0.1° and, at least in principle, rocking curves are impossible in any other direction because there is no grain alignment. To elaborate on the question of the 2θ dependence on the grain size we note that from the Scherrer formula the diffraction peak width $\delta\theta = \lambda / (s \cos\theta)$, where λ is the X-ray wavelength (1.54051 Å), s is the size of the difrracting volume and $\theta = 2\theta / 2$. The diffracting volume is really the diffracting length, because we are looking at a volume where two out of three dimensions are quasi-infinite. The two quasi-infinite dimensions are the penetration depth of the beam in the material (which is the same for equal reflections e.g. all 006 reflections have the same penetration depth for the same material and it is independent of the grain alignment) and the width of the beam spot which is parallel to ω. The only length of interest is the extension of the beam perpendicular to these two directions. This length, or size of the grain, is determined by the Scherrer formula given above and determines the peak width.

Along the χ cones one observes an equal intensity distribution which we refer to as a powder line and whose width can be set as being equal to 180°. This yields a FWHM ratio of $\omega(2\theta):\omega(\chi) \sim 0$, whereas the 'background-to-peak' intensity ratio along a χ cone is 1. This indicates that the signal is due to statistically distributed grains, in other words we observe 100% randomness.

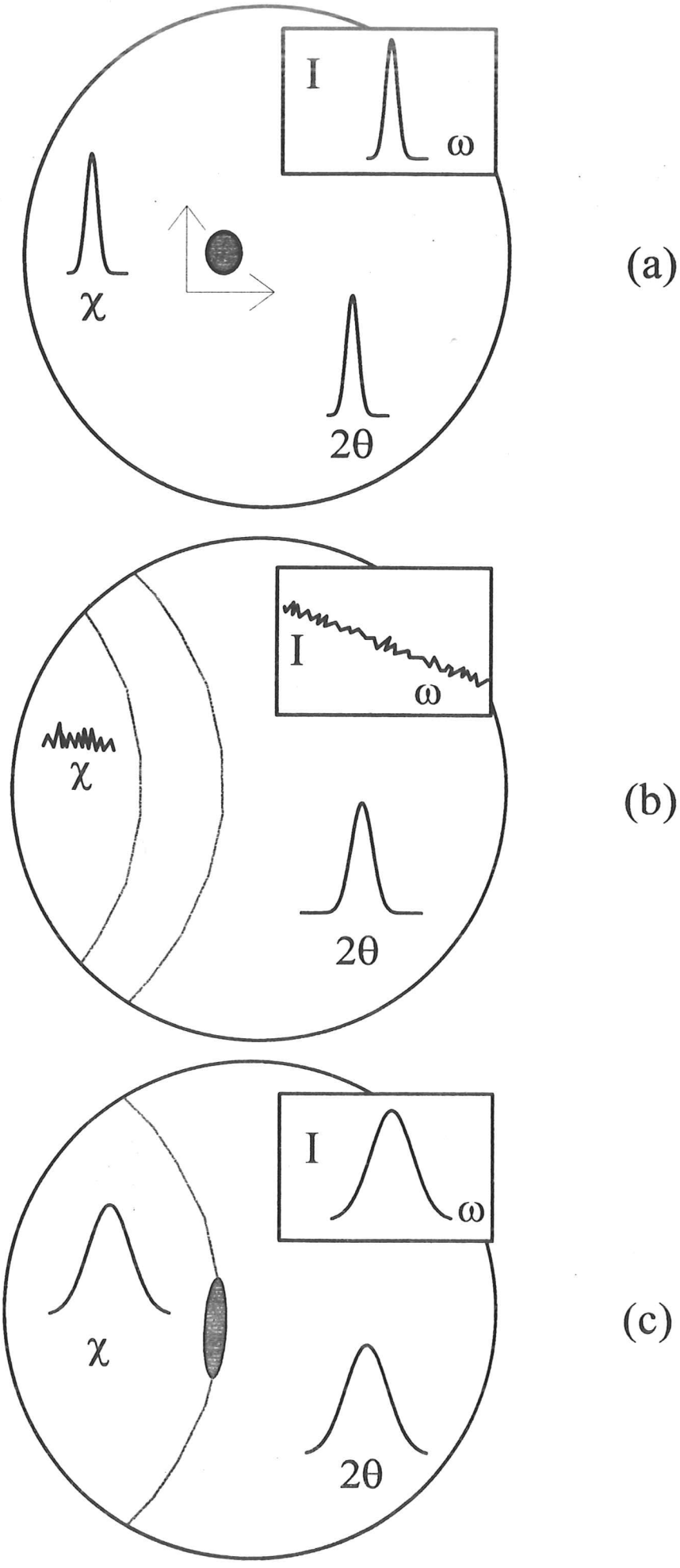

Fig. 3.2. Area detector display (idealized sketch) of reflection shapes and integration directions of a single crystal (a), an unaligned powder (b), and an aligned ceramic (c).

The above considerations allow us to calculate the amount of oriented grains and their degree of alignment in the case of a grain aligned sample. For the first part we consider the intensity distribution along a χ cone. In Table 3.1 we list the fit parameters of reflections (005), (006), and (007) for a variety of specimens each being characteristic of the set it represents. Taking the averaged background-to-peak ratios we obtain the unaligned fraction within the sample. This rocking curve (RC) method can now be compared (Table 3.1) to the simple conventional powder diffraction (CPD) method of taking the ratio of the intensity (I) sum of reflections (013) and (110), obtained using the 1D detector, of an unaligned (u) and an aligned (a) sample: $[I(013)+I(110)]_u$ / $[I(013)+I(110)]_a$ mentioned in the introduction as this ratio yields the amount of unaligned material as well. In both cases the resulting numbers are subtracted from 100 in order to obtain the aligned fraction in % (column 'quantitative DoA', Table 3.1).

In order to obtain the qualitative degree of alignment with the RC method the widths of the respective rocking curves were interpreted in the following way. First, an average width (w) is calculated using all measured reflections. Second, this value is multiplied by the maximum ratio of any two widths in χ and ω and the resulting number is subtracted from 100. This describes the degree of alignment in %. The second procedure can be understood in terms of determining the maximum 'eccentricity' of the diffraction spot. Our diffraction spots for aligned ceramics appear on the area detector as an ellipse whereas in the case of a single crystal we have a circular spot and thus the maximum eccentricity is equal to 1.

In less well-aligned samples the two procedures (quantity and quality of alignment) are not strictly independent as the background-to-peak ratio and the peak width are correlated, depending on the way the peak is fitted. For example for an Intensity versus χ plot, like in fig. 3.5(b) which we discuss in detail later, the high background makes it difficult to do a Lorentzian peak fit to the data. For samples with high background in the Intensity versus χ plots we find a systematic enhancement in the background in the peak / bgd ratio, used to evaluate the unaligned fraction within the sample, which suggests that the

"base" of the Intensity versus χ plot is due to the unaligned fraction of the grains. We thus regard the "base" of the peak as background (unaligned grains) and only use the rest of the peak to do the Lorentzian fit. In Table 3.1 (column 'qualitative DoA') we show the resulting degrees of alignment for several samples which were obtained using the fit parameters of the three reflections (005), (006), and (007).

Table 3.1. Intensity ratios (bg/ht) and linewidths w of reflections (005), (006), and (007) which are used together with the average widths and maximum eccentricities to determine the quantitative and qualitative degree of alignment (DoA, see text). The errors are less than 5% for intensities and less than 10% in the widths yielding errors of 2-3% in the resulting DoA's.

Sample	**reflection (005)**			**reflection (006)**			**reflection (007)**			**average width**	**maximum eccentricity**	**quantitative DoA**		**qualitative DoA**
$YBa_2(Cu_{1-x}Zn_x)_3O_{7-\delta}$	bg / ht	w(ω) (°)	w(χ) (°)	bg / ht	w(ω) (°)	w(χ) (°)	bg / ht	w(ω) (°)	w(χ) (°)	$\overline{w}$ (°)	∈	RC (%)	CPD (%)	(%)
x=0.00, δ=0.0	0.08	3.0	2.0	0.07	2.3	2.1	0.30	1.9	2.7	2.3	1.6	85	92	96
x=0.02, δ=0.0	0.12	1.9	1.9	0.12	1.8	2.0	0.25	1.2	1.7	1.75	1.7	84	95	97
x=0.05, δ=0.0	0.10	3.0	2.1	0.08	2.2	2.2	0.30	1.4	2.9	2.3	2.1	84	90	95
x=0.07, δ=0.0	0.19	3.0	3.2	0.25	3.3	3.4	0.43	2.9	1.9	2.95	1.8	71	30	95
x=0.10, δ=0.0	0.45	4.4	3.4	0.48	3.2	7.8	1.0	2.4	–	3.5	3.25	36	20	88.5
x=0.03, δ=0.0	0.04	1.7	1.3	0.05	1.6	1.3	0.17	1.7	1.65	1.5	1.3	91	90	98.0
x=0.03, δ=0.3	0.03	1.2	0.8	0.04	1.1	1.1	–	–	–	1.05	1.5	96	92	98.5
x=0.00, δ=0.3														
method I	0.03	1.5	1.0	0.03	1.2	1.1	0.11	1.2	1.3	1.2	1.5	95	95	98
method II	0.10	4.2	3.2	0.11	3.5	3.1	0.24	2.8	3.2	3.3	1.5	85	96	95
x=0.00, δ=0.0														
YBCO-A	0.06	4.3	6.5	0.07	4.8	6.8	0.25	4.9	7.4	5.8	1.7	87	40	80
YBCO-B	0.17	12.8	7.6	0.15	7.7	10.6	0.46	29.5	6.7	12.5	4.4	74	66	45
Hg-1223	0.29	2.9	2.1	0.06	2.3	1.9	0.15	2.4	2.2	2.3	1.5	84	92	97

	(005)		**(006)**		**(200)**		**(007)**	
	bg / ht	w(2θ)	bg / ht	w(2θ)	bg / ht	w(2θ)	bg / ht	w(2θ)
x=0.00, δ=0.0								
aligned	0.07	0.25°	0.05	0.27°	0.73	0.5°	0.33	0.3°
unaligned	0.66	0.39°	0.41	0.38°	0.62	0.45°	0.77	0.9°

3.3.2 Application of the analysis

We used the aforementioned RC method to estimate the quantity and quality of alignment of several samples. Characteristic results discussed here are those of Zn doped YBCO, Hg-1223 and oxygen deficient pure and Zn doped YBCO. These samples combine the variation of impurity doping, anisotropy, carrier concentration, number of CuO_2 planes per unit cell and two different cuprate families.

An example of the effects of different integration directions is given in figs 3.3 and 3.4. For the aligned sample, fig. 3.3(a), the intensity along χ shows a distinct peak, whereas in the unaligned reference, fig. 3.4(a), we only observe a statistical distribution in that direction. In contrast, the peaks in 2θ, figs 3.3(b) and 3.4(b), are quite similar in shape and intensity in both specimens, although the peak widths in the aligned sample are slightly smaller, indicating coherent scattering from oriented grains (see bottom of Table 3.1; comparison of aligned and unaligned YBCO, x =0.00, δ = 0.0 samples). In the unaligned reference we still find the pronounced diffraction signal from reflection (200) on the right hand side of (006) which is nearly completely suppressed in the aligned specimen. These two pictures were obtained by integrating in ω.

The two other possibilities of either integrating in χ or 2θ are shown in figs 3.3 and 3.4 (c), (d). For the aligned ceramic there are virtually no differences in peak shapes and intensities, whereas in the reference sample there seems to be a peak-like intensity distribution along ω obtained by integrating in χ which can indeed be fitted with a Lorentzian peak shape. Whether this is a real effect or not is currently being investigated.

Taking the above results into consideration we regard the intensity distribution along χ and the intensity integration in χ against ω as being the two most significant characteristics of these types of measurements as they determine the amount of oriented grains and the degree of alignment as discussed in section 3.3.1.

Fig. 3.3. Example of different integration directions and rocking curves of reflections (005) (solid line), (006) (dotted), and (007) (dashed) as obtained from an aligned pure YBCO sample: intensity distribution along χ (a) and 2θ (b), and ω rocking curves with integration in χ (c) and 2θ (d).

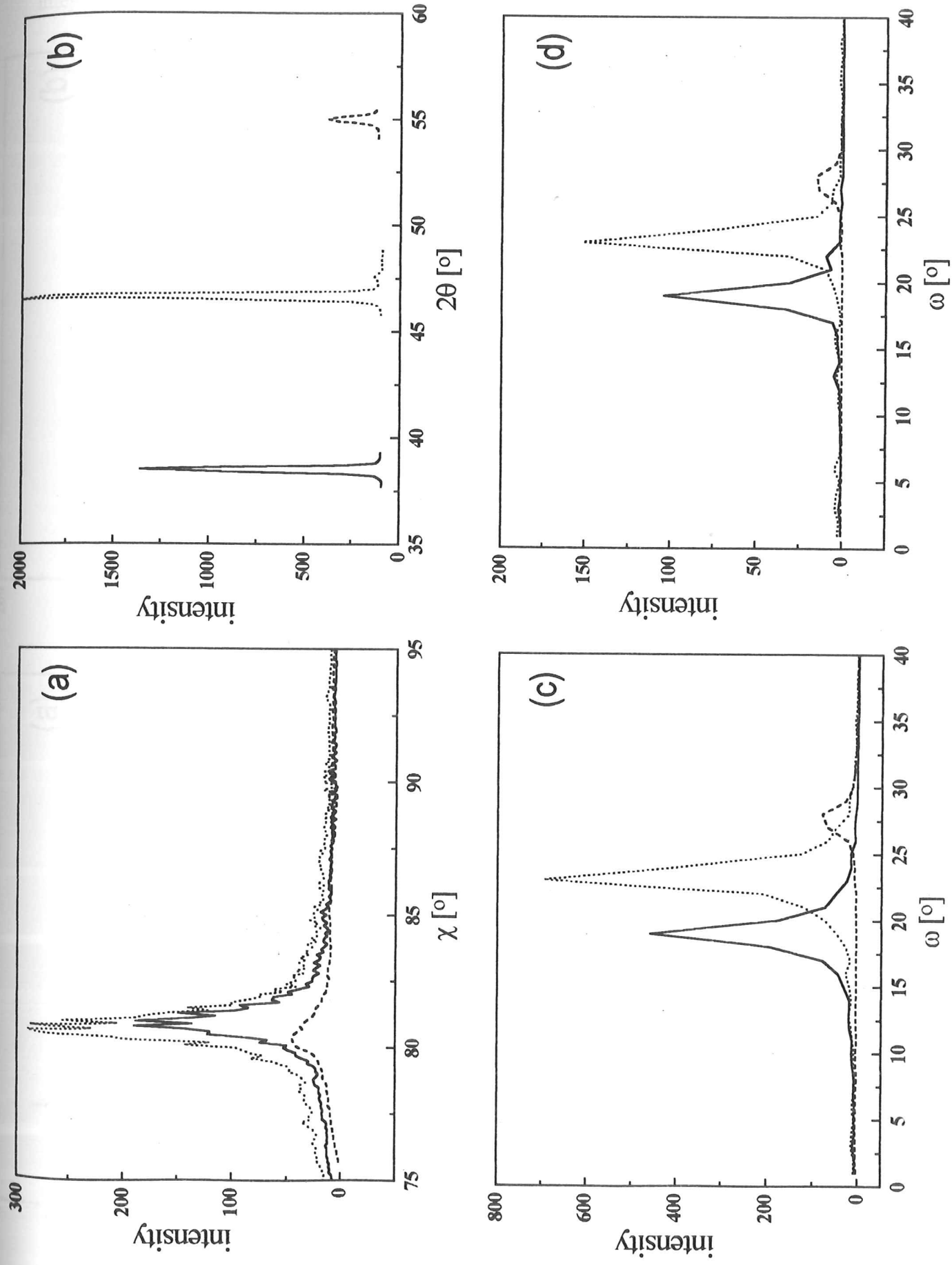

Fig. 3.4. Example of different integration directions and rocking curves of reflections (005) (solid line), (006) (dotted), and (007) (dashed) as obtained from an unaligned pure YBCO sample (reference): intensity distribution along χ (a) and 2θ (b), and ω rocking curves with integration in χ (c) and 2θ (d).

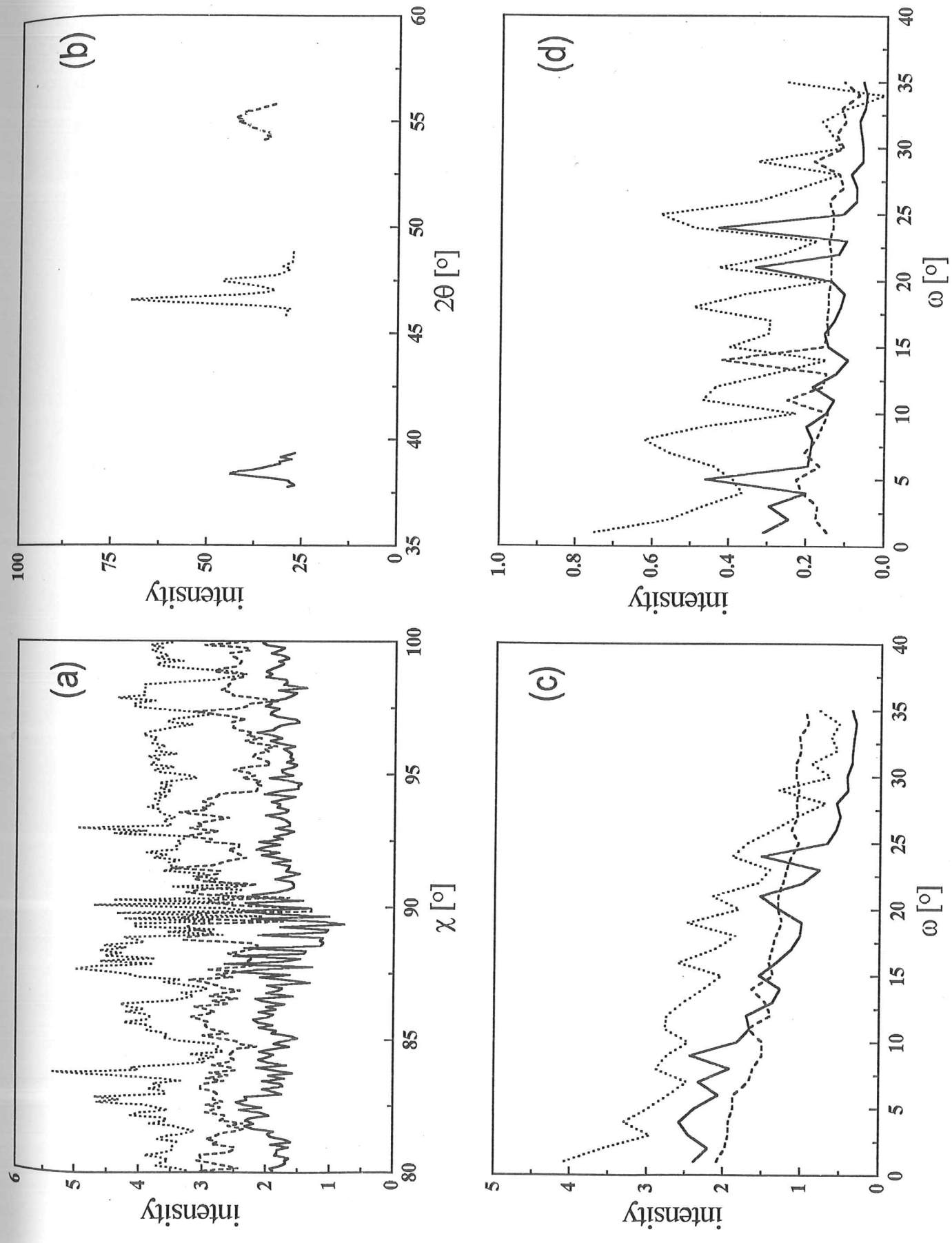

Figure 3.5 shows the rocking curves in ω of reflection (006) from the series of Zn-doped YBCO ceramics compared to the respective intensity distributions along χ. At low doping concentrations (≤5%) all curves are more or less identical with respect to shape and intensity, including the background. Higher Zn contents influence both peak widths and peak-to-background ratios indicating a considerably lower alignment (Table 3.1).

In fig. 3.6 we also illustrate the resulting rocking curves in both χ and ω direction of a magnetically aligned Hg-1223 ceramic (a,b) in comparison to the unaligned reference (c,d).

The 3% Zn-doped ceramic has been measured in the fully oxygenated as well as in the oxygen deficient phase (Table 3.1). The resulting curves are shown in fig. 3.7. Here we find an interesting effect that is present in all ceramics we investigated so far, namely that oxygen deficient samples are much easier to align quantitatively. This is confirmed by the measurements we performed on oxygen deficient (δ = 0.3) specimens with no Zn substitution which were aligned in two different ways (fig. 3.8). First of all, it is obvious from the curves that method I - as compared to method II - is the superior way of preparing aligned samples, and secondly the resulting alignment of this method has an average rocking curve width of ~1.2° and a background-to-peak ratio of 0.03 which is by far the best of all investigated ceramics (Table 3.1). We believe that the higher degree of alignment in the oxygen deficient samples is not due to the grain size variation between different samples since both the fully oxygenated and the oxygen deficient Zn doped samples have the same average grain size as discussed in section 3.2.2. It could be however, that the anisotropy of the room temperature susceptibility is enhanced with oxygen deficiency. Unfortunately, no systematic direct evidence is currently available, for example room temperature anisotropic susceptibility measurements in single crystals as a function of oxygen concentration.

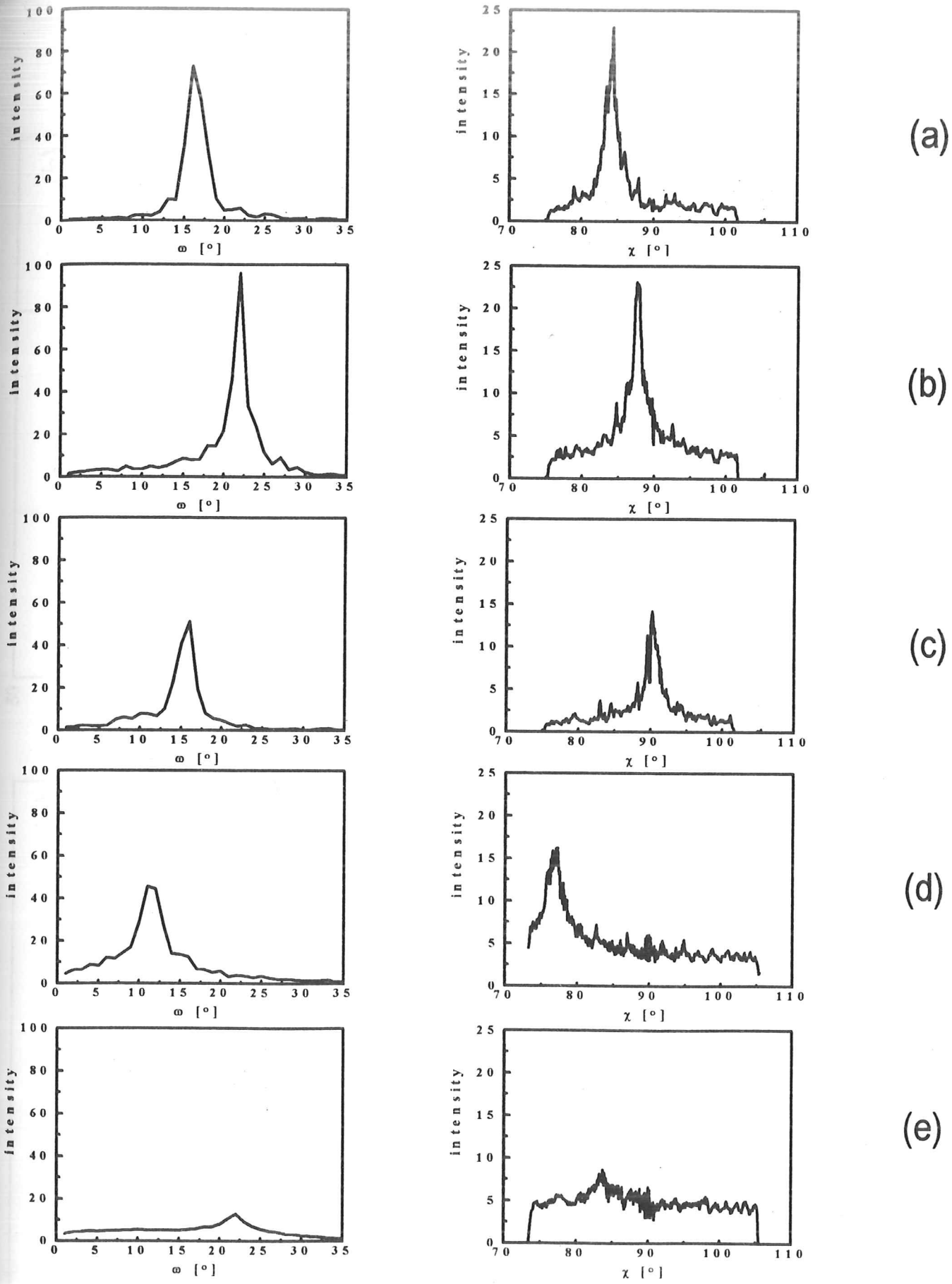

Fig. 3.5. Series of Zn-doped YBCO ceramics: ω rocking curves and intensity distributions along χ of reflection (006).

(a) pure YBCO, (b) +2% Zn, (c) +5% Zn, (d) +7% Zn, (e) +10% Zn.

Fig. 3.6. Rocking curves of reflections (005) (solid line), (006) (dotted), and (007) (dashed) in ω and χ as obtained from an aligned Hg-1223 ceramic (a,b) and its unaligned reference (c,d).

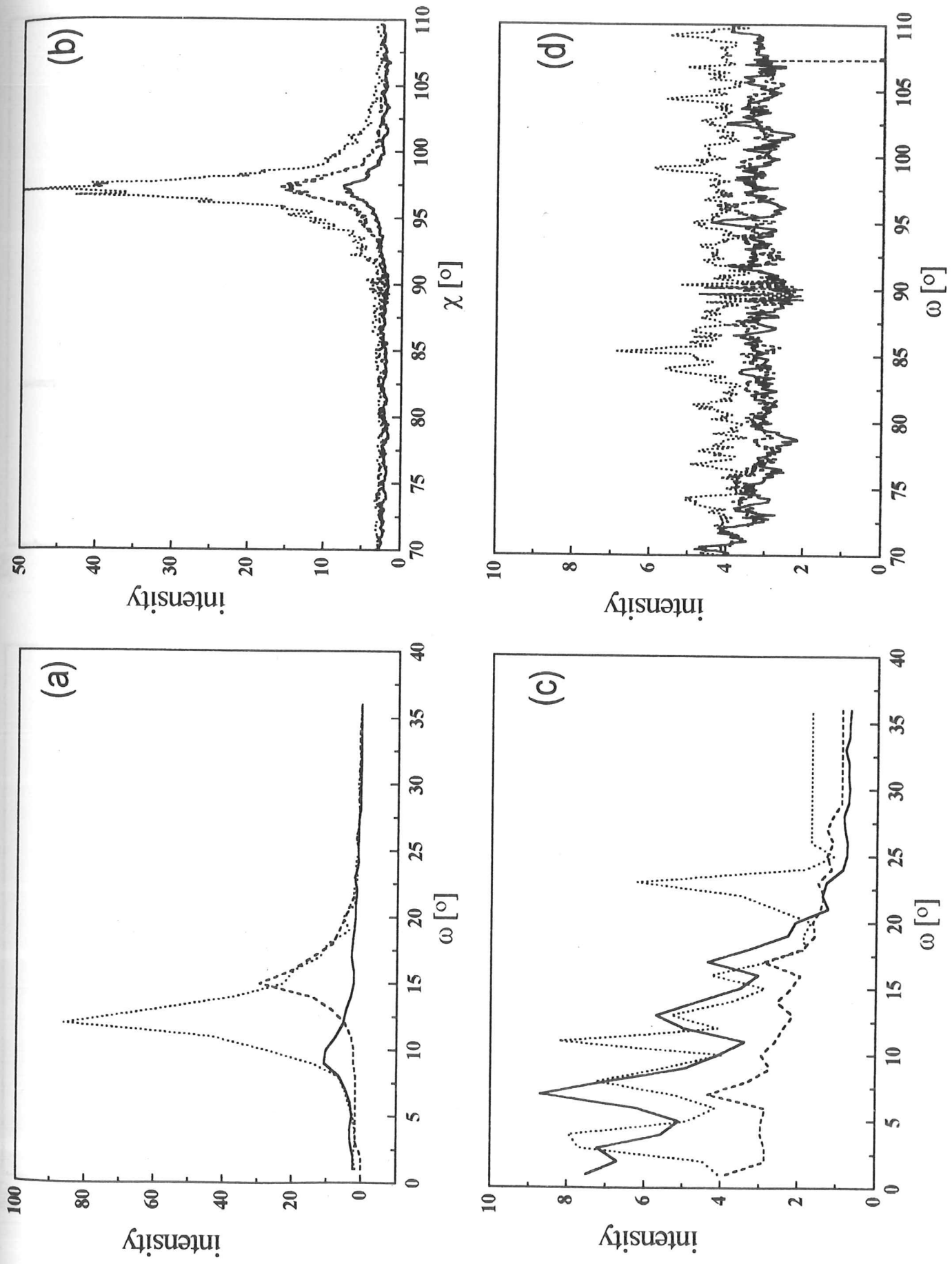

Fig. 3.7. Fully oxidized (a,b) and oxygen deficient (c,d) YBCO ceramic doped with 3% Zn: ω rocking curve and intensity distributions along χ of reflection (006).

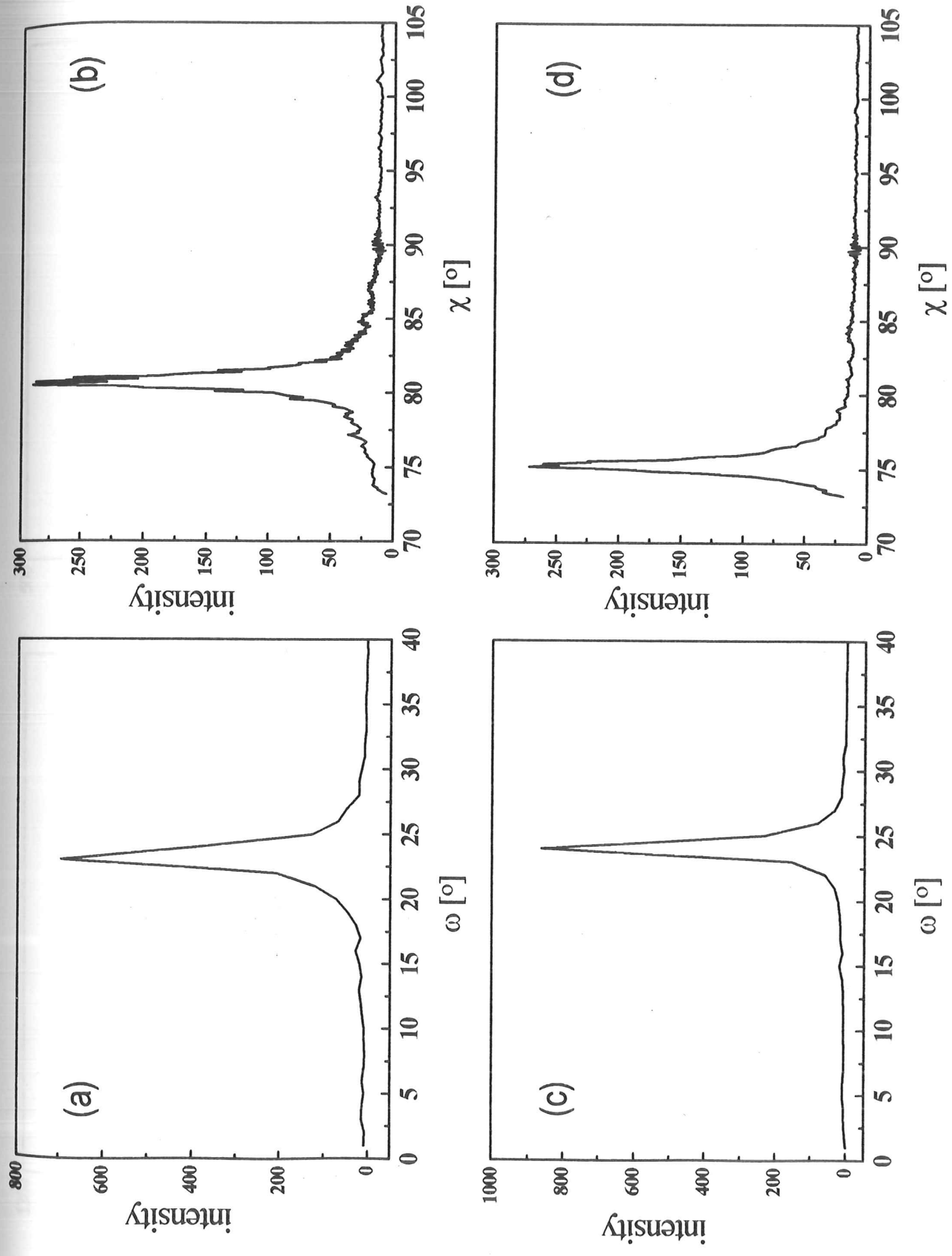

Fig. 3.8. Comparison of alignment methods I (a,b) and II (c,d) for $YBa_2Cu_3O_{6.7}$: ω rocking curves and intensity distribution along χ of reflection (006).

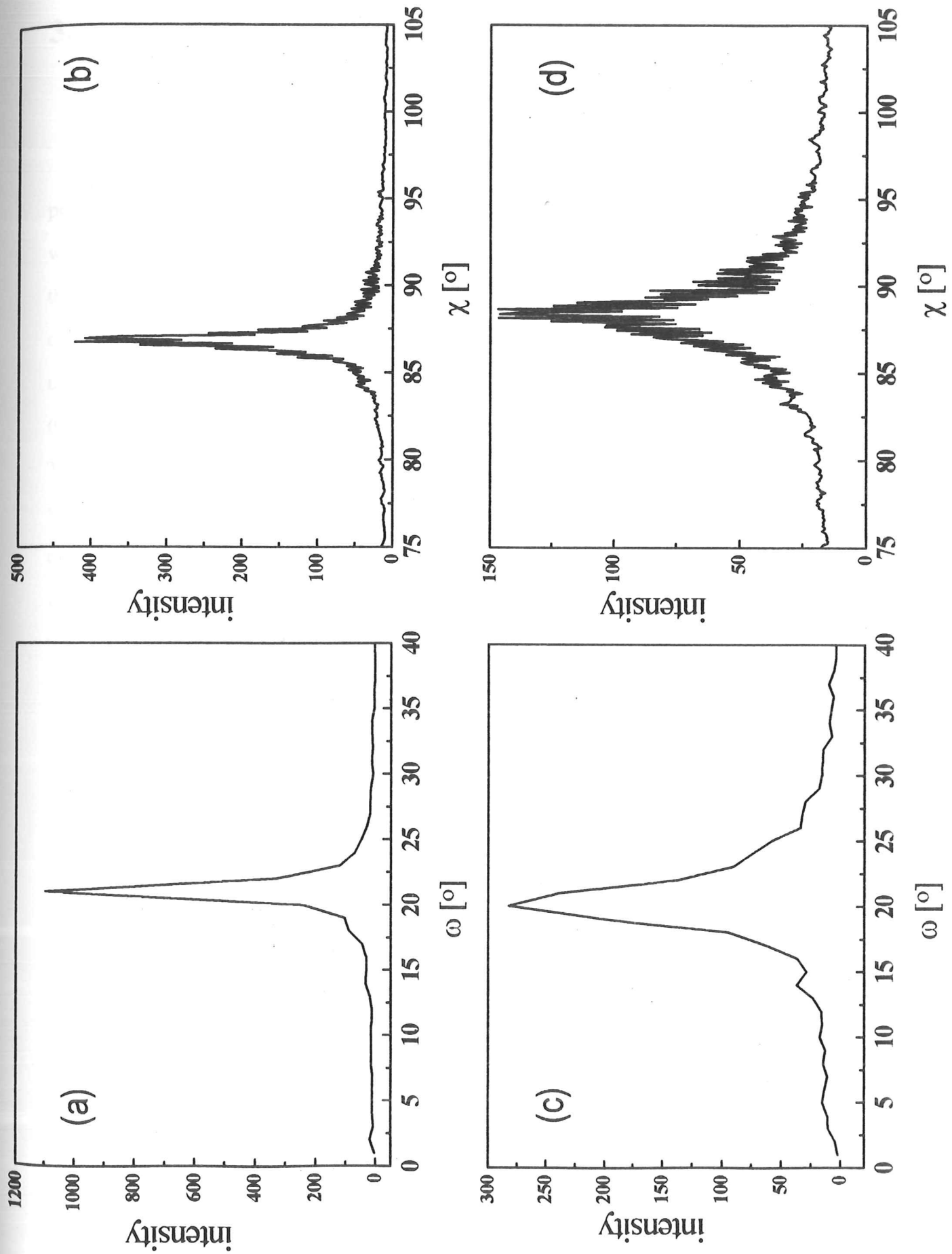

3.3.3 A brief comparison between the RC and CPD methods

Finally we would like to compare the new (RC) method to the simple conventional powder diffraction method (CPD) mentioned in the Introduction. In general, CPD, where we used a 1D detector, yields only information about the quantity of aligned powder not the quality of the alignment which is in addition not very accurate because it relies on the comparison of absolute intensities from two separate samples, namely the aligned and the unaligned reference specimens. The comparison of linewidths of reflections of the type (00l) was found to give a good estimate of the quality of the alignment. At the bottom of Table 3.1 we show the differences of background-to-peak ratios and diffraction peak widths for an aligned pure YBCO ($\delta = 0.0$) sample and the unaligned reference. As the quality of the alignment improves, we find an expected decrease in the linewidths and an increase in the intensities of the (00l) reflections. The opposite behaviour is observed for the (200) reflection (cf. figs 3.3 and 3.4). The average differences in the widths of the (005) and (006) reflections indicate a ~50% growth of the coherently diffracting volume.

In the determination of the quantitative degree of alignment both the conventional and the new method show similar trends i.e. the decrease in alignment with Zn-doping for >5% Zn. However, samples 'YBCO-A' and 'YBCO-B', which were aligned using method I, are a striking indication of the necessity to establish methods like those reported here (Table 3.1). In those two cases the results contradict each other completely. The main reason for this is mainly that it is very difficult to determine a lower amount of oriented grains by the conventional powder diffraction method. The degree of alignment measured by CPD represents mainly the big grains and the new (RC) method is able to detect both the big grains and the less intense signals.

3.4 Summary

We found that combining the information from both the CPD and RC methods for obtaining both quantitative and qualitative results on the degree of alignment in magnetically treated ceramics is highly recommendable.

To the best of our knowledge, the quantity and quality of alignment of the samples we used to study $\lambda(T)$ are the best reported to date for aligned ceramics. Furthermore, the $\lambda(T)$ data obtained, as shown in the following chapters, were independent of the quantity and quality of alignment within 5% of the values reported in each case.

References

[1] D.E. Farrell *et al.*, Phys. Rev. B 36, 4025 (1987).

[2] E.K.H. Salje, Phase Transitions 55, 37-56 (1995).

[3] K.R. Locherer *et al.*, Phil. Trans. R. Soc. Lond. A **354**, 2815 (1996).

[4] S. Zagoulaev, P. Monod and J. Jegoudez, Phys. Rev. B **52**, 10474 (1995).

Chapter 4

Surface-quality dependence of the low temperature magnetisation of $YBa_2Cu_3O_{7-\delta}$

4.1 Introduction

The surfaces of high-T_c superconductors (HTSC) are known to be reactive and environment sensitive. The surface structure and chemistry of the cuprates are often different from the bulk, for example carbonate phases [1], second phases [2] and crystallographic deformations [3,4] have been found at the surface of cuprate crystallites. An enhanced oxygen deficiency, $\delta = 0.8$, has been found by Auger electron spectroscopy [5] at scraped $YBa_2Cu_3O_{7-\delta}$ crystal surfaces. The tendency of HTSC to react with carbon dioxide and moisture present in the atmosphere degrades the superconducting properties of the material at the surface, although the greater part of the sample may remain unaffected. High resolution electron microscopy (HREM) has shown that during grinding most of the cuprates are unstable in air or acetone, and long exposure to air or acetone can cause serious changes to the structure and chemistry of the surface [3,4]. The surface reactivity of the cuprates is high during the grinding process itself and decays with time. For example grinding $HgBa_2CuO_{4+\delta}$ (Hg-1201) in air and then suspending the crystallites in ethanol did not significantly degrade their surface structure and chemistry. On the other hand, grinding in ethanol was found to deform the surface of the crystallites [3]. Therefore, it seems that any contact of the surface with contaminants during the grinding process can affect its properties. No such studies have been done for $YBa_2Cu_3O_{7-\delta}$, however, its tendency to react with water and carbon dioxide suggests that grinding in air can render the surface susceptible to unwanted chemical reactions.

Since one of the main merits of our technique is the use of powders to measure the penetration depth, we need to find a method to avoid extrinsic effects affecting our results. We note again, that the surface problem exists even in single crystals and particularly for the measurement of the penetration depth where one probes the surface of the sample we need to characterise their surfaces prior to the experiment.

The purpose of this investigation is to address the effects of surface degradation, see whether such surface defects cause significant changes in the low temperature (T) low field magnetic susceptibility (χ) data, and consequently the magnetic penetration depth. We also found new methods to avoid surface degradation and heat treat the damaged surfaces when necessary. The present study has been performed on a number of different batches of $YBa_2Cu_3O_7$ (YBCO). Characteristic results obtained from two of the batches are presented here.

4.2 Experimental

The YBCO powders, whose results are shown here were: (a) Newly purchased (Aldrich Chemical Co.) single phase powder [batch A (No. 35746-4)] with an average grain diameter (50% cumulative volume point) of 1 μm, and (b) phase pure YBCO powder prepared by Dr. J.R. Cooper at the IRC in Superconductivity using the standard solid state reaction method (batch B). All powders were annealed in flowing oxygen for 24 h at 380 °C and had a critical temperature T_c = 92.5 K as measured by low field ac susceptibility, χ, measurements. The $\chi(T)$ measurements were performed using the commercial low field ac susceptometer for an ac field H_{ac} = 3 G rms at a frequency f = 333 Hz. The separation of the grains and the absence of weak links were confirmed by checking the linearity of the pick-up voltage at 4.2 K for H_{ac} from 1 to 10 G rms and f from 16 to 667 Hz. The apparatus was calibrated using a Pb sphere (99.99% pure) at a low enough frequency to eliminate eddy current effects above T_c. High field normal state magnetic susceptibility measurements were also performed in a static magnetic field of 5

T using a Quantum Design SQUID magnetometer. In both cases the background signal was measured in separate runs and subtracted from the data at each temperature. The measured samples were either randomly oriented or magnetically aligned crystallites. The aligned samples were prepared by mixing the YBCO powder with a 5 min fast curing epoxy (Double Bubble; Perma Bond Europe) in a weight ratio YBCO : epoxy = 1 : 4. The mixture was then placed in a static field of 12 T at room temperature for 5 min. Details on the alignment procedure and characterisation can be found in chapters 2 and 3, respectively. The randomly oriented samples were also mixed with the 5 min fast curing epoxy but were left to cure in zero field. HREM images were taken by Dr. W. Zhou at the Department of Chemistry, on free crystallites from a Jeol JEM-200CX electron microscope operated at 200 kV, giving an interpretable resolution of ~1.85 Å. The vacuum in the microscope was maintained at $\sim 2 \times 10^{-7}$ Torr.

4.3 Results and discussion

The initial motivation for this investigation was the observation of an upturn below ~ 20 K in the low field susceptibility χ data of magnetically aligned YBCO crystallites of batch A [figs. 4.1(a) and (b)]. This upward curvature was independent of field, for H_{ac} = 1 - 10 G rms. Its presence was checked by carefully subtracting the background contribution of the sample holder and the epoxy. Similar curvatures were observed in free, unaligned, powders of the same batch.

A paramagnetic contribution from Cu free spins in the bulk of the crystallites was the first candidate for the observed effect. Thus, SQUID measurements were made in the normal state at high fields of 5 T yielding a Curie term $C = 4.8 \times 10^{-4}$ (emu K/ cm^3) from fits between 100 and 300 K. This Curie term is completely negligible on the scale of fig. 4.1(a), for example at 4.2 K it corresponds to 10^{-4} emu/cm^3, and suggests that bulk paramagnetism is not the cause for the upward curvature.

We knew from previous HREM work [4] that grinding YBCO in air introduces an amorphous surface layer several tens of Å thick, and therefore tried to remove the upturn in $\chi(T)$ by heat treatment. We found empirically that the curvature in the low temperature low field $\chi(T)$ data disappeared for samples treated in flowing oxygen at 850 °C for 12 h and then oxidised at 380 °C for 24 h, and instead obtained a linear T dependence below ~25 K. The product of the optimum heat treatment was examined by scanning electron microscopy (SEM) to confirm the absence of lumps and determine the grain size distribution. Furthermore, SQUID measurements on the powder showed that the Curie term had decreased from $C = 4.8 \times 10^{-4}$, before heat treatment, to 1.3×10^{-4} (emu K/ cm^3) after heat treatment. No upturn was observed in the low temperature $\chi(T)$ data after the heat treatment took place [figs. 4.1(a) & (b)]. We note that heat treating at lower temperatures such as 12 h in flowing oxygen at 750 °C and 800 °C did not remove the upturn, whereas 12h at 900 °C resulted in the formation of large lumps.

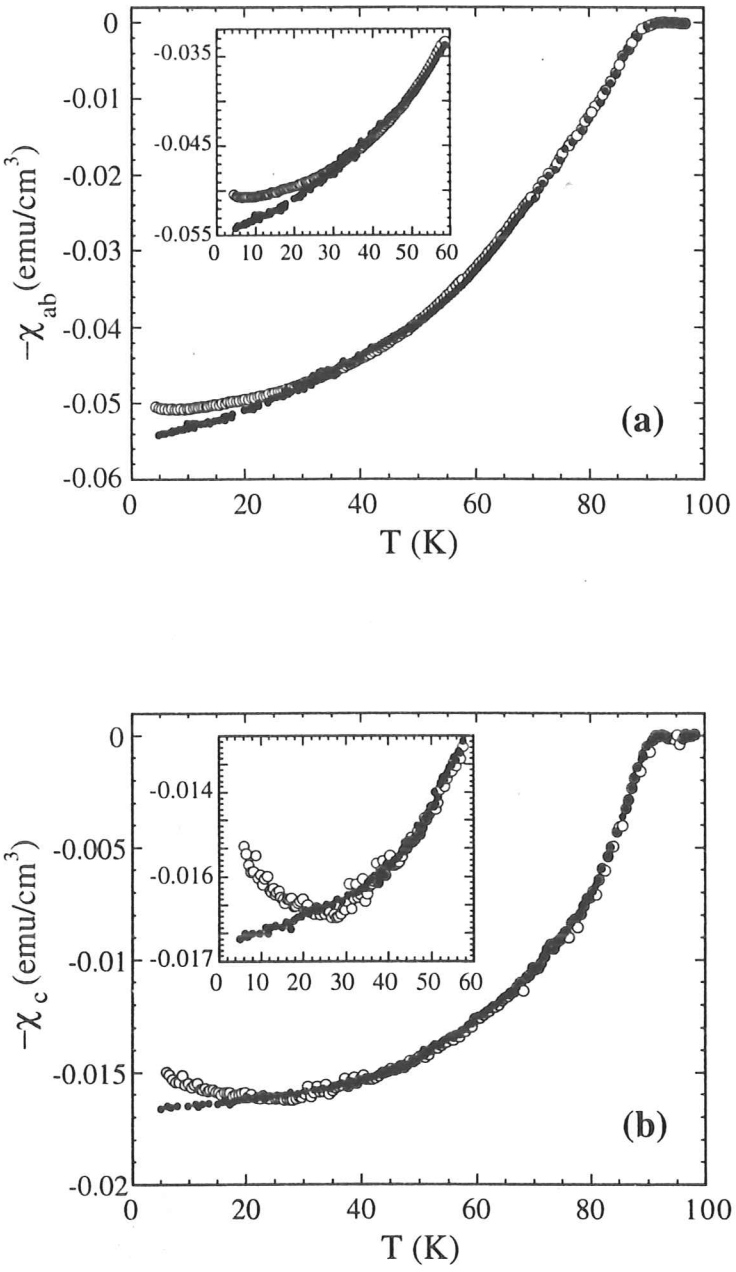

Fig. 4.1. The T dependence of the in-plane (H_{ac} // c) (a), and the out-of-plane (H_{ac} // ab) (b), diamagnetic susceptibilities of YBCO (batch A) grain aligned samples measured by the ac technique in the Meissner state. The open circles are for a sample which was not heat treated after being ground in air, whereas the solid circles are for a sample of the same material which was heat treated in O_2 flow at 850 °C for 12 h and then at 380 °C for 24 h, after being ground in air. The insets show the low temperature region of the curves.

The heat treated powder was mixed with epoxy and aligned in a field as described in section 4.2. The linear T dependences of the in-plane and out-of-plane $\chi(T)$, $\chi_{ab}(T)$ and $\chi_c(T)$, respectively, are also shown in figs. [4.1(a) and (b)]. By analysing the $\chi_{ab}(T)$ and $\chi_c(T)$, data of the magnetically aligned YBCO, and considering that the grains are approximately spherical, as indicated by SEM, the variation of the in-plane, λ_{ab}, and out-of-plane, λ_c , magnetic penetration depths with temperature can be obtained. Here it suffices to say that the low temperature dependences of λ_{ab} and λ_c resemble those of χ_{ab} and χ_c, respectively. Namely, $\lambda_{ab}(T)$ shows a linear term at low T which is now believed to be a characteristic feature of d-wave superconductivity. A linear T dependence is observed also in $\lambda_c(T)$ but with a somewhat lower relative slope. (More details on $\lambda_{ab}(T)$ and $\lambda_c(T)$ of YBCO will be given in chapters 6-8.)

To clarify the relevance of the surface structure and chemistry to the upturn seen in the low field $\chi(T)$ data we made a similar study on powder from batch B. The powder was dispersed in epoxy after being ground to an average grain diameter of 10 μm (50% cumulative volume point) in air and showed a smaller upturn in $\chi(T)$ to that seen in YBCO from batch A. (The ground powder was sedimented in acetone as described in chapter 2.) After the same heat treatment, in O_2 flow at 850 °C for 12 h and then 380 °C for 24 h, no upturn was observed in the low temperature χ data (fig. 4.2). (A portion of the sample was kept in the desiccator for a few days and we remeasured $\chi(T)$. No change was observed in the low temperature $\chi(T)$ data.) Regrinding the product in air caused a small increase in the Curie value, as obtained from high field SQUID measurements, but the upturn in the low temperature $\chi(T)$ data reappeared (fig. 4.2). The latter observation indicates that the upturn depends directly on the surface structure and chemistry of the sample.

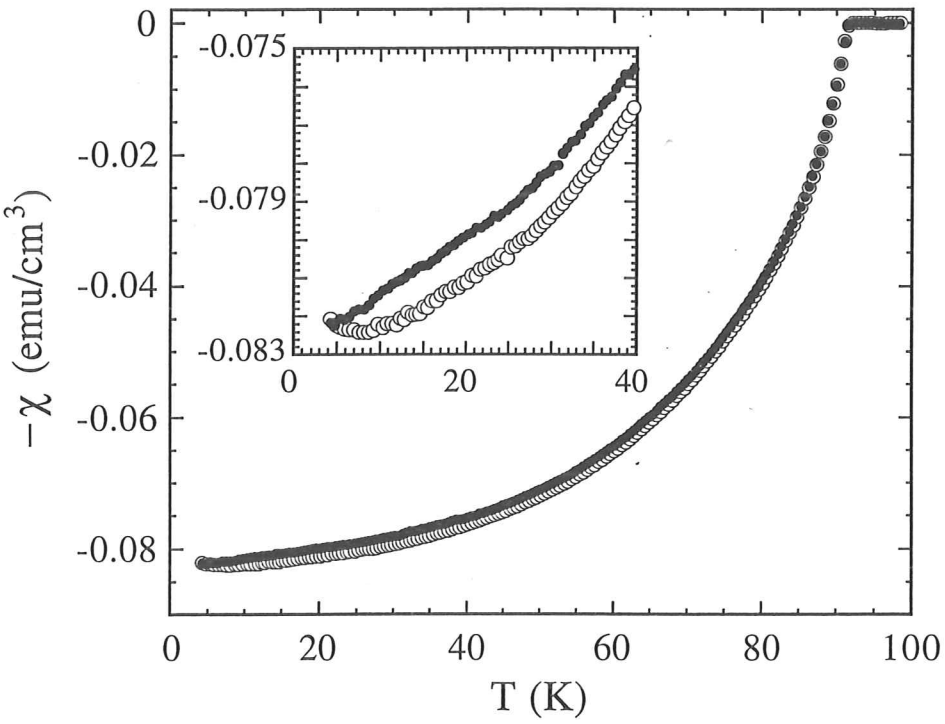

Fig. 4.2. The temperature dependence of the diamagnetic susceptibilities of an unaligned YBCO (batch B) sample measured by the ac technique in the Meissner state. The solid circles are for a sample which was first ground in air and then heat treated in O_2 flow at 850 °C for 12h and then at 380 °C for 24 h. The open circles are for the same sample but ground in air after the heat treatment (similar results, not shown, were found after the first grinding in air). The inset shows the low temperature region of the curves.

As discussed in the Introduction the sensitivity and reactivity of the surface is not restricted to YBCO but is general to the copper oxide superconductors. The optimum heat treatment conditions for each cuprate will vary for each material. However, grinding in a glove box with pure Ar helps to avoid significant surface degradation. The O_2 and H_2O contents inside the glove box were 10-40 ppm and 2-10 ppm, respectively. The ground crystallites of YBCO were removed from the glove box 10 min after grinding and kept in a vacuum desiccator for 30 min before starting the $\chi(T)$ measurements. No curvature was observed in the low temperature $\chi(T)$ data and consequently $\lambda(T)$ (chapters 5-7).

Samples from batch B were examined then by HREM. It was found that the surface properties of YBCO depend on how we treated the samples. The sample which was ground in air was deposited on a Mo grid with a holey carbon film, and then transferred to the electron microscope. A thick amorphous layer was observed on the surface [fig. 4.3(a)]. The thickness of such amorphous coating was $\approx$ 50 Å. We believe that this coating layer resulted from surface decomposition rather than from amorphous carbon contamination for the following reasons. Firstly, the thickness of the coating layer did not change and some microcrystals of metal oxides, Cu_8O, CuO, Y_2O_3 and $BaCu_2O_2$, developed gradually inside the layer under the electron beam irradiation. Second, surface energy dispersive X-ray microanalysis indicated a Y:Ba:Cu ratio on the surface, which was the same as that of the bulk. Furthermore, using the same technique, a heavy Hg loss was detected from a surface of Hg-1201 although the amorphous layer there was only about 20 Å thick [3]. Finally, when there was a carbon layer deposited on the surface, two amorphous layers were observed with significantly different image contrasts and the boundary between the particle and the amorphous carbon layer was clear. From the HREM image of fig. 4.3(a), we cannot see such a boundary along the [001] direction.

We then examined by HREM a sample from batch B which had been heat treated in O_2 flow at 850 °C for 12 h and consequently oxidised at 380 °C for 24 h, after being ground in air. The surfaces of the crystallites were found to be very clean without an amorphous layer coating. Figure 4.3(b) shows a typical profile image of such surface also viewed

down the [001] direction. The formerly decomposed surface, observed on the sample ground in air but not subjected to any heat treatment, has recrystallised into the parent structure. On the top of the surface we observe a very thin layer which shows a typical lattice relaxation, often seen on the surface of most copper oxide superconductors.

Fig. 4.3. Characteristic HREM surface profile images of an YBCO (batch B) sample viewed down the [001] direction. (a) The sample after grinding in air and (b) the sample which was first ground in air and then heat treated in O_2 flow at 850 °C for 12h and then at 380 °C for 24 h.

P.T.O

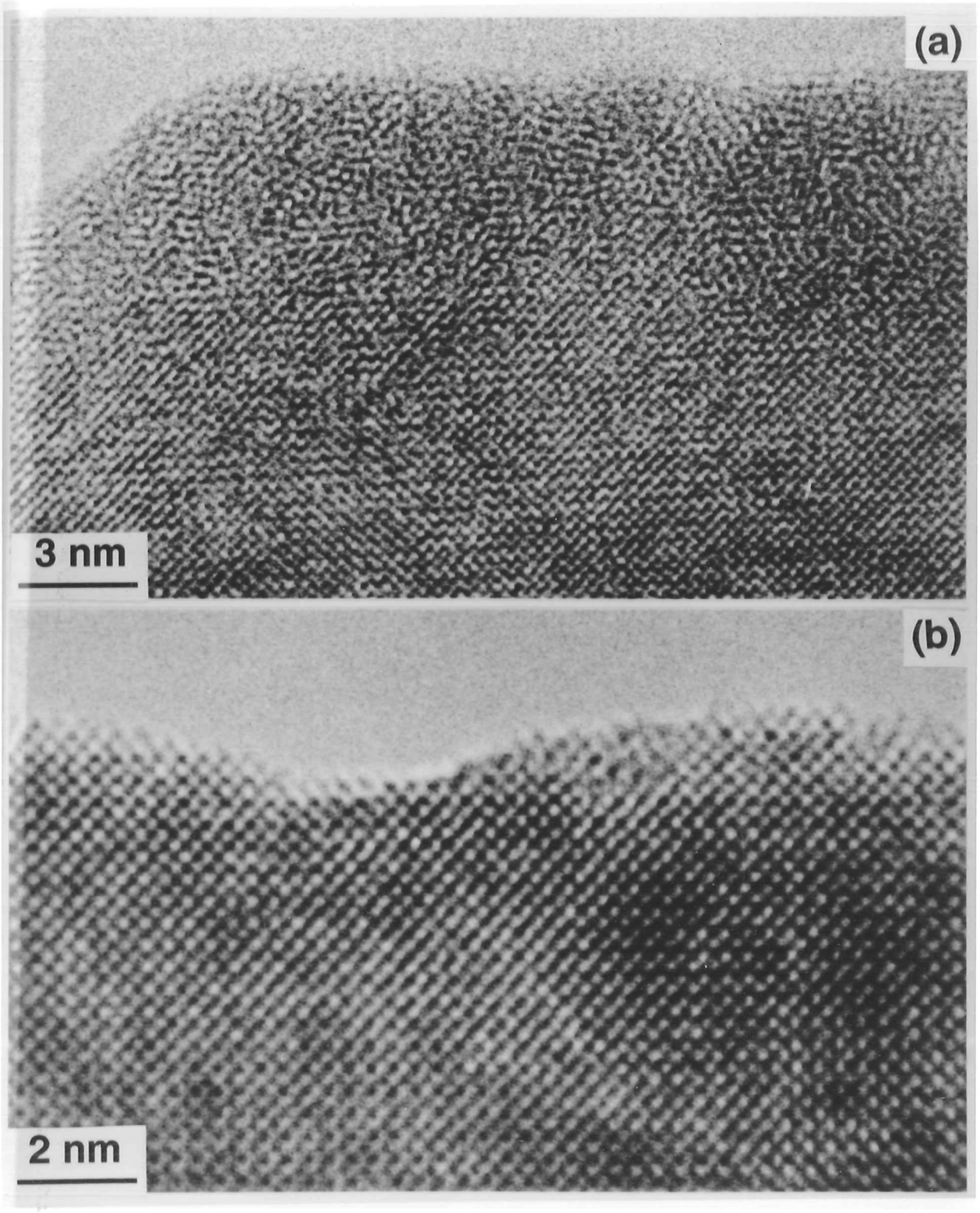
(a)
3 nm
(b)
2 nm

For the sample which was ground in Ar we deposited the dry powder on a Mo grid in a glove box and then transferred the specimen grid from the glove box to the electron microscope using an air-locked transfer. In this case we also observed an amorphous layer on the surface. However, the amorphous layer was thin (< 20 Å). Under the electron beam exposure, recrystallisation occurred starting from the interface between the crystal and the coating layer and then extending to the top surface. A clean surface was eventually observed. We suppose that the difference between the surface amorphous layers of YBCO ground in air and in Ar is not only in the thickness of the amorphous layer but also in their chemical composition and degree of disorder. Typical HREM images of YBCO samples ground in Ar can be seen in Ref. 4.

Finally, we wish to note that extrinsic behaviour of the low field susceptibility can have important consequences when determining the temperature dependence of the magnetic penetration depth of HTSC. It is well known that information regarding the type of the order parameter lies in the low temperature part of the data. In the case of YBCO for example, a linear temperature dependent $\lambda(T)$ has been found from microwave measurements [6] for high quality crystals whereas in the case of films and powders the results vary between different groups. Deviations from linearity, as those shown for example in fig. 4.1, start at $T \sim 20$ K a region crucial for understanding the behaviour of the order parameter.

4.4 Summary

We found that grinding in air can induce structural and chemical defects on the surface of YBCO crystallites. We find empirically that sometimes these can have significant effects on $\chi(T)$ and make the derived values of $\lambda(T)$ saturate or even increase again below 12-15 K. It is not well understood why surface defects can have such a strong effect on $\chi(T)$. Nevertheless, heat treating the crystallites at 850 °C for 12 h in flowing oxygen and reoxygenating at 380 °C, or grinding under argon yields a linear term in $\lambda(T)$.

With well-aligned samples, which we can carefully characterise by the method described in chapter 3, and with the knowledge as to how to prevent or cure sample surface degradation, we can now use the ac susceptibility technique to study the penetration depth of various families of HTSC. New results on various HTSC are presented in the following chapters.

References

[1] S. Nakahara *et al.*, J. Cryst. Growth 85 (1987) 639.

[2] Y. Ishida *et al.*, J. Electron. Microsc. 36 (1987) 251.

[3] W. Zhou, A. Asab, I. Gameson, D.A. Jefferson, P.P. Edwards, Physica C 248 (1995) 1 (and references therein).

[4] W. Zhou, D.A. Jefferson, and W. Y. Liang, Supercond. Sci. Tech., 6 (1993) 81.

[5] J. Hockertz, H.J. Clemens and W. Monch, Z. Phys. B 90 (1993) 331.

[6] W.N. Hardy *et al.*, Phys. Rev. Lett. 70 (1993) 3999.

Chapter 5

Magnetic penetration depth of anisotropic $HgBa_2Ca_2Cu_3O_{8+\delta}$ and the isotropic oxide $Ba_{0.6}K_{0.4}BiO_3$

5.1 Introduction

There is mounting evidence for d-wave superconductivity [1] in high-T_c superconductors and the measurement of the magnetic penetration depth λ is a useful probe [2-8] of the energy gap morphology at the Fermi surface and of the superfluid electrodynamics. Most studies have concentrated on fully oxygenated $YBa_2Cu_3O_7$ (YBCO) [3,6,7], and only a few [2,4,5,8] have examined highly anisotropic materials such as $La_{2-x}Sr_xCuO_4$ and $Bi_2Sr_2CaCu_2O_8$.

The $HgBa_2Ca_2Cu_3O_{8+\delta}$ (Hg-1223) compound has the highest known critical temperature [9-12] which makes it potentially attractive for practical applications. On the basis of its crystal structure [13] the transport properties are expected to be highly anisotropic. We report the values and temperature dependences of the in-plane, λ_{ab}, and out-of-plane, λ_c, magnetic penetration depths for c-axis aligned Hg-1223 powders obtained using the ac susceptibility technique. For comparison, the penetration depth of the cubic oxide superconductor $Ba_{0.6}K_{0.4}BiO_3$ was also investigated using the same technique.

5.2 Experimental

The Hg-1223 samples were prepared by G.B. Peacock in Prof. P.P. Edwards' group (Department of Chemistry, University of Birmingham) using a single-step method [14,15], whereas the $Ba_{0.6}K_{0.4}BiO_3$ (BKBO) powders were produced by grinding large single crystals (in argon atmosphere), grown by W. Schmidbauer (Clarendon Laboratory, University of Oxford) [16].

To magnetically align the Hg-1223 samples, the oxygenated powder was first lightly ground by hand to remove lumps and passed through a 20 μm sieve. This was carried out in an argon atmosphere using a glove box (chapter 2), in order to minimize surface degradation which can influence the low-temperature behaviour of the magnetisation (chapter 4). The powder was kept under argon atmosphere for 30 min before being mixed with a 5 min fast curing epoxy (Double Bubble; Perma Bond Europe) with a weight ratio Hg-1223 : epoxy = 1 : 5, and placed in a static field of 7 T at room temperature for 5 min. Part of the collected powder was used to determine the grain size distribution as described in chapter 2 (section 2.9). The grain size distribution of the powder for all grains measured is shown in the inset of fig. 5.1(a). Ac susceptibility, χ, measurements were performed with the ac field applied either in the ab-plane or along the c-axis. Measurements were performed using both ac susceptometers described in chapter 2 for an applied ac field H_{ac} = 1, 2 and 3 G rms at a frequency f = 333 Hz, but for all data presented here H_{ac} = 3 G rms and f = 333 Hz. The separation of the grains and the absence of weak links were confirmed, the background signal was subtracted from the data and the susceptometers were calibrated in a similar manner to that described in chapter 4 (section 4.2).

5.3 Results and discussion

From the X-ray analysis (chapter 3) more than 93% of the sample was found to be *c*-axis aligned to within ±2°.

Initial X-ray measurements of the oxygenated powder indicated a phase purity greater than 90%. SQUID measurements of the same powder two months later yielded a Curie term of $75 \times 10^{-3} / T$ (emu / mole) from fits between 250 and 300 K. This Curie term is negligible in comparison with the superconducting diamagnetism.

The inset of fig. 5.1(b) shows the temperature dependence of $-M / M_0$, in percent, near T_c for a *c*-axis aligned Hg-1223 sample. Here M_0 is the maximum possible diamagnetism. The way M_0 was determined, and the associated errors, are given in detail in chapter 2; section 2.9. The onset of superconductivity is observed to be at 134.5 K and the transition width (10 - 90 %) is 2 K. Taking the Hg-1223 grains in the composite to be approximately spherical, as indicated by scanning electron microscopy (chapter 2), the data were analysed on the basis of the model first suggested by Schoenberg [17] and described in more detail in chapter 2, and the variation of λ with temperature for both orientations was obtained [figs. 5.1(a) and (b)]. As discussed in chapter 2 (section 2.5), when $\lambda_c >> \lambda_{ab}$ one can safely take $\lambda_{eff} \sim 0.7\lambda_c$ for grains of arbitrary sizes in order to estimate λ_c, where λ_{eff} is the effective value of the penetration depth derived from the measured susceptibility for $H_{ac} // ab$.

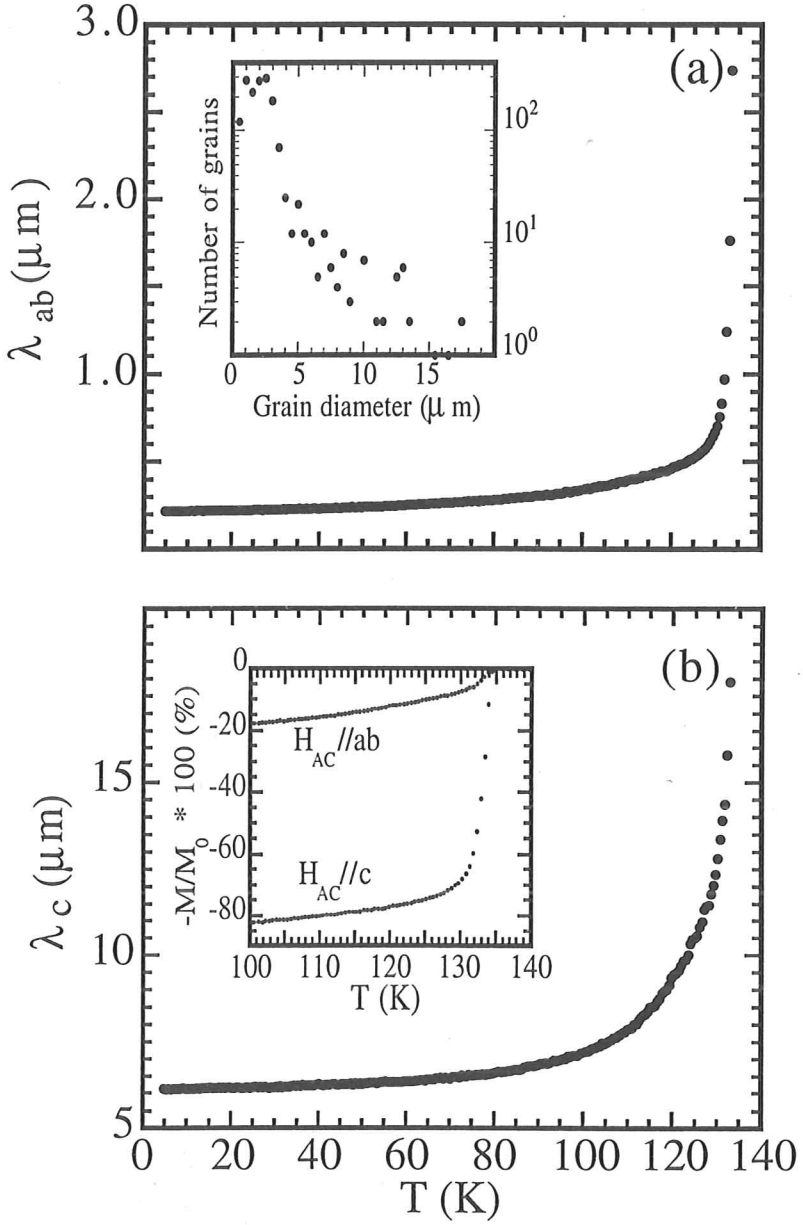

Fig. 5.1. The temperature dependence of the penetration depth for a grain aligned sample of $HgBa_2Ca_2Cu_3O_{8+\delta}$ for (a) H_{AC} // c, λ_{ab}, and (b) H_{AC} // ab, λ_c. Figure 1(a) (inset): Grain size distribution of the Hg-1223 powder. Figure 1(b) (inset): -M / M_0, in percent, of the same sample as a function of temperature close to T_c.

The values of $\lambda_{ab}(0)$ and $\lambda_c(0)$ are 2100 Å and 61000 Å, respectively. The value $\lambda_{ab}(0)$ = 2100 Å is in good agreement with that reported earlier for grain aligned Hg-1223 from high-field magnetisation studies [18]. (In high-field magnetisation measurements one uses the upper critical field slope to estimate $H_{c2}(0)$ [19], the coherence length $\xi_{ab}(0)$ and thus $\lambda_{ab}(0)$ through $\kappa = \lambda / \xi$ for a known value of κ.) Furthermore, the estimated anisotropy ratio $\gamma = [\lambda_c(0) / \lambda_{ab}(0)] \cong 30$ is close to that expected from resistivity results for Hg-1223 single crystals at 300 K, $\rho_c / \rho_{ab} \sim 1000$ [20].

Figure 5.2 shows plots of the temperature dependence of the normalised superfluid density $[\lambda(0) / \lambda(T)]^2$ for the *ab*-plane and the *c*-axis data, respectively. The data are compared with weak coupling theory for an *s*-wave [19] and a *d*-wave [21] superconductor with a maximum gap $\Delta(0) = 2.14\ k_B T_c$. It can be seen that the *d*-wave curve fits the data for $\lambda_{ab}(T)$ well. In contrast the data for $\lambda_c(T)$ are much flatter at low T and fit the expression suggested for Josephson coupling [22], $[\lambda(0) / \lambda(T)]^2 = [\Delta(T) / \Delta(0)] \tanh [\Delta(T) / 2k_B T]$ reasonably well, where $\Delta(T)$ is the weak coupling *d*-wave superconducting gap [21]. A similar behaviour has been reported for $\lambda_c(T)$ of $La_{1.85}Sr_{0.15}CuO_4$ single crystals by Shibauchi *et al.* [2]. However, their $\lambda_{ab}(T)$ data were close to what expected for a weak-coupled *s*-wave superconductor. We note that their low temperature data ($T / T_c < 0.25$) for both $\lambda_{ab}(T)$ and $\lambda_c(T)$ were quite scattered and rather inconclusive.

There are some deviations from the Josephson fit for λ_c in fig. 5.2 at low T corresponding to an almost T^2 power law. This behaviour is consistent with the Josephson-coupled layer model of Clem, Coffey and Hao [23] where the Josephson and the quasiparticle contributions to λ_c^2 are simply additive. The significant deviations seen in both λ_{ab} and λ_c near T_c are due to thermodynamic fluctuation effects as discussed below.

For comparison, we have performed similar measurements on BKBO powder samples dispersed in epoxy. $\lambda(0)$ was found to be $\cong$ 3500 Å and was reconfirmed by muon spin relaxation experiments. The temperature dependence of the normalised superfluid density

together with the behaviour expected from the weak coupling BCS theory for *s*-wave superconductors [19] are shown in fig. 5.3 for comparison. The temperature dependence of BKBO is found to resemble very well that predicted from the weak-coupling BCS theory for *s*-wave superconductors [19], except near T_c where the deviation seen may also arise from thermodynamic fluctuations. This result shows the conventional nature of the order parameter in BKBO, in contrast to YBCO (chapters 6-8) and Hg-1223, and indicates the importance of the CuO_2 planes for the *d*-wave symmetry of the order parameter.

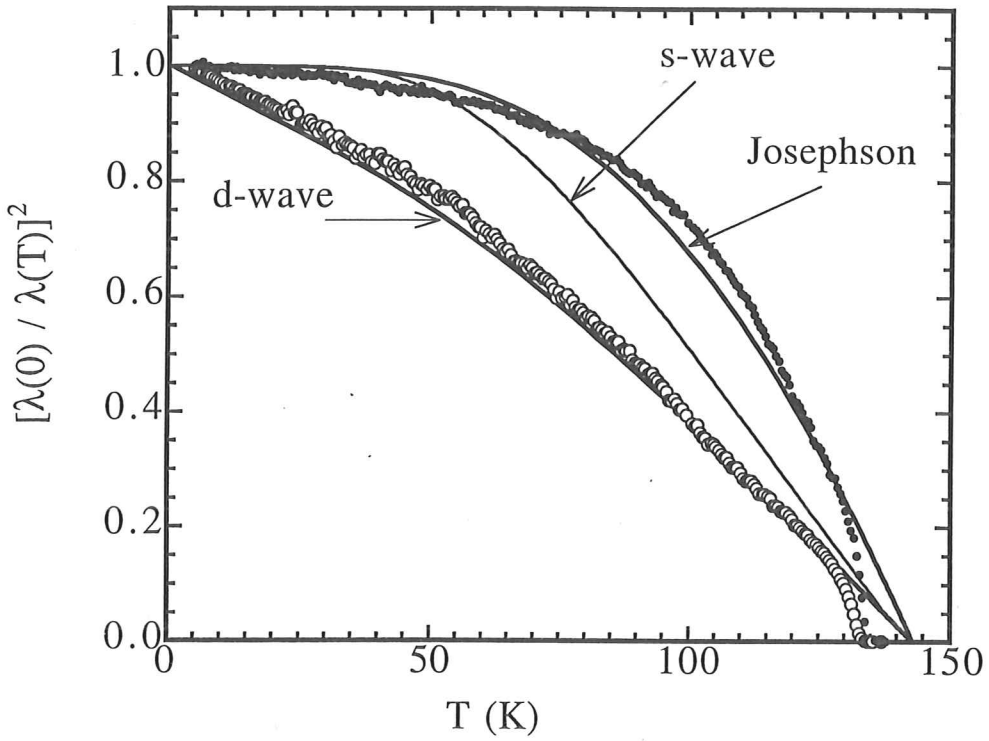

Fig. 5.2. (a) Plots of $[\lambda_{ab}(0) / \lambda_{ab}(T)]^2$ (open circles) and $[\lambda_c(0) / \lambda_c(T)]^2$ (closed circles) as functions of T for Hg-1223. Also shown, as solid lines, are the theoretical predictions for the normalised superfluid density from the weak coupling BCS theory for *s*-wave [19], the weak coupling BCS theory for *d*-wave [21], and the normalised superfluid density as calculated for a Josephson coupled *d*-wave superconductor [22].

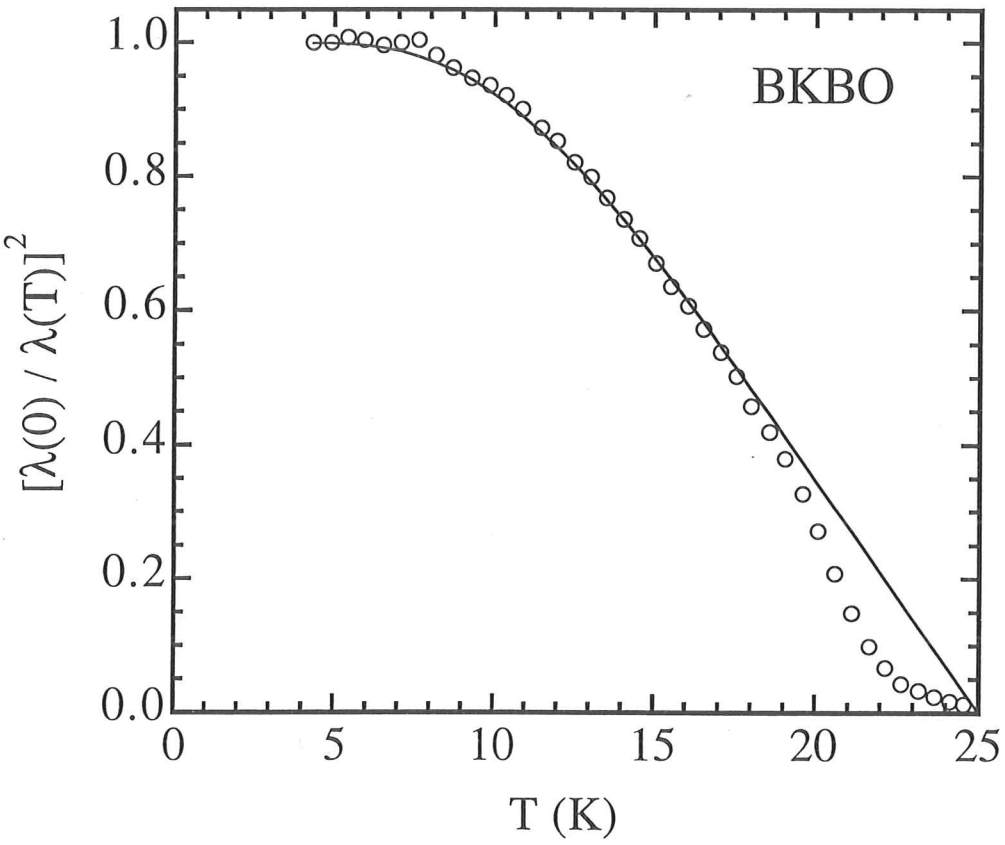

Fig. 5.3. (a) Plot of $[\lambda(0) / \lambda(T)]^2$ (open circles) as a function of T for BKBO. Also shown, as a solid line, is the theoretical prediction for the normalised superfluid density from the weak coupling BCS theory for *s*-wave superconductors [19].

There is marked curvature in the $[\lambda_{ab}(0)/\lambda_{ab}(T)]^2$, $[\lambda_c(0)/\lambda_c(T)]^2$ versus T plots (fig. 5.2) near T_c. Kamal *et al.* [24] have previously seen curvature in $[\lambda_{ab}(0)/\lambda_{ab}(T)]^2$ of YBCO crystals near T_c. By replotting their data as $[\lambda_{ab}(0)/\lambda_{ab}(T)]^3$, they obtained linear behaviour characteristic of 3D critical fluctuations. As shown in fig. 5.4(a), $[\lambda(0)/\lambda(T)]^3$ plots for our data (λ_{ab} and λ_c) are linear from $T / T_c = 0.8$ to ~ 0.97, but there are significant deviations nearer T_c which were independent of the magnitude of H_{ac}.

We do not fully understand this curvature but it may be caused by a dimensional cross-over [22] when the c-axis coherence length $\xi_c(T) \geq d$, where d is the largest distance between CuO_2 planes. We can elaborate this as follows. For Hg-1223 estimates of $\xi_c(0)$ range from ~ 1 to 2 Å [20,25]. Taking an average value $\xi_c(0) = 1.5$ Å and $d = 10$ Å [14], we obtain $\xi_c(0) / d = 0.15$, a value lying in the range empirically found to represent superconductors exhibiting interlayer Josephson coupling [26]. In the usual case where the coupling between CuO_2 planes within a unit cell is stronger than that between cells, d is the c-axis parameter (15.8 Å for Hg-1223 [13]) [27]. Taking $\xi_c(0) = 1.5$ Å and $d =$ 15.8 Å the 2D - 3D cross-over should occur at a reduced temperature $r = [2\xi_c^2(0) / d^2] =$ 0.018, i.e., $T / T_c \cong 0.98$ which corresponds rather well to the region where the curvature sets in fig. 5.4(a).

So one possible description of the results in fig. 5.4(a) is that there are critical fluctuations having an exponent 1/3 both in the 2D and 3D regions but with somewhat different prefactors. The similar behaviour of λ_{ab} and λ_c supports this viewpoint but as far as we know there are no theoretical predictions of critical exponents in the 2D region.

The inset to fig. 5.4(a) shows that BKBO does obey the law for 3D critical fluctuations better than the mean field law (fig. 5.3).

A second possibility for Hg-1223 is that the fluctuations are weaker and our data can be described by the theory of Baraduc and Buzdin (BB) for Gaussian fluctuations [27]. As shown in fig. 5.4(b) a reasonably good fit can be obtained for the λ_{ab} data using the BB 2D formula, taking $r = 0.018$ (as before) and the reduced Ginzburg temperature $G_i =$ 0.089. BB predict that in the 2D region the effect of fluctuations in λ_c^{-2} is equivalent to a

shift of $[0.5T_c\ (G_i r)^{1/2}]$ on the temperature axis. For the above values of G_i and r this shift is 3 K and is reasonably consistent with the *c*-axis data in fig. 5.2. However, in this picture one would expect a similar effect to occur in $YBa_2Cu_3O_7$ near 80 K and this is not observed (chapter 7).

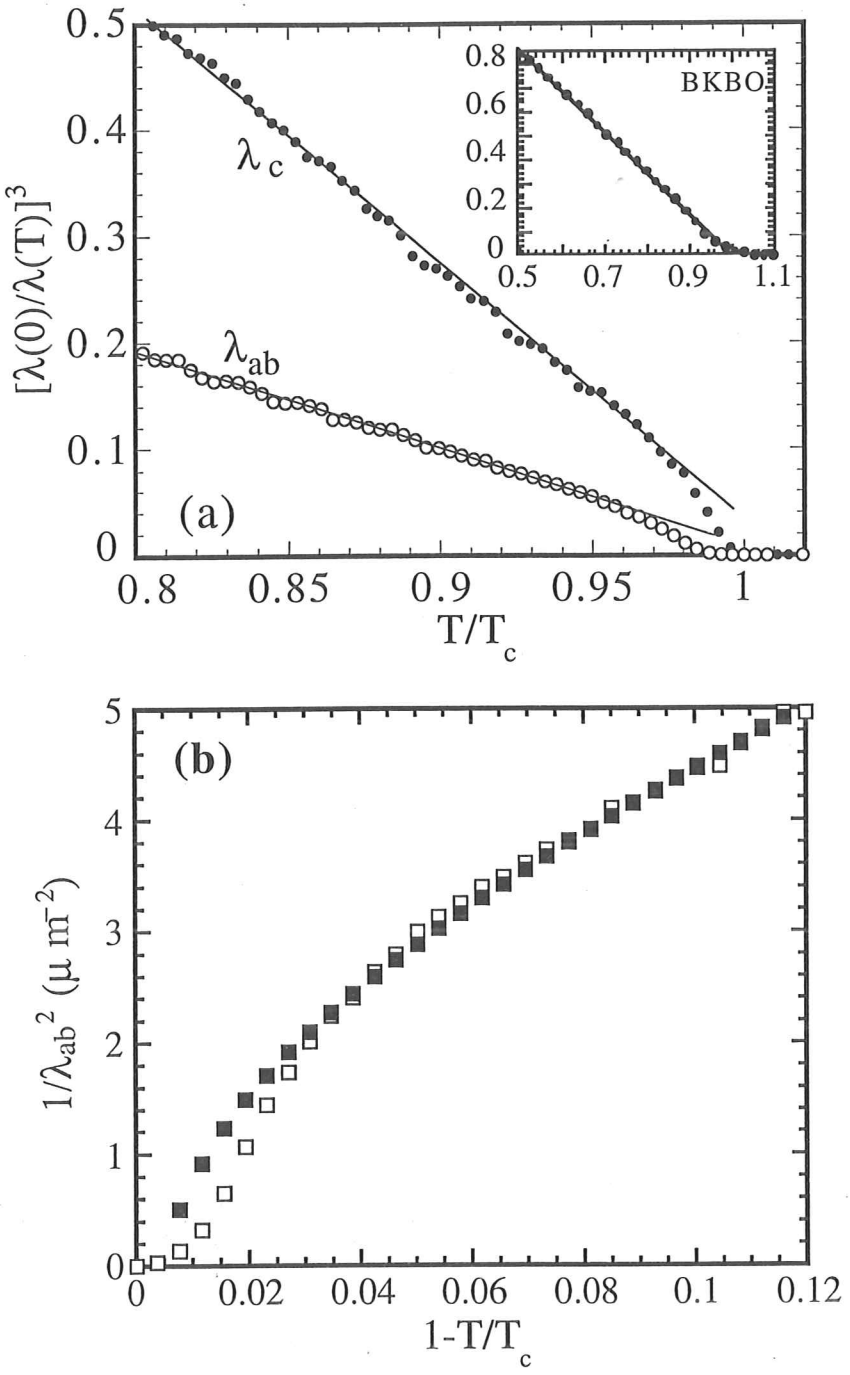

Fig. 5.4. (a) $\lambda^3(0) / \lambda^3(T)$ versus T/T_c for the *ab*-plane and *c*-axis penetration depths of Hg-1223. Solid lines are drawn as a guide to the eye. Inset: $\lambda^3(0) / \lambda^3(T)$ versus T/T_c for the BKBO sample. (b) $1 / \lambda_{ab}^2(T)$ versus $1\text{-}T/T_c$ (open squares) for Hg-1223 compared to the theory of Baraduc and Buzdin [27] (closed squares).

5.4 Summary

We have investigated the temperature dependence of the anisotropic penetration depth of high quality grain aligned Hg-1223. The anisotropy ratio $\gamma = [\lambda_c(0) / \lambda_{ab}(0)] \cong 30$ is very high, reflecting the 2D nature of Hg-1223. A kink was observed in $1 / \lambda^2(T)$ near T_c which was discussed in terms of a dimensional cross-over. The temperature dependence of $\lambda_{ab}(T)$ is indicative of d-wave superconductivity. However, $\lambda_c(T)$ approximately follows the behaviour expected for a superconductor with intrinsic Josephson coupling between the CuO_2 planes. The Josephson nature of Hg-1223 is further supported by the ratio $\xi_c(0) / d = 0.15$. BKBO on the other hand was found to be a weak-coupled s-wave superconductor.

Briefly, we conclude that Hg-1223 is a highly anisotropic two-dimensional Josephson type d-wave high-T_c superconductor, whereas BKBO is a weak-coupled s-wave superconductor, albeit with marked thermodynamic fluctuations near T_c.

References

[1] D. J. Van Harlingen, Rev. Mod. Phys. **67**, 515 (1995).

[2] T. Shibauchi *et al.*, Phys. Rev. Lett. **72**, 2263 (1994).

[3] J. F. Annet, N. Goldenfeld, and S. R. Renn, in *Physical Properties of High Temperature Superconductors II* edited by D. M. Ginsberg (World Scientific, Singapore, 1990).

[4] J. R. Cooper, L. Forro, and B. Keszei, Nature **343**, 444 (1990).

[5] A. Maeda *et al.*, Phys. Rev. B **46**, 14234 (1992).

[6] W. N. Hardy *et al.*, Phys. Rev. Lett. **70**, 3999 (1993).

[7] D.A. Bonn *et al.*, Phys. Rev. B **50**, 4051 (1994).

[8] A.Maeda *et al.*, Phys. Rev. Lett. **74**, 1202 (1995).

[9] A. Schilling *et al.*, Nature **363**, 56 (1993).

[10] C. W. Chu *et al.*, Nature **365**, 323 (1993).

[11] M. Nunez-Regueiro *et al.*, Science **262**, 97 (1993).

[12] E. V. Antipov *et al.*, Physica C **215**, 1 (1993).

[13] J. L. Wagner *et al.*, Phys. Rev. B **51**, 15407 (1995).

[14] G. B. Peacock, I. Gameson, and P. P. Edwards (in preparation).

[15] S. Lee *et al.*, J. Mater. Chem. **4**, 991 (1994).

[16] W. Schmidbauer *et al.*, Physica C **235-240**, 759 (1994).

[17] D. Shoenberg, *Superconductivity* (Cambridge University Press, Cambridge, 1954), p.164.

[18] M-S. Kim *et al.*, Phys. Rev. B **51**, 3261 (1995).

[19] B. Mühlschlegel, Z. Phys. **155**, 313 (1959).

[20] A. Carrington *et al.*, Physica C **234**, 1 (1994).

[21] A. Schofield, (private communication).

[22] W. E. Lawrence and S. Doniach, in *Proceedings of the 12th International Conference on Low-Temperature Physics* edited by E. Kanada (Academic Press of Japan, Kyoto, 1971).

[23] J. R. Clem, M. W. Coffey and Z. Hao, Phys. Rev. B **44**, 2732 (1991).

[24] S. Kamal *et al.*, Phys. Rev. Lett. **73**, 1845 (1994).

[25] M-K. Bae *et al.*, Physica C **231**, 249 (1994).

[26] N. E. Hussey *et al.*, Phys. Rev. B (in press).

[27] C. Baraduc and A. Buzdin, Physics Letters A **171**, 408 (1992).

Chapter 6

Probing the order parameter and the *c*-axis coupling of high- T_c cuprates by penetration depth measurements

6.1 Introduction

As shown in chapter 5 and in Refs [1-13] detailed knowledge of the behaviour of the superfluid density and the symmetry of the order parameter of high-T_c superconductors (HTSC) is important for understanding various properties of the superconducting state including the pairing mechanism in these materials.

The Hg-based cuprates are very interesting HTSC because of their high T_c's and the fact that there can be one or more CuO_2 planes per unit cell. Here we extend our study of chapter 5 and report the values and low temperature dependences of the in-plane (λ_{ab}) and out-of-plane (λ_c) penetration depths for *c*-axis grain aligned tetragonal [14] $HgBa_2CuO_{4+\delta}$ (Hg-1201) down to 1.2 K. We find characteristic T dependences, T^1 for λ_{ab} and T^5 for λ_c which are completely consistent with $d_{x^2-y^2}$ symmetry of the order parameter. For comparison we report low T anisotropic penetration depth data for tetragonal [15] Hg-1223 and $\lambda_c(T)$ of orthorhombic [16] $YBa_2Cu_3O_7$ ($YBCO_7$) and $YBa_2Cu_3O_{6.57}$ ($YBCO_{6.57}$). The results allow us to provide a coherent picture on the differences between the in-plane and the out-of-plane penetration depths of high T_c cuprates, and give a physical picture on the *c*-axis coupling of these materials.

6.2 Experimental

The Hg-1201 and Hg-1223 samples were prepared by G.B. Peacock in Prof. P.P. Edwards' group at the Department of Chemistry of the University of Birmingham using a single-step technique, described in detail elsewhere [17,18]. Initial characterisation by X-ray diffraction showed the phase purity of Hg-1201 to be at least 95% and that of Hg-1223 to be at least 90% with no other superconducting phases present. The Hg-1201 and Hg-1223 samples had T_c = 93 and 134.5 K, respectively. Bulk pieces were ground in argon atmosphere using a glove box to minimise surface degradation (chapter 4). The collected powders were sieved, kept in an argon atmosphere for 30 min and then magnetically aligned as described in chapters 2 and 5. The average grain diameters corresponding to the 50% cumulative volume point, as determined by analysing scanning electron microscopy photographs (chapter 2), were 4 and 10 μm for the Hg-1201 and Hg-1223 samples, respectively. Quantitative and qualitative checks of the sample alignment were made by X-ray diffraction using the high resolution technique described in chapter 3 and Ref. 19. The fraction of the unoriented powder in both Hg-1201 and Hg-1223 was estimated to be ~ 5%. Rocking curve analysis of the aligned Hg-1201 and Hg-1223 samples gave a full width at half maximum of ~1.6° and 2.0°, respectively.

Bulk $YBa_2Cu_3O_{7-\delta}$ was prepared by Dr. J.R. Cooper at the IRC in Superconductivity in the standard way by solid state reaction from CuO_2, Y_2O_3 and $BaCO_3$. The bulk product was ground in air, sedimented in acetone (to obtain a narrow grain size distribution; chapter 2) and finally heat treated at 845 °C in flowing oxygen for 12 hours to repair the damaged surface of the grains (chapter 4). The fully oxygenated, $\delta = 0.0$ ($YBCO_7$, T_c = 92 K) samples were prepared by annealing in pure oxygen atmosphere at 380 °C for 24 hours and then slowly cooled to room temperature. The oxygen deficient, δ = 0.43 ($YBCO_{6.57}$, T_c = 55 K) samples were prepared by annealing in 0.2% O_2 / N_2 atmosphere at 550 °C for 12 hours and then quenching into liquid nitrogen. The final oxygen contents of $\delta = 0.0$ and $\delta = 0.43$ were verified from the weight change of a fully

oxygenated sintered sample used as a reference which was heat treated together with the respective samples. The annealed powders were then magnetically aligned, as described in chapter 2. The average grain diameters were 5 and 10 μm for the fully oxygenated and the oxygen deficient samples, respectively.

Low field ac susceptibility, χ, measurements were performed using both the commercial, down to 4.2 K, and the home built, down to 1.2 K, susceptometers. Measurements were performed for H_{ac} = 0.3 - 3 G rms at f = 333 Hz. The earth's field was screened out using a mu-metal shield. For all data presented here H_{ac} = 1 G rms and f = 333 Hz. The separation of the grains and the absence of weak links were confirmed by checking the linearity of the signal at 4.2 K for H_{ac} from 0.3 to 3 G rms and f from 33 to 333 Hz. The background signal was subtracted and the apparatus was calibrated as described in chapters 2 and 5. The data were analysed using London's model (chapter 2 and Ref. 20), and the variation of λ with temperature was obtained for both orientations.

6.3 Results and discussion

The values of $\lambda_{ab}(0)$ and $\lambda_c(0)$ obtained for Hg-1201 are 1710 ± 100 and 13 600 ± 1200 Å, respectively. The $\lambda_{ab}(0)$ value was also confirmed by μSR measurements at PSI. These measurements were performed using polycrystalline pellets of the same batch as the one used to prepare the aligned samples. Figures 6.1 (a) and (b) show characteristic plots of the low T dependence of the ac susceptibility (plotted as fractional diamagnetism) for the ab-plane and the c-axis Hg-1201 data, respectively. The temperature dependences of λ_{ab} and λ_c are shown in the respective insets. The linear term in λ_{ab} (T) seen in fig. 6.1(a), characteristic for d-wave superconductivity [1], has a slope of 6.5 Å/K. In contrast, the data for $\lambda_c(T)$, fig. 6.1(b), are much flatter at low T. The $\lambda_c(T)$ data fit the expression suggested by Xiang and Wheatley for tetragonal HTSC with relatively low anisotropy [eq. (3) in Ref. [21]]: $\lambda_c(T) \sim \lambda_c(0)\ [1+ \alpha(T/T_c)^5]$, with $\alpha \sim 3$. The parameter α depends strongly on the ratio of the superconducting transition

temperature and the zero temperature energy gap, namely $\alpha = 225(T_c/\Delta_0)^5$. The experimental value of α, yields $(\Delta_0/T_c) \sim 2.37$, 10% larger than the weak coupling BCS value $(\Delta_0/T_c) = 2.14$, for a *d*-wave superconductor. We also tried to fit the data using an exponential or other power-law functions of T/T_c but found that these were less satisfactory than the above expression for $\lambda_c(T)$. Furthermore, it is physically unlikely for λ_{ab} to vary linearly with T, as observed experimentally, while the *c*-axis penetration depth shows an exponential T dependence. This is so, because a low temperature linear term in λ_{ab} indicates the presence of low energy quasiparticle excitations and shows that there is no isotropic *s*-wave energy gap. These low energy quasiparticles will also contribute to λ_c (unless there is a mechanism preventing them doing so) and make $\lambda_c(T)$ to behave as a power law at low T. For a clean cuprate with tetragonal crystal structure, like the Hg-1201 samples we measured, $\lambda_c(T)$ was actually predicted to vary as a T^5 [21] as observed.

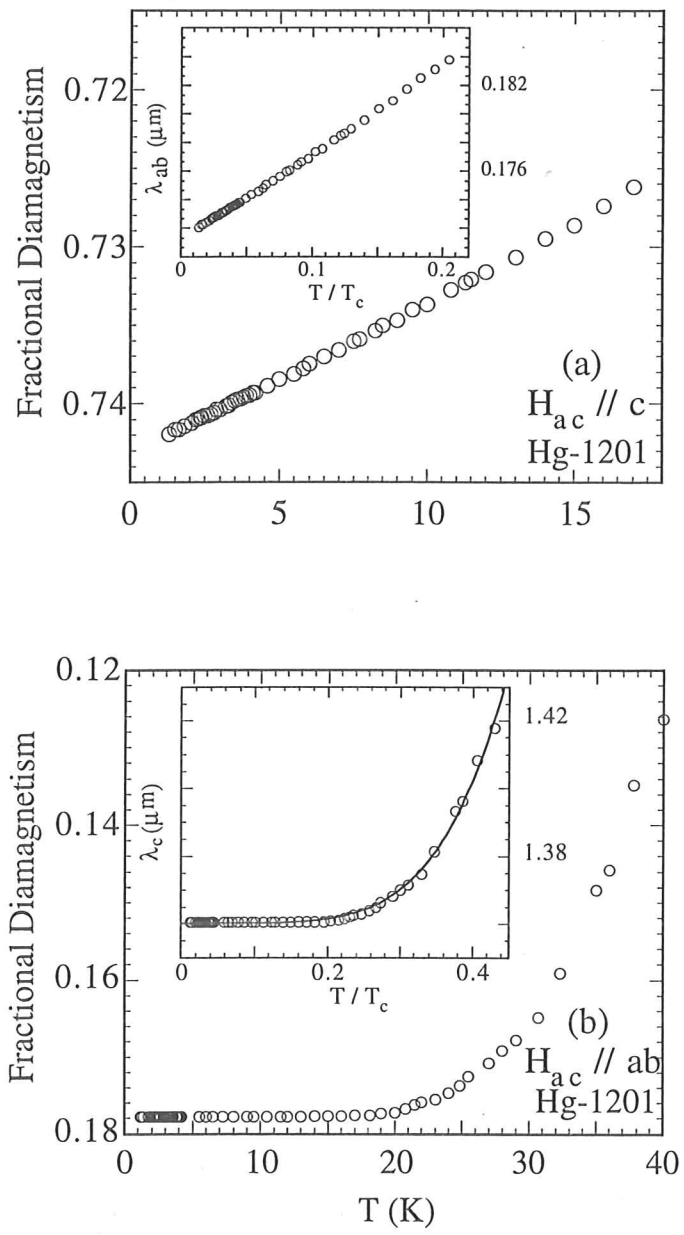

Fig. 6.1. The low temperature dependence of the fractional diamagnetism for a grain aligned sample of $HgBa_2CuO_{4+\delta}$ for (a) H_{ac} // c and (b) H_{ac} // ab. The insets in (a) and (b) show the temperature dependence of λ_{ab} and λ_c, respectively, of the same sample. Also shown, by the solid line in the inset (b) is a fit to the expression $\lambda_c\,(T) \sim \lambda_c\,(0)\,[1+ a(T/T_c)^5]$, with $a \sim 3$.

We believe that the weaker T dependence of λ_c compared to λ_{ab} is a consequence of the unusual c-axis electronic structure of high T_c oxides. In clean tetragonal samples, the c-axis hopping of holes mainly occurs through large radius Cu 4s orbitals [22]. It has been shown [21] that in this case the interlayer hopping constant of holes (t_c) is a function of the in-plane momentum $k_{//} = (k_x, k_y)$ and t_c is proportional to $(\cos k_x - \cos k_y)^2$. This unusual $k_{//}$ dependence of t_c originates from the wave function overlap between the bonding O 2p orbital and Cu 4s orbital that is proportional to $(\cos k_x - \cos k_y)$. Therefore, t_c vanishes along the lines (i.e. $k_x = \pm k_y$) where the $d_{x^2-y^2}$ wave gap nodes develop and will thus have a strong impact on the low T behaviour of λ_c if the superconducting pairing has $d_{x^2-y^2}$ symmetry. This leads to the T^5 dependence described above. This $k_{//}$ dependence of t_c is clearly apparent in band structure calculations for all tetragonal cuprates, including those with more than one CuO_2 layer per unit cell [23]. However, it is strongly violated for $YBa_2Cu_3O_{7-\delta}$ because of the presence of the Cu-O chain bands [22, 24].

The agreement between the theoretical analysis and the experimental result for the T^5 behaviour of λ_c implies that the gap nodes do in fact lie along the directions where t_c vanishes, i.e. $k_x = \pm k_y$, since otherwise this special $k_{//}$ dependence of t_c would have little effect and the T dependences of λ_{ab} and λ_c should be similar. Thus our results are consistent with not only the existence of the gap nodes but also the positions of the nodes on the Fermi surface.

The T^5 term in λ_c is small [$\sim (k_B T / \Delta_0)^5$]. It can be observed only in clean tetragonal samples of relatively low anisotropy where the coherent hopping of holes is the main contribution to the c-axis superfluid response. The contribution to λ_c from disorder effects is expected to vary as T^2 at low T [21, 25]. If disorder effects are important in the c-axis superfluid response, then the T^5 behaviour of λ_c will be completely masked by this T^2 behaviour. We believe this is the reason why the T^5 behaviour of λ_c has not been observed in Hg-1223 (see chapter 5 and below). The effect of impurities has been seen in penetration depth results of Zn doped YBCO (chapter 8). It

was also found that Zn substitution slightly increases the c-axis coupling which is consistent with the idea that the c-axis coupling in the cuprates is influenced by the in-plane Cu 4s orbitals.

We have performed similar measurements on Hg-1223 samples for which the values of $\lambda_{ab}(0)$ and $\lambda_c(0)$ are 1770 ± 90 and $61\,000 \pm 3000$ Å, respectively. As for Hg-1201 the $\lambda_{ab}(0)$ values were also confirmed on polycrystalline pellets by μSR measurements. $\lambda_{ab}(0)$ here is lower to that found in chapter 5 but roughly within the error of the experiment. Figures 6.2 (a) and (b) show the T dependence of the fractional diamagnetism for the ab-plane and the c-axis data, respectively. The T dependences of λ_{ab} and λ_c are again shown in the respective insets. The linear term in $\lambda_{ab}(T)$ has a slope of 4.2 Å/K. The data for $\lambda_c(T)$ are much flatter and a T^2 term develops at low T. As mentioned above, the T^2 behaviour of $\lambda_c(T)$ in Hg-1223 at low temperatures [fig. 6.2(b) (inset)] could be due to its high anisotropy. In highly anisotropic materials one expects a significant decrease in the coherent tunneling component of the superfluid along the c-direction [21]. This takes place without affecting $\lambda_{ab}(T)$ because propagation in the ab plane remains coherent. However, we note that the new $\lambda_c(T)$ data for Hg-1223 agree with those of chapter 5 for $T > 4.2$ K which entirely could be fitted reasonably well to a Josephson tunnelling model.

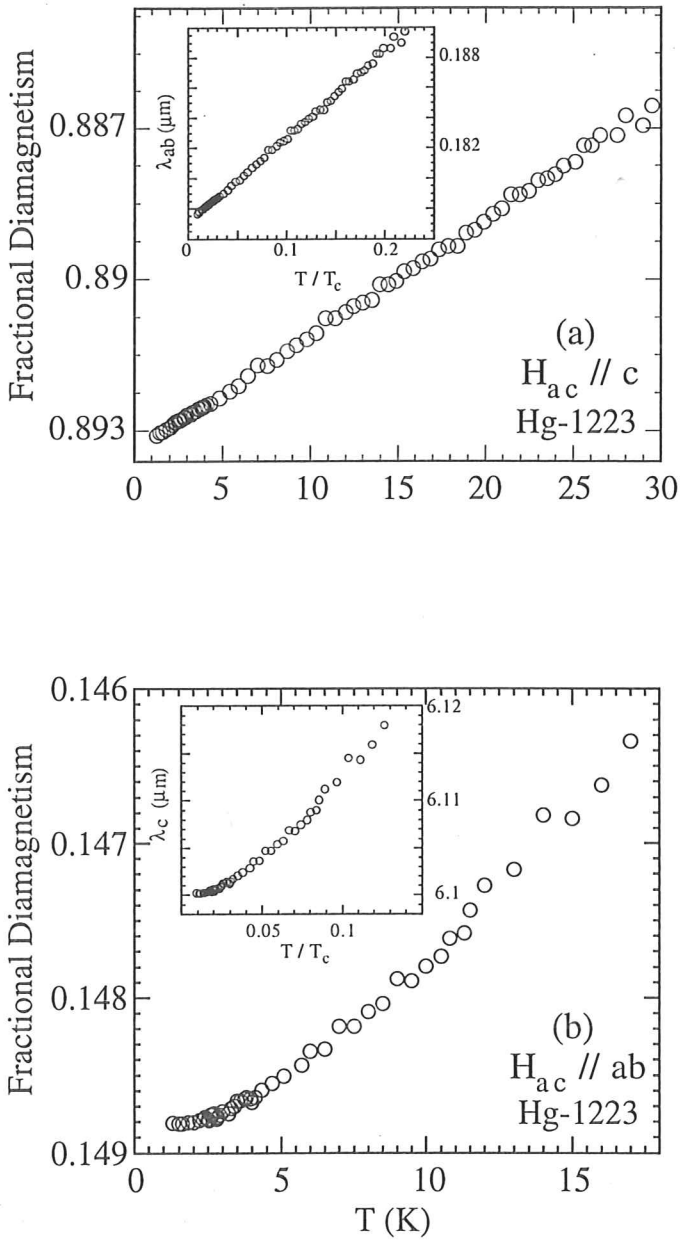

Fig. 6.2. The low temperature dependence of the fractional diamagnetism for a grain aligned sample of $HgBa_2Ca_2Cu_3O_{8+\delta}$ for (a) H_{ac} // c and (b) H_{ac} // ab. The insets in (a) and (b) show the temperature dependence of λ_{ab} and λ_c of the same sample.

Figure 6.3 shows typical data for high-quality grain aligned $YBCO_7$ and $YBCO_{6.57}$. For the more isotropic $YBCO_7$ (chapters 7 and 8) we observe a linear T dependence in λ_c at low temperatures but the relative change is about a factor of 2 smaller than in $[\lambda_{ab}(T) / \lambda_{ab}(0)]$ (taken from chapter 8 and shown as an inset in fig. 6.3). The weaker T dependence of λ_c may arise from the inter-band hopping between the planar and chain CuO bands [24, 26]. In $YBCO_7$ or other materials with Cu-O chains, t_c is finite around the d-wave gap nodes [i.e. t_c is no longer proportional to $(\cos k_x - \cos k_y)^2$] due to the hybridisation between the one-dimensional CuO chains and the CuO_2 planes. Thus the above discussion of the T^5 law is not applicable to $YBCO_7$. By removing oxygen from $YBCO_7$ one can significantly reduce the chain contribution. $YBCO_{6.57}$ has an anisotropy ratio $\gamma = [\lambda_c(0) / \lambda_{ab}(0)] \sim 25$ (chapter 7). As in Hg-1201, Hg-1223 and $YBCO_7$, $\lambda_{ab}(T)$ in $YBCO_{6.57}$ is linear at low temperatures but with a slope 20 Å/K. The systematic variation of λ_{ab} with oxygen content in YBCO will be discussed in chapter 7. Here we only mention $\lambda_c(T)$ of $YBCO_{6.57}$, fig. 6.3, which at low T obeys a T^2 behaviour similar to Hg-1223 which is of similar anisotropy.

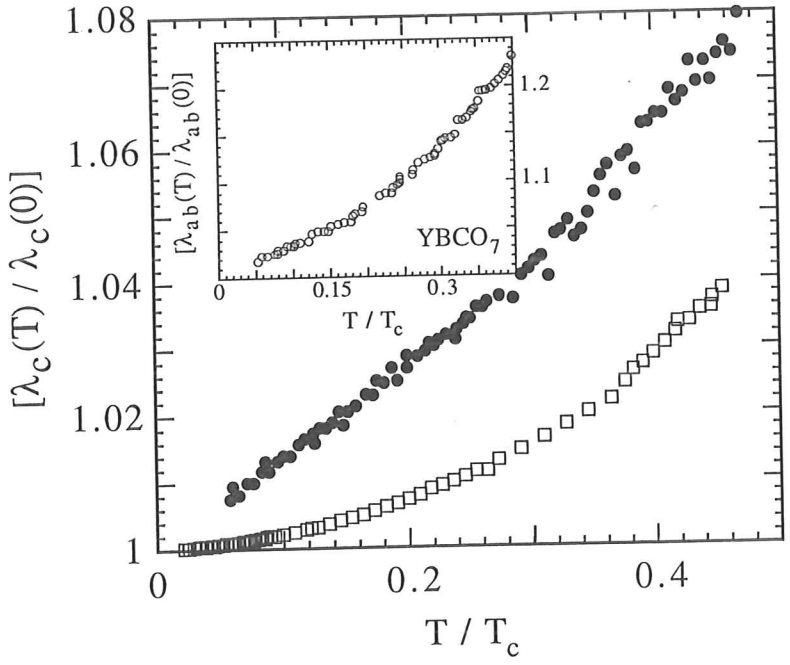

Fig. 6.3. The low temperature dependence of $[\lambda_c\ (T)\ /\ \lambda_c\ (0)]$ for grain aligned $YBa_2Cu_3O_7$ (closed circles) and $YBa_2Cu_3O_{6.57}$ (open squares). $\lambda_c(0)$ for these samples are 12 600 Å and 71 700 Å, respectively. For comparison with $[\lambda_c\ (T)\ /\ \lambda_c(0)]$ the inset shows $[\lambda_{ab}(T)\ /\ \lambda_{ab}\ (0)]$ data of $YBa_2Cu_3O_7$ (chapter 7).

We should mention that SQUID measurements of the Hg-1201 and Hg-1223 powders used to make the aligned composites yielded normal state Curie terms $C = 52 \times 10^{-3}/T$ and $75 \times 10^{-3}/T$ (emu / mole), respectively. In principle such Curie terms could affect our low T ac susceptibility data especially those for $H_{ac} // ab$. However, the ac measurements have been made down to 1.2 K, for both $H_{ac} // c$ and $H_{ac} // ab$ and it is clear that a Curie Weiss law $\chi = [C / (T+\Theta)]$ with $\Theta = 0$ does not describe the low T data for either field orientation. If $\Theta \geq 10$ then the effects of these Curie terms are completely negligible. The worst case scenario is $\Theta = 2$ - 3 which gives small correction to $\lambda_c(T)$, of the size of the symbols used in figs. 6.1(b) and 6.2(b), while $\lambda_{ab}(T)$ is unchanged.

6.4 Summary

We have investigated the low temperature dependence of the anisotropic magnetic penetration depth of magnetically aligned powders of crystalline $HgBa_2Ca_{n-1}Cu_nO_{2n+2+\delta}$ (n=1 and 3) down to 1.2 K. The values of $\lambda_{ab}(0)$, $\lambda_c(0)$ for n=1 and 3 were estimated to be 1710 ± 100, 13 600 ± 1200 Å and 1770 ± 90, 61 000 ± 3000 Å, respectively. The T dependence of λ is not affected by this level of uncertainty in $\lambda(0)$. A linear $\lambda_{ab}(T)$ was observed at low temperatures for both Hg-1201 and Hg-1223 with slopes 6.5 and 4.2 Å/K, respectively. On the other hand, the out-of-plane component, $\lambda_c(T)$, varied as T^5 and T^2 for Hg-1201 and Hg-1223, respectively. Furthermore, $\lambda_c(T)$ for $YBCO_7$ varies as T whereas a T^2 power law was observed for $YBCO_{6.57}$.

References

[1] For example, J.F. Annett, N. Goldenfeld, and A. Leggett, in *Physical Properties of High Temperature Superconductors* edited by D. M. Ginsberg (World Scientific, Singapore, 1996), cond-mat / 9601060.

[2] D. J. Van Harlingen, Rev. Mod. Phys. **67**, 515 (1995).

[3] W. N. Hardy, D.A. Bonn, D.C. Morgan, Ruixing Liang, and Kuan Zhang, Phys. Rev. Lett. **70**, 3999 (1993); D.A. Bonn, S. Kamal, K. Zhang, R.X. Liang and W. N. Hardy, J. Phys. Chem. Solids, **56**, 1941 (1995) .

[4] C. Panagopoulos, W. Zhou, N. Athanassopoulou and J.R. Cooper, Physica C **269**, 157 (1996).

[5] A. Porch, J.R. Cooper, D.N. Zheng, J.R. Waldram, A.M. Campbell and P.A. Freeman, Physica C **214**, 350 (1993).

[6] C. Panagopoulos, J.R. Cooper, N. Athanassopoulou and J.Chrosch, Phys. Rev. B **54**, R12721 (1996).

[7] T. Shibauchi, H. Kitano, K. Uchinikura, A. Maeda, T. Kimura, and K. Kishio, Phys. Rev. Lett. **72**, 2263 (1994).

[8] J.R. Cooper, Phys. Rev. B **54**, R3753 (1996), and references therein.

[9] J.R. Cooper, L. Forro, and B. Keszei, Nature **343**, 444 (1990).

[10] A. Maeda, Y. Iino, T. Hanaguri, N. Motohira, K. Kishio and T. Fukase, Phys. Rev. Lett. **74**, 1202 (1995).

[11] T. Jacobs, S. Sridhar, Q. Li, G.D. Gu and N. Koshizuka, Phys. Rev. Lett. **75**, 4516 (1995).

[12] S.-F. Lee, D.C. Morgan, R.J. Ormeno, D. Broun, R.A. Doyle, J.R. Waldram and K. Kadowaki, Phys. Rev. Lett. **77**, 735 (1996).

[13] C. Panagopoulos, J.R. Cooper, G.B. Peacock, I. Gameson, P.P. Edwards, W. Schmidbauer and J.W. Hodby, Phys. Rev. B **53**, R2222 (1996).

[14] J.L. Wagner, P.G. Radaelli, D.G. Hinks, J.D. Jorgensen, J.F. Mitchell, B. Dabrowski, G.S. Knapp and M.A. Beno, Physica C **210**, 447 (1993).

[15] J.L. Wagner, B.A. Hunter, D.G. Hinks and J.D. Jorgensen, Phys. Rev. B **51**, 15407 (1995).

[16] R. Beyers and T.M. Shaw in "Solid State Physics - Volume 42" edited by H. Ehrenreich and D. Turnbull (Academic press, inc. London 1989).

[17] G. B. Peacock, I. Gameson, and P. P. Edwards (in preparation).

[18] G. B. Peacock, I. Gameson, and P. P. Edwards, Adv. Mater. (in press)

[19] J. Chrosch, C. Panagopoulos, N. Athanassopoulou, J.R. Cooper and E.K.H. Salje, Physica C **265**, 233 (1996).

[20] D. Shoenberg, *Superconductivity* (Cambridge University Press, Cambridge, 1954), p.164.

[21] T. Xiang and J.M. Wheatley, Phys. Rev. Lett. **77**, 4632 (1996).

[22] O.K. Andersen, A.I. Liechtenstein, O. Jepsen and P. Paulsen, J. Phys. Chem. Solids, **56** 1573 (1995).

[23] D.L. Novikov and A.J. Freeman, Physica C **212**, 233 (1993); D.L. Novikov, V.A. Gubanov and A.J. Freeman, *ibid* **210**, 301 (1993).

[24] T. Xiang and J.M. Wheatley, Phys. Rev. Lett. **76**, 134 (1996).

[25] R.J. Radtke, V.N. Kostur and K. Levin, Phys. Rev. B **53**, R522 (1996).

[26] W.A. Atkinson and J.P. Carbotte cond-mat / 9612058.

Chapter 7

The systematics of the in-plane penetration depth of high- T_c cuprates

7.1 Introduction

In chapter 6 we reported the values and temperature dependences of the in-plane (λ_{ab}) and out-of-plane (λ_c) penetration depths for slightly overdoped [1,2] $HgBa_2CuO_{4+\delta}$ (Hg-1201) with critical temperature T_c = 93 K and underdoped [3,4] $HgBa_2Ca_2Cu_3O_{8+\delta}$ (Hg-1223) with T_c = 134.5 K. For both Hg-cuprates the low temperature dependence of the in-plane penetration depth, $\lambda_{ab}(T)$, was found to be strongly linear with slopes 6.5 Å/K for Hg-1201 and 4.2 Å/K for Hg-1223. The difference in the values of the linear term of the two Hg-cuprates is rather interesting and deserves further attention. To this aim we have extended our investigation in fully oxygenated and deoxygenated (underdoped) pure $YBa_2Cu_3O_{7-\delta}$ and measured the penetration depth of grain aligned powder composites.

In this chapter we report experimental results on the values and temperature dependences of λ_{ab} and λ_c of high quality c - axis grain aligned orthorhombic [5] $YBa_2Cu_3O_{7-\delta}$ with δ = 0.0, 0.3 and 0.43, which have two CuO_2 planes per unit cell as well as Cu-O chains and compare them to those of tetragonal [6] Hg-1201 with one CuO_2 plane per unit cell and tetragonal [7] Hg-1223 with three CuO_2 planes per unit cell. We find that irrespective of the carrier concentration, number of CuO_2 planes per unit cell, crystal structure, presence of Cu-O chains, and anisotropy, the low temperature λ_{ab} varies linearly with T and the maximum superconducting energy gap (Δ_0) in cuprate superconductors with d- wave order parameter scales linearly with T_c.

7.2 Experimental

Sample preparation was carried out by the standard solid state reaction process using high purity (99.999%) Y_2O_3, $BaCO_3$ and CuO oxides. (The solid state reaction process was carried out by Dr. J.R. Cooper at the IRC in Superconductivity.) Bulk pieces were separately annealed in appropriate oxygen atmospheres and temperatures for 12h to obtain the required δ values. The fully oxygenated, $\delta = 0.0$ ($YBCO_7$, $T_c = 92$ K), samples were prepared by annealing in pure oxygen atmosphere at 380 °C for 24 hours and then slowly cooled to room temperature. The $\delta = 0.3$ ($YBCO_{6.7}$, $T_c = 66$ K) samples were prepared by annealing in pure oxygen atmosphere at 650° for 12 h and then quenching in liquid nitrogen. Finally, the $\delta = 0.43$ ($YBCO_{6.57}$, $T_c = 55$ K) samples were prepared by annealing in 0.2% O_2 / N_2 atmosphere at 550 °C for 12 hours and then quenching into liquid nitrogen. The final oxygen contents of $\delta = 0.0$, 0.3 and $\delta = 0.43$ were verified from the weight change of a fully oxygenated sintered sample, used as a reference, which was heat treated together with the respective samples. The $\delta = 0.0$ bulk piece was lightly ground and sedimented in acetone to obtain well defined grain size distribution. The sedimented powders were heat treated as discussed in chapter 4 to repair any structural damages to the surface of the grains. For $\delta = 0.3$ and 0.43 a bulk piece for each δ was lightly ground and sieved through a 20 μm sieve in an argon glove box to avoid surface degradation of the crystallites (chapter 4) and obtain a well defined grain size distribution (chapter 2). The collected powders were then kept in argon atmosphere for 30 min. All powders were magnetically aligned. The average grain diameters were 5 and 10 μm for the fully oxygenated and the oxygen deficient samples, respectively. Quantitative and qualitative checks of the sample alignment were made by the X-ray diffraction technique described in chapter 3. The fraction of the unoriented powder in all grain aligned samples was estimated to be < 5%. Rocking curve analysis of the $\delta = 0.0$ and $\delta > 0.0$ samples gave a full width at half maximum of approximately $\pm 1.4^\circ$ and $\pm 1^\circ$, respectively.

Low field susceptibility, χ, measurements were performed using the commercial equipment (down to 4.2 K) for samples with $\delta = 0.0$, 0.3 and 0.43. Samples with $\delta =$ 0.43 were also measured at low temperatures using the home built susceptometer (down to 1.2 K). The earth's field was screened out using a mu-metal shield. Measurements were performed for an applied ac field $H_{ac} = 0.3$ - 3 G rms at $f = 333$ Hz. For all data presented here $H_{ac} = 3$ G rms and $f = 333$ Hz. The separation of the grains and the absence of weak links were confirmed and the background signal was subtracted from the data at each temperature. The apparatuses were calibrated as described in chapters 4-6 and the data were analysed using London's model (chapter 2).

7.3 Results and discussion

The measured values of $\lambda_{ab}(0)$ for $\delta = 0.0$, 0.3 and 0.43 are 0.14, 0.21 and 0.29 μm whereas the $\lambda_c(0)$ values are 1.26, 4.53 and 7.17 μm, respectively. These results are in contrast to previous work [8] in which the surfaces of the particles were probably not as clean and the degree of grain alignment was significantly lower. As T_c is reduced with oxygen deficiency, $[1 / \lambda_{ab}^2(0)]$ falls very quickly in close agreement to the Uemura relation [9,10], which holds when T_c is reduced by lowering the carrier concentration. The anisotropy ratio $\gamma = [\lambda_c(0) / \lambda_{ab}(0)]$ increases with oxygen deficiency signifying the increase of the system's anisotropy.

Figures 7.1 (a) and (b), show characteristic low temperature plots of $[\lambda(T) / \lambda(0)]$ for the *ab*-plane and *c*-axis data, respectively, for the three oxygen concentrations studied. The maximum error in $\lambda(T)$ is less than the size of the symbols used in figs. 7.1(a) and (b). The low temperature linear term in $\lambda_{ab}(T)$, consistent with *d*-wave superconductivity, for $YBCO_7$ gives ~ 4.7 Å/K. Furthermore, it is in very good agreement with that found earlier from microwave measurements on $YBCO_{6.95}$ single crystals [11]. As oxygen is removed from the lattice (the chains) the linear term increases to 12 and 20 Å/K for $\delta =$ 0.3 and 0.43, respectively. For $YBCO_7$ we also observe a linear T dependence in λ_c at

low temperatures but the relative change is about a factor of two smaller than in [$\lambda_{ab}(T)$ / $\lambda_{ab}(0)$]. The T dependence in λ_c for $YBCO_7$ is in strong contrast to that of Hg-1201 (chapter 6) which showed a T^5 dependence due to the c-axis hopping of holes through large radius Cu 4s orbitals. The linear $\lambda_c(T)$ in $YBCO_7$ may arise from the inter-band hopping between the planar and chain CuO bands [12]. In $YBa_2Cu_3O_{7-\delta}$ or other materials with Cu-O chains, the interlayer hopping constant of holes is finite around the d-wave gap nodes due to the hybridisation between the one-dimensional Cu-O chains and the CuO_2 planes. Removing oxygen from the chains causes this "proximity" effect from the chains to the neighbouring planes to be suppressed and eventually get a lower dimensionality and thus higher anisotropy [12,13]. $\lambda_c(T)$ of $YBCO_{6.7}$ and $YBCO_{6.57}$ at low T obeys a T^2 behaviour similar to Hg-1223 which is of similar anisotropy (chapter 6). Details on the systematics of $\lambda_c(T)$ of cuprate superconductors were discussed in chapter 6.

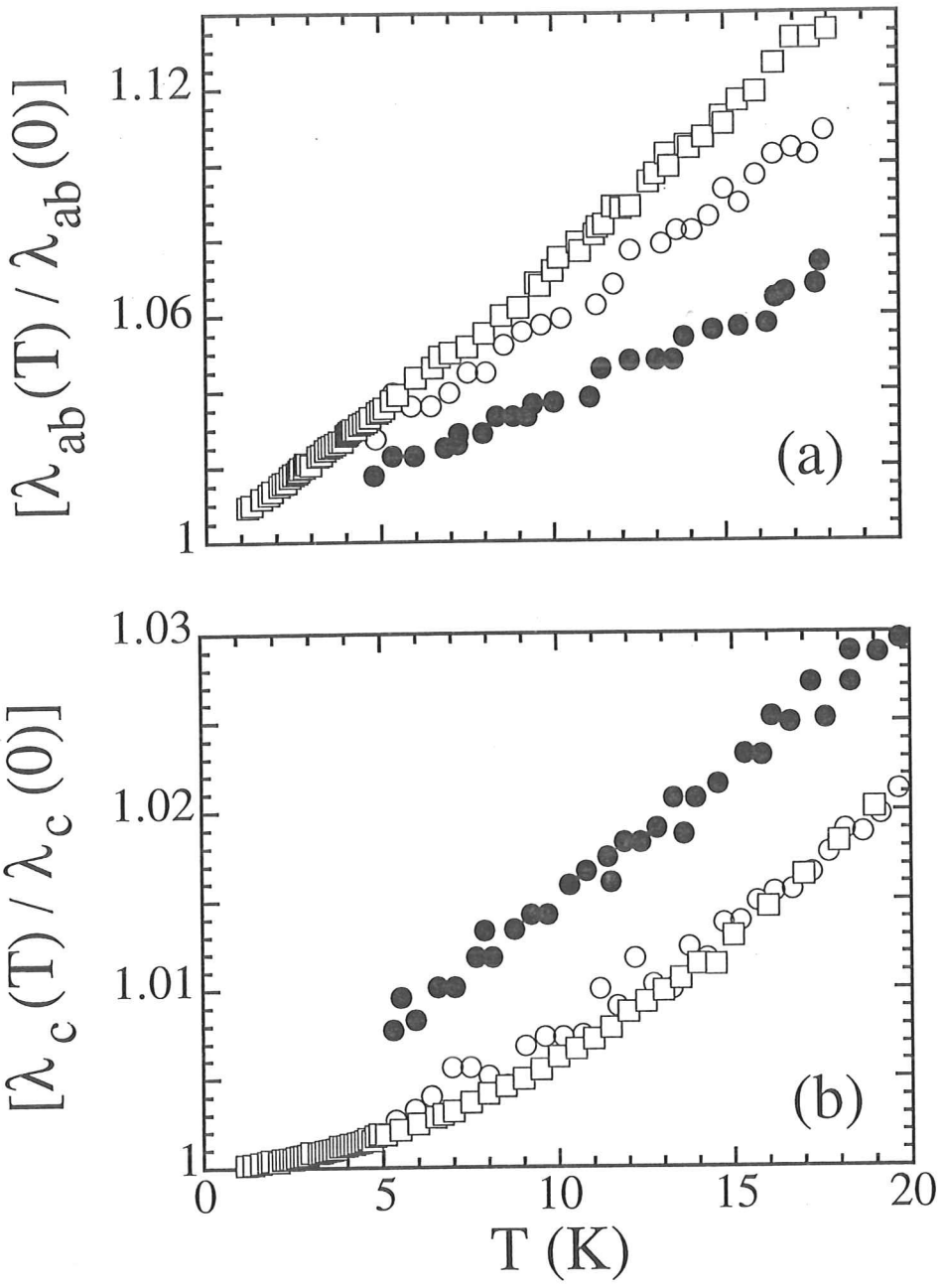

Fig. 7.1. Low temperature plots of (a) $[\lambda_{ab}(T) / \lambda_{ab}(0)]$ and (b) $[\lambda_c(T) / \lambda_c(0)]$ for $YBCO_7$ (closed circles), $YBCO_{6.7}$ (open circles) and $YBCO_{6.57}$ (open squares). The T_c, $\lambda_{ab}(0)$ and $\lambda_c(0)$ values are given in the text.

Figure 7.2, depicts the temperature dependences of the normalised superfluid densities $[\lambda_{ab}(0) / \lambda_{ab}(T)]^2$ and $[\lambda_c(0) / \lambda_c(T)]^2$, for $\delta = 0.0$, 0.3 and 0.43. There is an excellent agreement between the $[\lambda_{ab}(0) / \lambda_{ab}(T)]^2$ curves for the three oxygen concentrations. The $[\lambda_c(0) / \lambda_c(T)]^2$ curves on the other hand slightly differ from each other probably due to the sensitivity of $\lambda_c(T)$ to the anisotropy of the system. The sensitivity of $\lambda_c(T)$ to the anisotropy of the system was discussed in chapters 5 and 6 and further evidence is given in chapter 8. The agreement of the $[\lambda_{ab}(0) / \lambda_{ab}(T)]^2$ curves for $\delta = 0.0$, 0.3 and 0.43 indicates that the BCS ratio ($2\Delta_0 / k_B T_c$) does not change, at least for the δ values studied here.

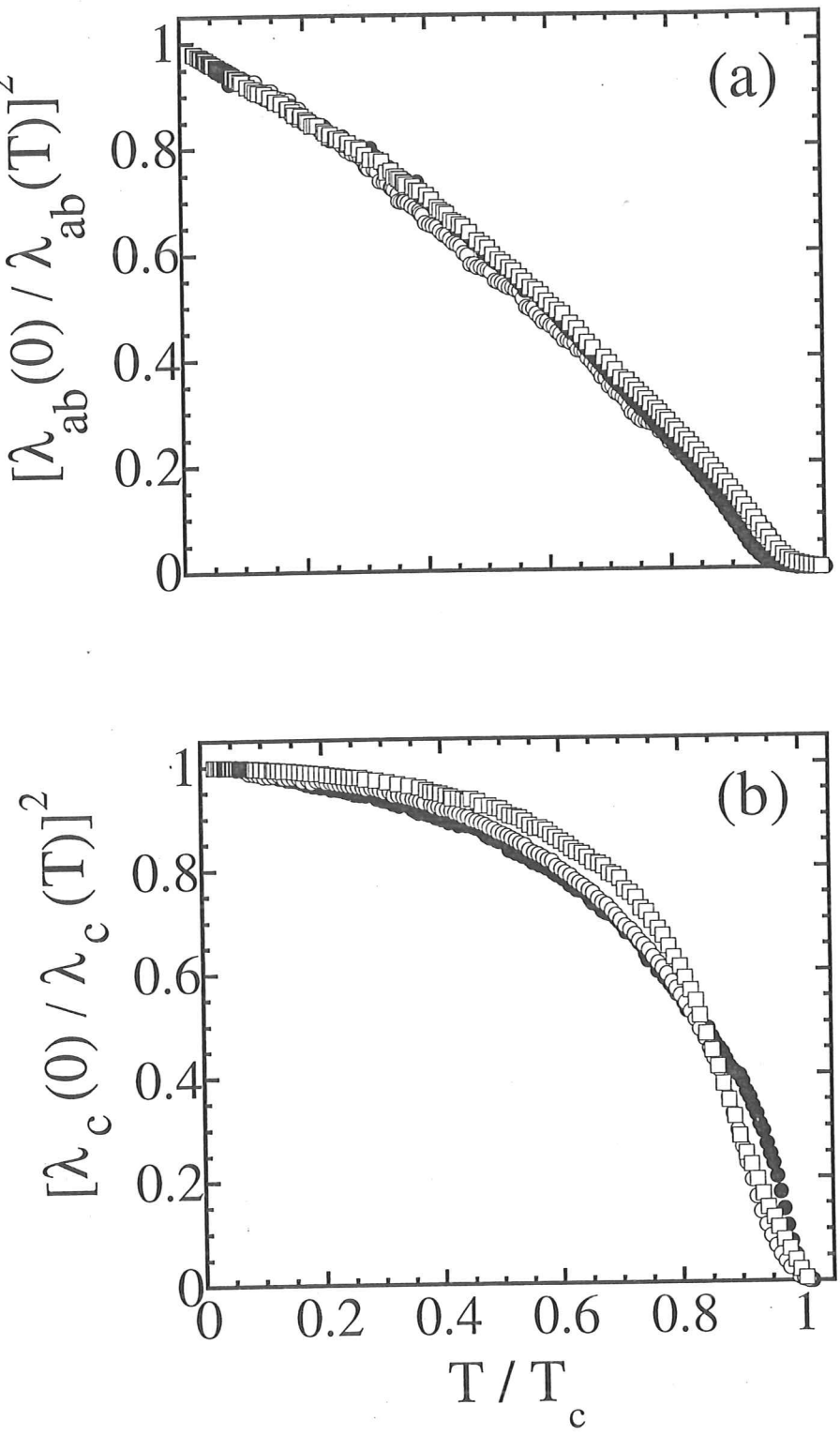

Fig. 7.2. Plots of (a) $[\lambda_{ab}(0) / \lambda_{ab}(T)]^2$ and (b) $[\lambda_c(0) / \lambda_c(T)]^2$ as functions of T / T_c for $YBCO_7$ (closed circles), $YBCO_{6.7}$ (open circles) and $YBCO_{6.57}$ (open squares).

Using a simple mean field weak-coupling model Won and Maki [14] predict that in the clean limit the low temperature superfluid density is given by

$$[\lambda(0) / \lambda(T)]^2 \approx 1 - 2\,(T / \Delta_0)\,\ln 2. \qquad (1)$$

In fig. 7.3(a), we plot $\{1-[\lambda_{ab}(0) / \lambda_{ab}(T)]^2\}$ vs T for all the cuprate superconductors we have measured so far. The cuprate with the highest T_c, Hg-1223, has the smallest slope and the latter increases as T_c decreases. Using eq. (1) and the slopes of the curves in fig. 7.3(a) we plot fig. 7.3(b) which gives $\Delta_0 \approx 2T_c$. For comparison we also include data for the *s*-wave perovskite $Ba_{0.6}K_{0.4}BiO_3$ (BKBO) (taken from chapter 5) where we have multiplied Δ_0, as obtained from a fit of the weak-coupling curve for a BCS *s*-wave superconductor, by its T_c. On the basis of the materials plotted in fig. 7.3(b), the scaling of T_c to Δ_0 is independent of the number of CuO_2 planes per unit cell, carrier concentration, crystal structure, presence of chains and anisotropy of the cuprate.

The penetration depth results for the samples in the underdoped regime are in contrast to results obtained from angle-resolved photoemission spectroscopy (ARPES) [15], at least for the $YBa_2Cu_3O_{7-\delta}$ samples where direct comparison with ARPES data is currently possible, where Δ_0 was found to be constant or slightly increasing while T_c is reduced. The contradiction between these measurements is an important puzzle and more systematic investigation is required in order to gain a deeper understanding of the pairing state.

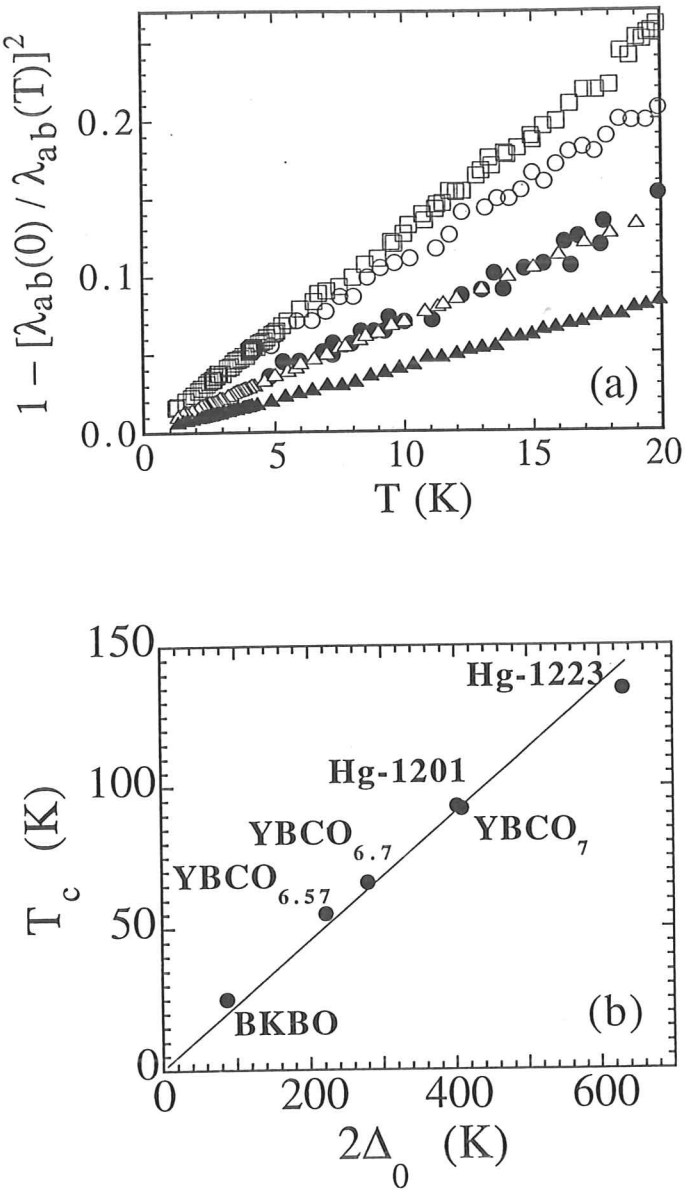

Fig. 7.3. (a) Plot of {1- [$\lambda_{ab}(0)$ / $\lambda_{ab}(T)$]^2} versus T for Hg-1223 [$\lambda_{ab}(0) \approx 1770$ Å and $\lambda_c(0) \approx 61\,000$ Å] (closed triangles), Hg-1201 [$\lambda_{ab}(0) \approx 1710$ Å and $\lambda_c(0) \approx 13600$ Å] (open triangles), $YBCO_7$ (closed circles), $YBCO_{6.7}$ (open circles) and $YBCO_{6.57}$ (open squares). (b) T_c versus $2\Delta_0$ as derived from the plot in panel (a) using eq. (1) in the text. BKBO is included for comparison (see text for details). The solid line is drawn as a guide to the eye. The maximum error in (b) is of the size of the symbols.

7.4 Summary

We have studied $\lambda_{ab}(T)$ and $\lambda_c(T)$ of high quality grain-aligned $YBa_2Cu_3O_{7-\delta}$ with $\delta =$ 0.0, 0.3 and 0.43. The values of $\lambda_{ab}(0)$, $\lambda_c(0)$ and γ were found to increase with oxygen deficiency. The temperature dependences of λ_{ab} for all three oxygen concentrations follow very closely the behaviour expected for a weak-coupling *d*-wave superconductor. We find that the presence of the linear term in $\lambda_{ab}(T)$ is independent of the number of CuO_2 planes per unit cell, carrier concentration, crystal structure, presence of chains and anisotropy. From the change of the low temperature linear slope of $\lambda_{ab}(T)$ for $YBa_2Cu_3O_{7-\delta}$ (δ = 0.0, 0.3 and 0.43), $HgBa_2Ca_{n-1}Cu_nO_{2n+2+\delta}$ (n=1 and 3) and using the Won and Maki model [14] we find that in *d*- wave cuprate superconductors Δ_0 scales linearly with T_c. Finally, the low temperature $\lambda_c(T)$ behaviour was linear for $YBCO_7$ but T^2 for the oxygen deficient samples.

References

[1] G. B. Peacock, I. Gameson, and P. P. Edwards (in preparation).

[2] Q. Xiong, Y.Y. Xue, Y. Cao, F. Chen, Y.Y. Sun, J. Gibson, C.W. Chu, L.M. Liu and A. Jacobson, Phys. Rev. B **50**, 10346 (1994).

[3] G. B. Peacock, I. Gameson, and P. P. Edwards, Adv. Mater. (in press)

[4] A. Carrington, D. Colson, Y. Dumont, C. Ayache, A. Bertinotti and J.F. Marucco, Physica C **234**, 1 (1994); C.K. Subramaniam, M. Paranthaman and A.B. Kaiser, Phys. Rev. B **51**, 1330 (1995).

[5] R. Beyers and T.M. Shaw in "Solid State Physics - Volume 42" edited by H. Ehrenreich and D. Turnbull (Academic press, inc. London 1989).

[6] J.L. Wagner, P.G. Radaelli, D.G. Hinks, J.D. Jorgensen, J.F. Mitchell, B. Dabrowski, G.S. Knapp and M.A. Beno, Physica C **210**, 447 (1993).

[7] J.L. Wagner, B.A. Hunter, D.G. Hinks and J.D. Jorgensen, Phys. Rev. B **51**, 15407 (1995).

[8] N. Athanassopoulou, J.R. Cooper and J. Chrosch, Physica C **235-240**, 1835 (1994).

[9] J. L. Tallon *et al*, Phys. Rev. Lett. **74**, 1008 (1995); C. Bernhard*et al*, Phys. Rev. B **52**, 10 488 (1995).

[10] Y.J. Uemura *et al.*, Phys. Rev. Lett. **66**, 2665 (1991).

[11] W. N. Hardy, D.A. Bonn, D.C. Morgan, Ruixing Liang, and Kuan Zhang, Phys. Rev. Lett. **70**, 3999 (1993).

[12] T. Xiang and J.M. Wheatley, Phys. Rev. Lett. **76**, 134 (1996).

[13] T. Xiang and J.M. Wheatley, Phys. Rev. Lett. **77**, 4632 (1996).

[14] H. Won and K. Maki, J. Phys. I France **6**, 1 (1996)

[15] J.M. Harris, Z.-X. Shen, P.J. White, D.S. Marshall, M.C. Schabel, J.N. Eckstein and I. Bozovic, Phys. Rev. B **54**, R15 665 (1996).

Chapter 8

The effects of Zn doping on the anisotropic penetration depth of $YBa_2Cu_3O_7$

8.1 Introduction

In $YBa_2Cu_3O_7$ (YBCO), one of the substituents of much interest is Zn, with a nonmagnetic d^{10} configuration, because it replaces the in-plane copper atoms Cu(2) and rapidly suppresses the superconducting transition temperature T_c [1]. Previous penetration depth studies [2] showed that as little as 0.31% Zn substitution causes a crossover from a linear temperature (T) dependence of the in-plane penetration depth to a T^2. This was interpreted as the effect of strong scattering on a d-wave superconductor [3]. The reason Zn causes a rapid decrease in T_c is still unclear. On the basis of the existence of a linear term in the heat capacity data below T_c it was initially suggested that Zn acts as a pair breaker [4]. Since then others have proposed that Zn induces a small magnetic moment on neighbouring Cu sites [5,6] and that magnetic scattering is responsible for the depression of T_c. On the other hand recent analysis [7] of specific heat and susceptibility data of Zn doped YBCO and $La_{2-x}Sr_xCuO_{4-y}$ leads to a picture in which Zn doping simply causes a shift of spectral weight to low energies rather than the formation of a true magnetic moment on neighbouring Cu sites. The latter picture is perhaps more consistent with the NMR study of Ishida et al [8] where well defined magnetic moments on Ni atoms, which also substitute on the Cu(2) sites of YBCO, have a much smaller effect on the low temperature Knight shift than Zn.

To the best of our knowledge, there are no systematic studies on the effects of Zn doping to the absolute values and T dependences of the in-plane, λ_{ab}, and out-of-plane,

λ_c, magnetic penetration depths of the cuprates. Furthermore, no complete theory is currently available to predict the possible effects of high concentrations of scattering impurities to the anisotropic penetration depth of *d*-wave superconductors. It is thus important to have systematic experimental evidence to determine the empirical effects of Zn substitution. Using the ac-susceptibility technique we obtained the absolute values and T dependences of λ_{ab} and λ_c for high quality magnetically aligned YBCO, which show large systematic changes with Zn content.

8.2 Experimental

Bulk $YBa_2(Cu_{1-x}Zn_x)_3O_7$ samples with x = 0.00, 0.02, 0.03 and 0.05 were prepared by solid state reaction, from CuO, Y_2O_3, ZnO and $BaCO_3$. (The solid state reaction procedure was carried out by Dr. J.R. Cooper at the IRC in Superconductivity.) Each bulk sample was lightly ground and sedimented in acetone to obtain well defined grain size distributions. The sedimented powders were heat treated as described in chapter 4 to repair any structural damages to the surface of the grains and obtain maximum oxygen concentration. After the heat treatment part of the collected powder for each Zn concentration was used to determine the grain-size distribution. The average grain diameter, 50% cumulative volume point, for all samples studied here was 5 μm. The powders were mixed with a 5 min fast curing epoxy and aligned in a static field of 12 T at room temperature. Details on the degree of alignment can be found in chapter 3. The T_c's for the different Zn compositions were 92.5 K, 68.2 K, 55 K and 46.4 K for x = 0.00, 0.02, 0.03 and 0.05, respectively, in reasonable agreement with values reported previously in the literature for fully oxygenated samples of similar Zn contents [6]. Actually our unpublished data for several sets of Zn : YBCO samples show that the T_c value of the 0.05 Zn sample corresponded to 0.045 Zn. We use the latter value in subsequent analysis.

Ac susceptibility (χ) measurements were performed using the commercial ac susceptometer with the ac field applied either in the *ab*-plane or along the *c*-axis. The χ data were analysed in the manner described in chapter 2 and Ref. 9 and the variation of λ with temperature for both orientations was obtained.

8.3 Results and discussion

The values of T_c, $\lambda_{ab}(0)$, $\lambda_c(0)$ and the anisotropy ratio $\gamma = [\lambda_c(0) / \lambda_{ab}(0)]$, for the Zn concentrations studied here are listed in Table 8.1. As T_c is reduced by Zn doping $\lambda_{ab}^{-2}(0)$ falls very quickly. The fall is even faster than the Uemura relation [10], $\lambda_{ab}^{-2}(0) \propto T_c$, which holds for underdoped materials (chapter 7) where T_c is reduced by lowering the carrier concentration rather than by adding impurities to the CuO_2 planes. Our $\lambda_{ab}(0)$ values for $x \geq 0.02$ are in good agreement with those obtained from muon spin relaxation measurements independently at the same time on optimally doped polycrystalline $Y_{0.8}Ca_{0.2}Ba_2(Cu_{1-y}Zn_y)_3O_{7-\delta}$ [11]. In the latter work the Cu-O chain contribution to $\lambda_{ab}(0)$ was deliberately suppressed by incorporating Ca and adjusting the oxygen content for maximum T_c. This implies that in our work the Cu-O chain contribution has been suppressed by $x = 0.02$ or more Zn which is consistent with the analysis described later.

x	T_c (K)	$\lambda_{ab}(0)$ (μm)	$\lambda_c(0)$ (μm)	$\lambda_c(0)/\lambda_{ab}(0)$
0.00	92.5	0.14	1.26	9.0
0.02	68.2	0.26	1.42	5.6
0.03	55.0	0.30	1.55	5.2
0.05	46.4	0.37	1.64	4.4

Table 8.1. Table of T_c, $\lambda_{ab}(0)$, $\lambda_c(0)$ and $[\lambda_c(0) / \lambda_{ab}(0)]$ as a function of $x = 0.00$, 0.02, 0.03 and 0.05 for $YBa_2(Cu_{1-x}Zn_x)_3O_7$.

The temperature dependences of λ_{ab} and λ_c are shown in figs 8.1(a) and 8.1(b) as plots of $1/\lambda^2$ versus T because in the London model $1/\lambda^2 = 4\pi\, n_s e^2/m^*$, where n_s is the superfluid density and m^* is the effective mass. Figure 8.1(a) shows that as Zn is added the quasi-linear dependence of $1/\lambda_{ab}^2(T)$ gradually evolves into a T^2 behaviour at low T consistent with the single crystal results at lower x values [2]. On these unnormalised plots the slopes near T_c are independent of x for $x \geq 0.02$. Figure 8.1(b) shows that $1/\lambda_c^2(T)$ for $x = 0.00$ also has an initial linear dependence at low T but is much flatter. Possible explanations for this behaviour were given in chapters 6 & 7 and are also briefly mentioned below. This linear dependence becomes T^2 with the addition of Zn. Again the slopes near T_c are independent of x for $x \geq 0.02$. Normalised plots of $[\lambda(0)/\lambda(T)]^2$ versus T/T_c are shown in figs. 8.2(a) and 8.2(b). These show similar overall behaviour for $\lambda_{ab}(T)$ in the region $0 < x \leq 0.03$ and for $\lambda_c(T)$ for $0.02 < x \leq 0.05$.

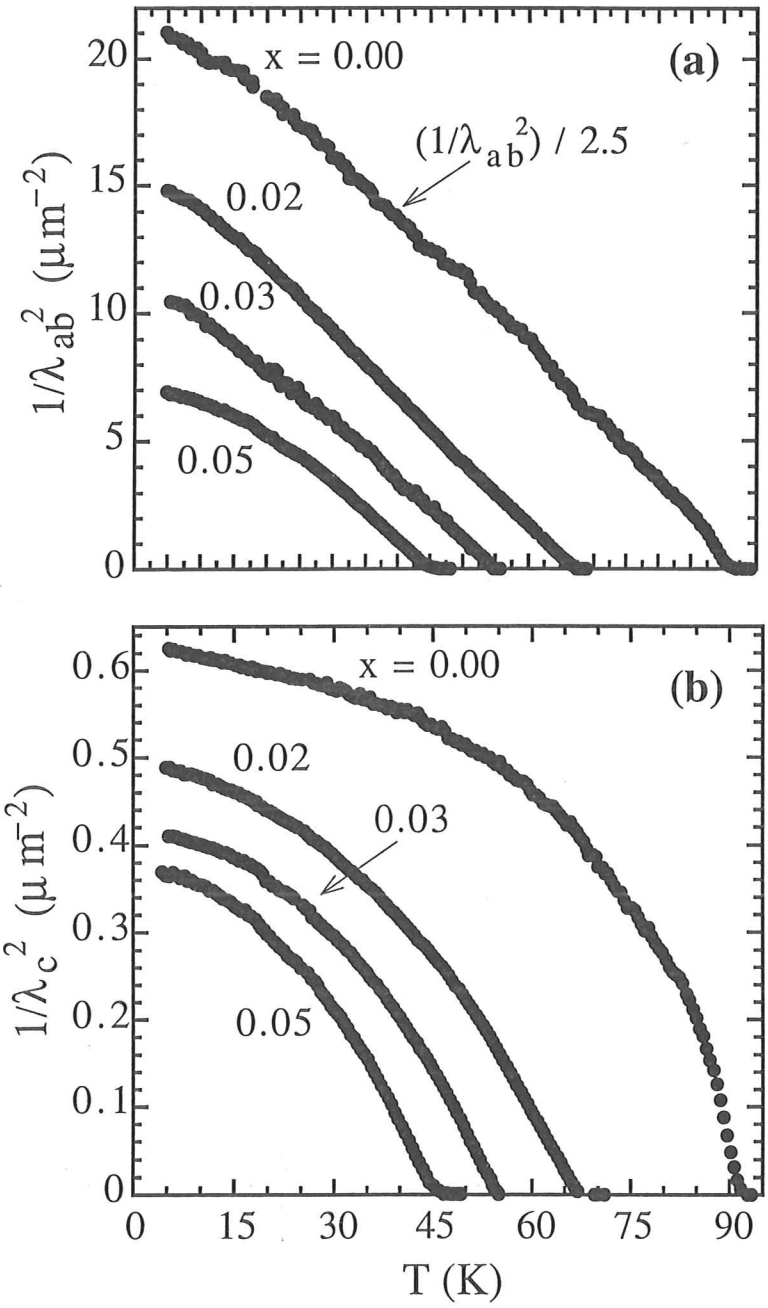

Fig. 8.1. Plots of (a) $(1 / \lambda_{ab})^2$ and (b) $(1 / \lambda_c)^2$ as functions of T for $YBa_2(Cu_{1-x}Zn_x)_3O_7$ with $x = 0.00$, 0.02, 0.03 and 0.05. The $[1 / \lambda_{ab}^2(T)]$ data for $x = 0.00$ in (a) have been divided by 2.5 for clarity.

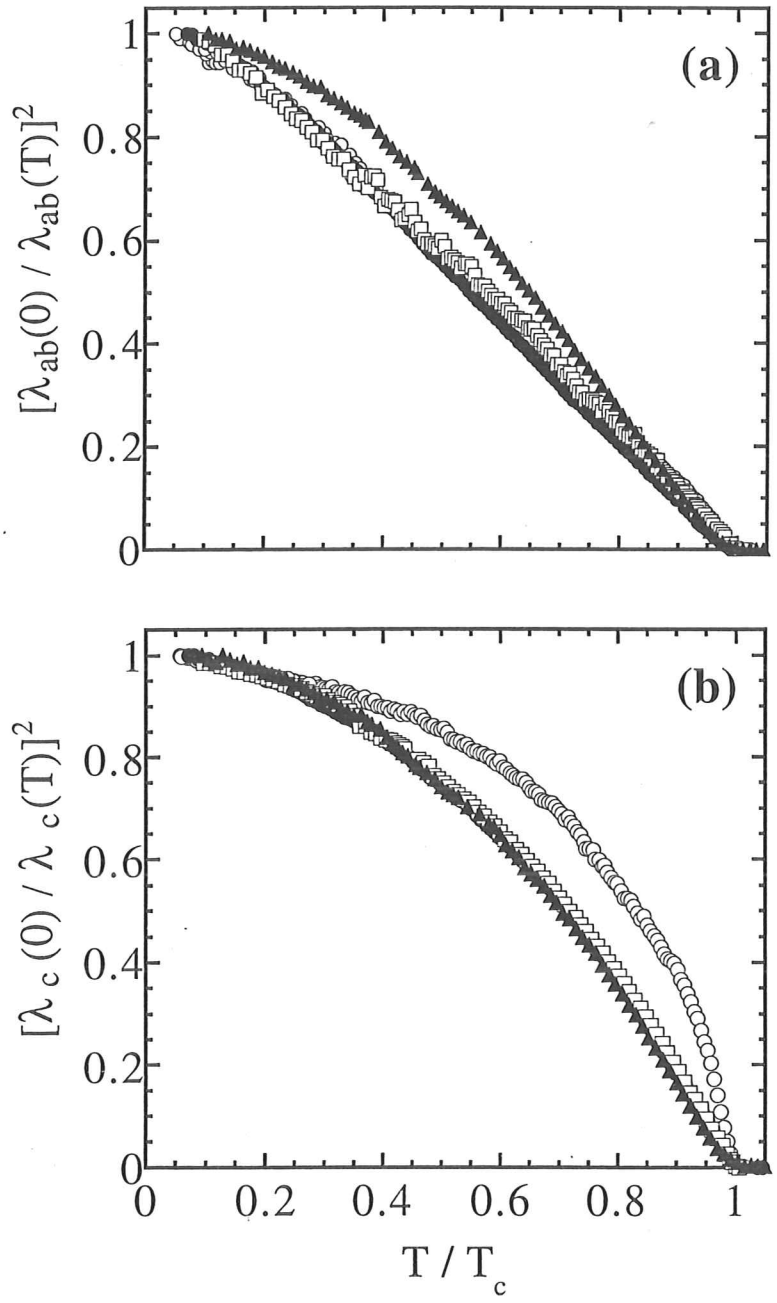

Fig. 8.2. Plots of (a) $[\lambda_{ab}(0) / \lambda_{ab}(T)]^2$ and (b) $[\lambda_c(0) / \lambda_c(T)]^2$ as functions of T/T_c for $YBa_2(Cu_{1-x}Zn_x)_3O_7$ with $x = 0.00$ (open circles), 0.02 (closed circles), 0.03 (open squares) and 0.05 (closed triangles).

Figure 8.3(a) shows a comparison of $\lambda_{ab}(T)$ with $\lambda_c(T)$, plotted as $[\lambda_{ab}(0) / \lambda_{ab}(T)]^2$ and $[\lambda_c(0) / \lambda_c(T)]^2$, for $x = 0.00$ and also the behaviour expected for a weakly coupled BCS d-wave superconductor with a maximum gap $\Delta(0) = 2.14\ k_B T_c$ [12]. (Note that the same agreement between the data and the BCS d-wave fit holds for all the data sets shown in chapter 7, fig. 7.2. In the latter case no theoretical fit was included due to the large number of plots in the figure.) There is striking agreement between $\lambda_{ab}(T)$ and the d-wave curve over the whole temperature range which is observed for the first time for YBCO although it is in agreement with results for $HgBa_2Ca_2Cu_3O_{8+\delta}$ (Hg-1223) (chapter 5). As mentioned earlier in the text, although $[\lambda_c(0) / \lambda_c(T)]^2$ is flatter it is linear below 30 K (see inset to fig. 8.3(a)). In Hg-1223 which is much more anisotropic, $\lambda_c(T)$ was even flatter and this was ascribed to incoherent pair tunneling along the c-direction or possible Josephson coupling between the planes. In the present case the anisotropy is much smaller and other possibilities for example proximity effect coupling via the Cu-O chains [13] or a variation in the c-axis transfer integral around the CuO_2 plane Fermi surface [14] are possible.

Figure 8.3(b) shows that for $x = 0.05$, $[\lambda_{ab}(0) / \lambda_{ab}(T)]^2$ and $[\lambda_c(0) / \lambda_c(T)]^2$ have essentially the same T dependence. (The data are also compared with the behaviour expected for a weak coupling BCS s-wave superconductor [15].) It is probably mainly because 5% Zn smears out the anisotropy of the d-wave gap. However, as discussed below, Zn substitution also increases the c-axis coupling slightly and probably increases the superconducting coherence lengths in all directions via the effect on T_c.

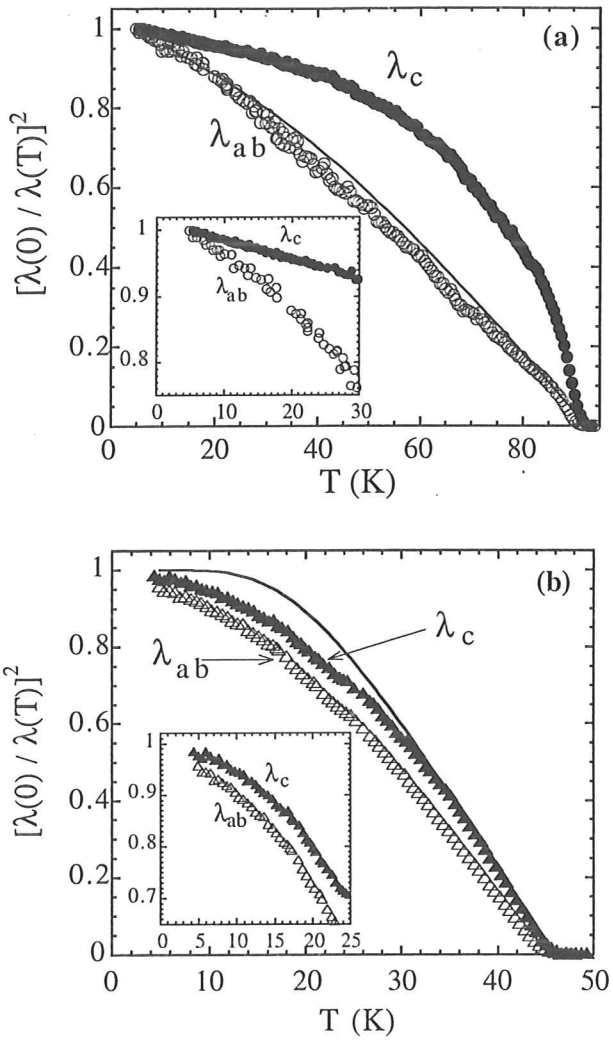

Fig. 8.3. Plots of $[\lambda_{ab}(0) / \lambda_{ab}(T)]^2$ and $[\lambda_c(0) / \lambda_c(T)]^2$ as functions of T for $YBa_2(Cu_{1-x}Zn_x)_3O_7$ with $x = 0.00$ (a) and $x = 0.05$ (b). Also shown, by the solid lines, in (a) is the theoretical prediction for the normalised superfluid density from the weak coupling BCS theory for a *d*-wave superconductor [12] and in (b) the weak coupling BCS theory for an *s*-wave superconductor [15]. The insets show the low temperature regions.

The probable effect of Zn doping on the superfluid density (n_S) has been analysed by using published specific heat [4], NMR [8] and Gd^{3+} ESR [16] results which give consistent values for the residual density of states at the Fermi energy in the superconducting state [16]. We assume that this residual density of states (N_R) corresponds to unpaired electrons and therefore, plot our values of $\lambda_{ab}^2(0)$ and $\lambda_c^2(0)$ versus $1/N_S$, where in our notation $N_S = N_T - N_R$, N_T is the total density of states and (N_R / N_T) is given in Ref. [16]. As shown in fig. 8.4(a), $\lambda_{ab}^2(0)$ increases linearly with $1/N_S$, except for the $x = 0.00$ sample where the deviation possibly arises from the chain contribution to $\lambda_{ab}(0)$ [17]. From this deviation we estimate the value of $\lambda_{ab}(0)$ from the CuO_2 planes to be 1870 Å. The values of $\lambda_c^2(0)$ do not increase linearly with $1/N_S$. This is probably due to a decrease in anisotropy with Zn doping as has also been found from resistivity studies for Zn doped $Bi_2Sr_2CaCu_2O_{8+y}$ crystals [18]. As shown in fig. 8.4(b), [$\lambda_c(0)$ / $\lambda_{ab}(0)$] decreases linearly with Zn content (here we use the CuO_2 plane value for $\lambda_{ab}(0)$, $x = 0.00$, derived above). In chapter 6 we mentioned that the *c*-axis coupling in the cuprates is influenced by the 4*s* electrons of the in-plane Cu atoms which is possibly consistent with our finding that Zn substitution increases the *c*-axis coupling (of course there is a net increase in λ_c because the superfluid density is reduced by Zn doping). As discussed below this relatively small increase in *c*-axis coupling combined with the strong reduction in T_c leads to a larger superconducting coherence length (ξ_c (T)) in the *c*-direction and fluctuation effects near T_c should be reduced.

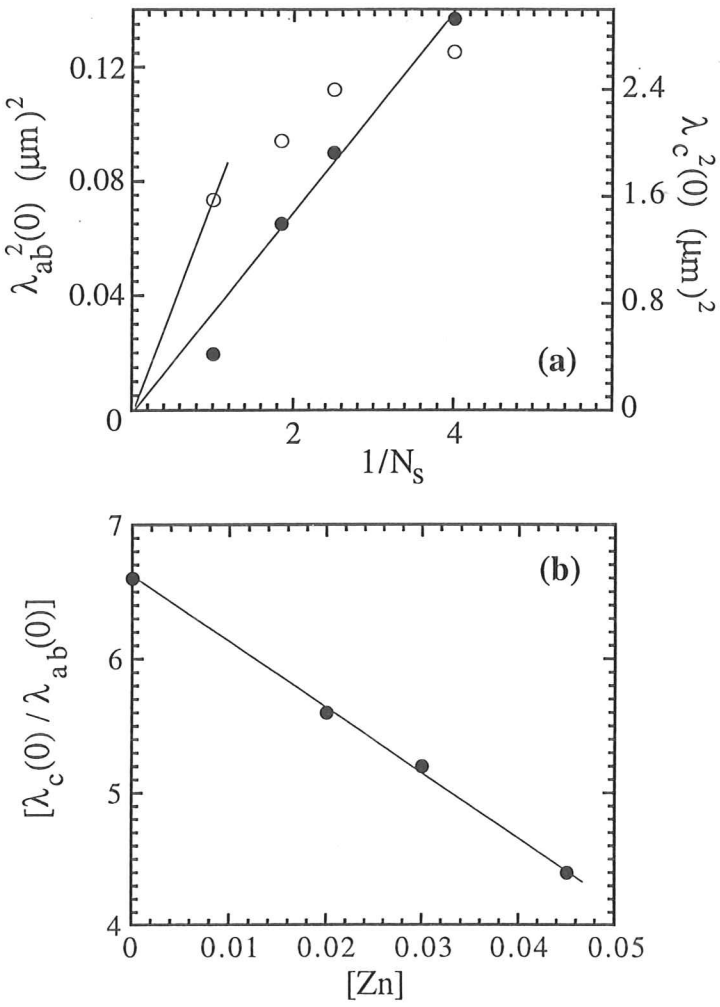

Fig. 8.4. (a) $\lambda_{ab}^2(0)$ (closed circles) and $\lambda_c^2(0)$ (open circles) versus $1/N_S$ for $YBa_2(Cu_{1-x}Zn_x)_3O_7$ with $x = 0.00$, 0.02, 0.03 and 0.05. Here $N_S = N_T - N_R$, where N_T is the total density of states and N_R the residual density of states below T_c which corresponds to unpaired electrons [16]. (b) $[\lambda_c(0) / \lambda_{ab}(0)]$ versus Zn concentration (x = 0.00, 0.02, 0.03 and 0.05). Solid lines are drawn as a guide to the eye. For $x = 0.00$ we have used the value of $\lambda_{ab}(0)$ for the CuO_2 planes (see text).

Finally, we discuss the kinks seen in $[1/\lambda_{ab}(T)]^2$ and $[1/\lambda_c(T)]^2$ for $x = 0.00$ near T_c (figs. 8.1(a) and 8.1(b)). The kinks may be caused by superconducting fluctuations. When the coupling between CuO_2 planes within a unit cell is stronger than that between cells, a 2D - 3D crossover in YBCO is expected at a reduced temperature $r = [2\xi_c^2(0) / d^2] = 0.06$ [19], i.e., $T / T_c \approx 0.94$ which is close to where the kinks are seen (fig. 8.1). Here $\xi_c(0)$ is the c-axis coherence length (2 Å for YBCO [20]) and d is the c-axis parameter (11.7 Å for YBCO [21]). However, as shown in fig. 8.1 this kink is not detected for $x \geq 0.02$. From the values of T_c and the changes in anisotropy discussed above we would expect $r = 0.11$ for 0.02 Zn that is, a kink near 66 K in fig. 8.1. It is perhaps possible that superconducting fluctuations are smeared out by 0.02 Zn.

8.4 Summary

In summary, we have investigated the dependences of the anisotropic magnetic penetration depth of high quality grain aligned YBCO on Zn doping and temperature. The values of $\lambda_{ab}(0)$ and $\lambda_c(0)$ were found to increase systematically with Zn doping. The observed increase in the values of $\lambda_{ab}(0)$ with Zn content is consistent with the residual density of states determined by other measurements. In contrast, the values of $\lambda_c(0)$ do not increase as quickly, probably because of a moderate increase in the c-axis coupling strength. Below ~ 25 K $\lambda_{ab}(T)$ and $\lambda_c(T)$ for pure YBCO obey a linear T power law characteristic of d-wave superconductivity. These linear T dependences change to T^2 with the addition of Zn ($x = 0.02$, 0.03 and 0.05). While $\lambda_{ab}(T)$ for $x = 0.00$ is consistent with a weak coupling d-wave model over the whole temperature range $\lambda_c(T)$ shows a flatter temperature dependence. However, for high Zn doping ($x = 0.05$) both quantities have essentially the same behaviour suggesting that 5% Zn smears out the anisotropy of the d-wave gap, or leads to the increase of the superconducting coherence length in all directions.

References

[1] For example, B. Jayaram *et al.*, Phys. Rev. B **38**, 2903 (1988).

[2] D. A. Bonn *et al.*, Phys. Rev. B **50**, 4051 (1994).

[3] P.J. Hirschfeld and N. Goldenfeld, Phys. Rev. B **48**, 4219 (1993)

[4] J. W. Loram, K. A. Mirza and P. A. Freeman, Physica C **171**, 243 (1990).

[5] H. Alloul *et al.*, Phys. Rev. Lett. **67**, 3140 (1991).

[6] S. Zagoulaev, P. Monod and J. Jegoudez, Phys. Rev. B **52**, 10474 (1995).

[7] J. W. Loram, (unpublished).

[8] K. Ishida *et al.*, J. Phys. Soc. Jpn. **62**, 2803 (1993).

[9] D. Shoenberg, *Superconductivity* (Cambridge University Press, Cambridge, 1954), p.164.

[10] Y.J. Uemura *et al.*, Phys. Rev. Lett. 66, 2665 (1991).

[11] C. Bernhard *et al.*, Phys. Rev. Lett. (submitted).

[12] A. Schofield, (private communication).

[13] T. Xiang and J.M. Wheatley, Phys. Rev Lett. **76**, 134 (1996).

[14] J. M. Wheatley, (private communication).

[15] B. Muhlschlegel, Z. Phys. **155**, 313 (1959).

[16] A. Janossy *et al.*, Phys. Rev. B **50**, 3442 (1994).

[17] J. L. Tallon *et al.*, Phys. Rev. Lett. **74**, 1008 (1995).

[18] D-S. Jeon *et al.*, Physica C **253**, 102 (1995).

[19] C. Baraduc and A. Buzdin, Physics Letters A **171**, 408 (1992).

[20] L.N. Bulaevskii, Int. J. Mod. Phys. B 4, 1849 (1990).

[21] R.M. Hazen *et al.*, Phys. Rev. B **35**, 7238 (1987).

Chapter 9

Conclusions

The penetration depth of several high-T_c superconductors (HTSC) has been investigated through low field ac susceptibility measurements on grain aligned samples.

We have prepared magnetically oriented HTSC. These samples consist of thousands of tiny crystallites of known grain size distribution dispersed in epoxy with their crystallographic *c*-axis oriented in the same direction. The high degree of alignment is uniquely characterised by a special X-ray technique.

An amorphous layer on the surface of $YBa_2Cu_3O_7$ ($YBCO_7$) crystallites was found to account partially for the discrepancy in the literature in the temperature, T, dependence of the penetration depth, λ, at temperatures lower than 20 K. New methods to avoid surface degradation and heat treat the degraded surfaces were found. In particular heat treating the $YBCO_7$ crystallites at 850 °C for 12 h in flowing oxygen and reoxygenating at 380 °C, or grinding HTSC under argon yields clean surfaces.

Penetration depth data were taken using home built and commercial susceptometers over a wide temperature range, $1.2\ K \leq T \leq 150\ K$.

We first studied the penetration depth of grain aligned tetragonal $HgBa_2Ca_2Cu_3O_{8+\delta}$ (Hg-1223) down to 4.2 K. Hg-1223 is of particular interest because it has the highest T_c among all HTSC and contains three CuO_2 planes. We reported the values and T dependences of the in-plane λ_{ab} and out-of-plane λ_c penetration depths. The isotropic perovskite oxide superconductor $Ba_{0.6}K_{0.4}BiO_3$ (BKBO) was also studied for comparison. The anisotropy ratio $\gamma \sim 30$ as obtained from the ratio of the measured $\lambda_c(0)$ and $\lambda_{ab}(0)$ values reflects the 2D nature of Hg-1223. The 2D nature is further supported by a kink observed in $1 / \lambda^2(T)$ near T_c suggesting a dimensional cross-over. The T dependence of λ_{ab} shows excellent agreement with the theoretical prediction for *d*-wave

superconductivity. $\lambda_c(T)$ followed the behaviour expected for a superconductor with intrinsic Josephson coupling between the CuO_2 planes. BKBO, is found to be an *s*-wave superconductor.

We have also investigated the low temperature dependence of the anisotropic magnetic penetration depth of grain aligned tetragonal $HgBa_2Ca_{n-1}Cu_nO_{2n+2+\delta}$ (n=1 and 3) down to 1.2 K. The linear term in $\lambda_{ab}(T)$ for Hg-1201, characteristic of *d*-wave superconductivity, has a slope of 6.5 Å/K. In contrast the data for $\lambda_c(T)$ are much flatter at low T. The $\lambda_c(T)$ data fit the expression for tetragonal d_{x2-y2} HTSC: $\lambda_c(T) \sim \lambda_c(0)$ [1+ $\alpha(T/T_c)^5$], with $\alpha \sim 3$. The experimental value of α yields $(\Delta_0/T_c) \sim 2.37$. The weaker T dependence of λ_c compared to λ_{ab} is a consequence of the unusual *c*-axis electronic structure of high-T_c oxides. In clean tetragonal samples, the *c*-axis hopping of holes mainly occurs through large radius Cu 4*s* orbitals. In this case, the *c*-axis hopping constant is a function of the in-plane momentum $k_{//} = (k_x, k_y)$ and vanishes at $k_x = k_y$. This unusual $k_{//}$ dependence of the *c*-axis hopping constant leads to the T^5 dependence in λ_c. The linear term in $\lambda_{ab}(T)$ for Hg-1223 has a slope of 4.2 Å/K. $\lambda_c(T)$ is much flatter than $\lambda_{ab}(T)$ and depends quadratically on T. This T^2 behaviour could be due to the high anisotropy of Hg-1223 since for weakly coupled planes, disorder can give rise to a T^2 term in $\lambda_c(T)$ without significantly affecting the T^1 term in $\lambda_{ab}(T)$. However, one cannot rule out the possibility of Josephson coupling effects as mentioned in the last paragraph. All results are consistent with the picture of d_{x2-y2}-wave superconductivity in low and high anisotropic cuprates provided one accepts that disorder effects are indeed important for $\lambda_c(T)$ of more highly anisotropic compounds.

The effects of oxygen concentration on the values and temperature dependences of λ_{ab} and λ_c of high quality *c* - axis grain aligned orthorhombic $YBa_2Cu_3O_{7-\delta}$ with $\delta = 0.0$, 0.3 and 0.43, which have two CuO_2 planes per unit cell as well as Cu-O chains were also studied. These were compared to those of Hg-1201 with one CuO_2 plane per unit cell and Hg-1223 with three CuO_2 planes per unit cell. $\lambda_{ab}(0)$, $\lambda_c(0)$ and the anisotropy ratio $\gamma = [\lambda_c(0) / \lambda_{ab}(0)]$ were found to increase with δ. For the above values of δ, both

$\lambda_{ab}(T)$ and $\lambda_c(T)$ follow the behaviour expected for a superconductor with nodes in the energy gap. The linear term in $\lambda_{ab}(T)$ increases with oxygen deficiency, namely, from 4.5 to 12 and 20 Å/K, for δ = 0.0, 0.3 and 0.43, respectively. From the change of the low temperature linear slope of $\lambda_{ab}(T)$ for $YBa_2Cu_3O_{7-\delta}$ (δ = 0.0, 0.3 and 0.43) and $HgBa_2Ca_{n-1}Cu_nO_{2n+2+\delta}$ (n=1 and 3) we find that in BCS d- wave cuprate superconductors the superconducting energy gap Δ_0 scales linearly with T_c. For the less anisotropic YBCO7 ($\gamma \sim$ 6.5, using $\lambda_{ab}(0)$ = 0.187 μm, i.e., the value from the planes only), we observe a linear T dependence in λ_c at low temperatures but the relative change is about a factor of two smaller than in [$\lambda_{ab}(T)$ / $\lambda_{ab}(0)$]. This probably arises from the effects of hopping between planar and chain bands. By removing oxygen from YBCO7 one can reduce the effects of the chains. $\lambda_c(T)$ of $YBCO_{6.7}$ ($\gamma \sim$ 22) and $YBCO_{6.57}$ ($\gamma \sim$ 25) vary as T^2, like Hg-1223 which has similar anisotropy.

Finally, we investigated the effects of Zn doping to the absolute values and temperature dependences of λ_{ab} and λ_c of YBCO7. The values of $\lambda_{ab}(0)$ and $\lambda_c(0)$ were found to increase systematically with Zn doping in $YBa_2(Cu_{1-x}Zn_x)_3O_7$, x = 0.00, 0.02, 0.03 and 0.05. A fast increase of $\lambda_{ab}(0)$ with Zn is found which is consistent with an increase in the residual density of states. In contrast, $\lambda_c(0)$ does not increase as quickly which we attribute to an enhanced c-axis coupling strength caused by Zn doping. The linear low T dependences of $\lambda_{ab}(T)$ and $\lambda_c(T)$ change to T^2 with the addition of Zn. As mentioned above, while $\lambda_{ab}(T)$ for x = 0.00 is consistent with a weak-coupling d-wave model over the whole T range, $\lambda_c(T)$ shows a flatter, but linear, temperature dependence. However, for x = 0.05 both quantities have almost the same behaviour, suggesting that either 5% Zn smears out the anisotropy of the d-wave gap, or leads to the increase of the superconducting coherence length in all directions.

In brief, we have been able with our technique to systematically probe the superfluid density and the order parameter of various HTSC. We have found that the presence of the linear term in $\lambda_{ab}(T)$, characteristic of d-wave superconductivity, is independent of the number of CuO_2 planes per unit cell, carrier concentration, crystal structure, presence of

chains and anisotropy. The superconducting energy gap of BCS *d*- wave cuprate superconductors was found to scale linearly with T_c. It was shown experimentally that for HTSC with tetragonal symmetry and moderate anisotropy the Cu 4s orbital is important for the *c*-axis hopping of holes. Namely a T^5 dependence of $\lambda_c(T)$ was observed for Hg-1201 and a T^2 law for more anisotropic materials (e.g. Hg-1223). $\lambda_c(T)$ for $YBCO_{6.7}$ and $YBCO_{6.57}$, which have similar anisotropy to Hg-1223, also varied as T^2. $YBCO_7$ shows a flatter but linear T dependence in $\lambda_c(T)$ at low T. Zinc substitution in $YBCO_7$ affects the anisotropy and the residual density of states. Finally, results for BKBO emphasise the importance of the CuO_2 planes for *d*- wave pairing symmetry.

Publications

Surface Quality Dependence of the Low Temperature Magnetisation of $YBa_2Cu_3O_7$

C. Panagopoulos, W. Zhou, N. Athanassopoulou and J. R. Cooper

Physica C, Vol. 269, p.157 (**1996**)

High-Resolution X-Ray Diffraction Analysis of Magnetically Aligned High-T_c Superconducting Ceramics

J. Chrosch, C. Panagopoulos, N. Athanassopoulou, J. R. Cooper and E.K.H. Salje

Physica C, Vol. 2655, p.233 (**1996**)

Magnetic Penetration Depth of Grain Aligned $HgBa_2Ca_2Cu_3O_{8+\delta}$

C. Panagopoulos, J.R. Cooper, G.B. Peacock, I. Gameson, P.P. Edwards,

W. Schmidbauer and J.W. Hodby:

Phys. Rev. B Vol. 53 (6) R2222 (**1996**)

The Effects of Zn Doping on the Anisotropic Penetration Depth of $YBa_2Cu_3O_7$

C. Panagopoulos, N. Athanassopoulou, J. R. Cooper and J. Chrosch

Phys. Rev. B Vol. 54 (18) R12 721 (**1996**)

Anisotropic Penetration Depth Measurements of High- T_C Superconductors

C. Panagopoulos, J.R. Cooper, T. Xiang, G.B. Peacock, I. Gameson, P.P. Edwards,

W. Schmidbauer and J.W. Hodby

Invited paper for M^2S, Beijing 1997, (To appear in Physica C) (**1997**)

Probing the Order Parameter and the c-axis Coupling of High- T_C Cuprates by Penetration Depth Measurements

C. Panagopoulos, J.R. Cooper, T. Xiang, G.B. Peacock, I. Gameson and P.P. Edwards

Phys. Rev. Lett. (**1997**) (*in press*)

Scaling of T_C with Superconducting Energy Gap in d-wave Cuprates as Probed by Penetration Depth Measurements

C. Panagopoulos, J.R. Cooper and T. Xiang

Phys. Rev. Lett. (submitted)